On the surface interaction between *Cylindrotheca fusiformis* and aerospace aluminum alloys

S. Zalman

Technische Universiteit Delft

TU Delft

On the surface interaction between *Cylindrotheca fusiformis* and aerospace aluminum alloys

by

S. Zalman

to obtain the degree of Master of Science
at the Delft University of Technology,
to be defended publicly on Monday February 28, 2022 at 14:00.

Student number: 4394550
Project duration: February 1, 2021 – February 28, 2022
Thesis committee:

Dr. S. J. Garcia,	TU Delft, thesis supervisor
Dr. M. Nijemeisland,	TU Delft
Dr. C. D. Rans,	TU Delft
Prof. dr. C. P. D. Brussaard,	Royal Netherlands Institute for Sea Research

Cover image from Kunstformen der Natur (1904), plate 84: Diatomeae by Ernst Haeckel [1]

TU Delft

Abstract

Microbes, and the biofilms they form on surfaces, generally have a negative impact on performance. Well-known examples are the increase of drag in ships and pipes, and the accelerated corrosion of metallic structures known as MIC. Among microbes, diatoms form a large unicellular algae group known to play a relevant role in the first stages of biofilm formation. Diatoms are well-known for their species-dependent silica exoskeletons, but they also produce, as other microbes, extracellular polymeric substances (EPSs) that may offer opportunities for the development of novel bio-based surface treatments. In this work we studied the interaction between a marine diatom species named *Cylindrotheca fusiformis* and aerospace aluminum alloys as a first step towards novel surface protection treatments of aircraft structures.

Two routes were followed to study the interaction of *C. fusiformis* with aluminum alloys after studying diatom population growth. The first route focused on the biofilm formation on aluminum 99.5%, AA20204-T3 and AA7075-T6 to study the effect of surface composition. The effect of the surface preparation (degreased vs. polished) was then studied with AA2024-T3 substrates. The second route focused on the study of diatoms' motility on aluminum 99.5% and AA2024-T3 with various surface pretreatments. In this work, a number of characterization techniques such as FTIR, SEM/EDS, Raman spectroscopy and image correlation techniques were used.

It was found that *C. fusiformis* forms well-adherent biofilms on all aluminum substrates, independently of the surface composition and surface pre-treatment. Nevertheless, the biofilms appeared to be most homogeneous on AA7075-T6, while the EPS layer was more homogeneous on aluminum 99.5% and AA2024-T3. The motility studies showed that *C. fusiformis* lowers its surface motility rapidly when on aluminum 99.5% until cells stop being motile. On AA2024-T3, cells maintain their motility for longer periods of time. The motility dependency on surface chemistry is hypothesized to come from speciation-dependent aluminum toxicity. Post-mortem chemical analysis of the exposed surfaces showed traces of organic material in the form of proteins and carbohydrates attributed to displacement trails. The results confirm that monocultures of *C. fusiformis* are able to generate biofilms on aerospace aluminum alloys and release water-insoluble organic matter on the surface. The promising results here obtained pave the way for more dedicated research to understand the relationships between surface chemistry and topology, and diatom motility and biofilm formation and composition.

Acknowledgments

This thesis project was not an easy journey and taught me a lot about myself. Now it has come to an end and with it, ends an era. There are many people who guided me along the way. First, I would like to thank my supervisor Dr. Santiago Garcia for giving me this opportunity, many good ideas and for motivating me to think out of the box. I also thank Prof. Dr. Corina Brussaard, for assisting in this interdisciplinary project and providing us with the necessary knowledge and material to do this project. Special thanks to Dr. Marlies Nijemeisland, whom without this project would not have succeeded. Thank you for teaching me the ropes in the lab and always looking for practical solutions with me. And thanks to Dr. Calvin Rans for freeing up time to be part of my committee.

The support staff at TU Delft and NIOZ were of immeasurable value, thank you for always being there to help Durga, Shanta, Anna, Kirsten, Michele, Ilsa and of course the DASML crew. Hugo, Tinashe and Jingjing, thank you so much for all help with my research, you were always there for me when I got stuck or just to talk. To all the other PhD students of NovAM, thank you so much for your input and nice snacks during the meetings. Paul, thanks for introducing me to the world of ImageJ and all the tips and tricks.

I would have been lost without my fellow master students. Thank you Anniek, for all the nice coffee breaks at Jenny and Maurizio, for listening to me and helping me navigate through the start of my project. Mark, my fellow aerospace biologist, thanks for the fruitful discussions we had and for motivating me till the end. Thanks to Willem for the nice walks, good talks and LaTeX tips. And to all the other master students at NovAM, all of you brightened my time here. Thanks to the ”Vliegende Eekhoorns” and all other friends I have made in almost 6 years in Delft for the good times. To Daan, who came to the rescue when all appeared to be lost. And to Sifra, who is the most patient listener I know.

Finally, I would like to thank my parents Chris and Lucien, my little brother Sam and m’oma Marij, thank you for all the support you have given me throughout this difficult journey. Thank you Arnold, for standing by me, for giving me love and support and for all the nice dinners, I would have never been able to complete this without you.

S. Zalman
Delft, February 2022

List of Figures

List of Tables

Contents

1

Introduction

One of the biggest challenges in the aerospace engineering and engineering in general is corrosion protection. Corrosion often severely impedes performance and comes with significant costs. It is estimated that the global cost of corrosion is equivalent to 3.4% of the global gross domestic product, which is about US$2.5 trillion [2]. While there are many techniques of corrosion prevention, hexavalent chromium is a widely used and efficient form of corrosion protection. However, it is carcinogenic and not environmentally-friendly [3]. The aerospace industry, among others, faces the challenge of finding saver and better ways to protect against corrosion.

With the demand for greener alternatives increasing, so does the bio-based trend in engineering. This is often in the form of bio-inspired or bio-based materials. Examples are adhesives based on mussels' attachment proteins or high strength fibers based on spiders' silk through synthetic biology [4]. Alternatively, naturally built structures can be applied almost directly, for example by using algae exoskeletons as carriers for corrosion inhibitors [5] or using biofuel made from algae [6]. Another example of nature's engineering is the formation of natural coatings or *biofilms* on structures such as trees (natural) or ships (man-made). These biofilms are almost always undesired as they may impede performance, for example by increasing drag on ship hulls [7] or by increasing the corrosion rate [8].

However, these biofilms could also serve as the basis for a bio-based coating or pre-treatment. They may also add new functionalities, for example, some microorganisms can inhibit corrosion. They can do this passively, by for example forming a protective barrier or actively, by neutralizing corrosive species [9]. Examples include bacterium *Bacillus brevis* that inhibits corrosion by eliminating the corrosion enhancing sulfate-reducing bacteria and the bacterium *Bacillus licheniformis* which was found to reduce corrosion on AA2024 by producing sticky protective layer [10]. Furthermore, the extracellular polymeric substances (EPSs) that are excreted by microorganisms show interesting properties. EPSs can have antiviral, anti-inflammatory or even anti-tumor properties [11]. Other EPSs have functions that could also be interesting for the aerospace industry, such as anti-adhesive qualities [11] or on the other hand, good adhesiveness even under wet circumstances [12]. The natural film formation in combination with the production of functional biopolymers make microbially produced coatings a promising development to explore.

Here we explore this alternative view of using biofilms for surface protection. This research takes a unique approach by studying a subgroup of microalgae called *diatoms* for protective coating applications on aerospace aluminum alloys. Diatoms were selected because they form biofilms on a wide variety of surfaces, even on fouling-release coatings [13]. The interaction of marine diatom species *Cylindrotheca fusiformis* and various aluminum alloy substrates was investigated. Unraveling the interaction will increase the understanding of how biofilms form on aluminum substrates, which is crucial to evaluate the potential of using diatoms to form coatings. Because of the interdisciplinary nature of this project, it was a collaboration between TU Delft's Faculty of Aerospace Engineering and the Royal

Netherlands Institute for Sea Research. This chapter provides the necessary background information on diatoms and the aluminum alloys used in this work and outlines the research objective and thesis structure.

1.1. Diatom biology

Diatoms are a kind of unicellular microalgae that live in all kinds of aquatic environments. They play an important role in global carbon fixation, as it is estimated that they are responsible for about 20% of the global carbon fixation [14]. Their morphology is characterized by a SiO_2 exoskeleton, called the *frustule*, which contains the organic material. Based on the shape of their frustule, diatoms can be divided into two categories: *centric* and *pennate*. Centric diatoms are radially symmetric and are generally pelagic (free floating), while pennate diatoms are bilaterally symmetric and often of the benthic kind (living on a substrate) [13]. The frustule is composed of two halves called *thecae*, that fit together like a petri dish. The smaller one is called the *hypotheca* and the larger one the *epitheca*. They are built up from a valve and several girdle bands, as can be seen schematically in Figure 1.1a. Pennate species can also have a slit in their valves, called the *raphe*. The raphe(s) play a role in diatoms adhesion and motility.

The specific species that was used for this work is *Cylindrotheca fusiformis*, which is a benthic, raphid, pennate species. A micrograph showing the cell wall and its different structures can be seen in Figure 1.1b [15]. This species was selected because it showed good biofilm formation on titanium and PMMA in preliminary work [16], as can be seen in Figure 1.2.

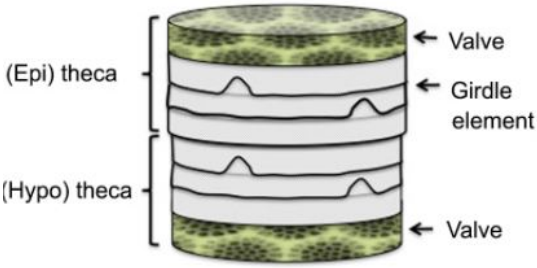

(a) Schematic representation of the frustule; adapted from [17]

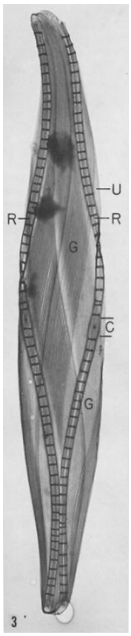

(b) Electron micrograph of the cell wall of *Cylindrotheca fusiformis*; R is the raphe, G is the girdle composed of several girdle bands; adapted from [15]

Figure 1.1: Diatom morphology

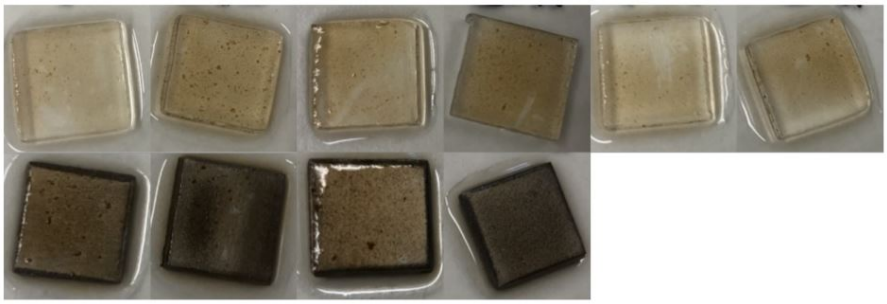

Figure 1.2: Biofilms formed by *Cylindrotheca fusiformis* on titanium and PMMA after 6 day immersion in a culture with a starting concentration of 8.0×10^4 cells/mL [16]

The diatoms were kept as liquid monocultures, for which the typical growth pattern can be seen in Figure 1.3 [18]. The growth curve can be divided into four phases:

1. The lag phase; this is the phase right after inoculation in which the cells are still adjusting to their new surroundings and growth is slow
2. The exponential or log phase; during this phase, the culture grows exponentially
3. The stationary phase; growth rate declines because there is a limiting factor, such as nutrients, light or CO_2, this leads to the growth rate to become equal to the death rate, resulting in a constant cell concentration
4. The death phase; eventually the growth stops and the cells will start dying and the culture will collapse

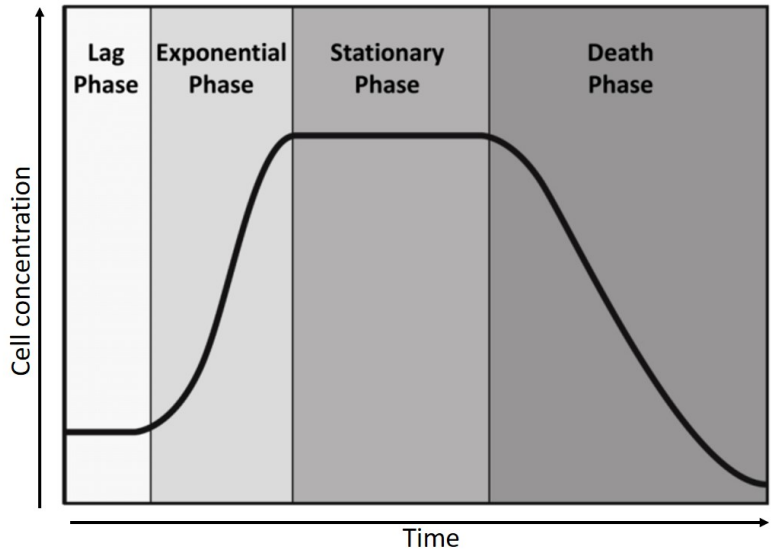

Figure 1.3: Typical growth curve for a diatom culture; adapted from [18]

Cells from different growth phases may have different properties, for example, generally more EPS is secreted during stationary phase [19]. The duration of each of the phases and the exact cell concentration are dependent on the species and growing conditions.

1.1.1. Extracellular Polymeric Substances (EPSs)

Extracellular Polymeric Substances (EPSs) are composed of high molecular weight biopolymers. Diatom EPS is mainly composed of polysaccharides and proteins. The exact composition and amount of EPS is determined by the species, growth phase and environmental factors [20]. EPSs are interesting to research, because they may possess useful functionalities. For example, several diatom EPSs have been found to have antiviral or (anti-)adhesive properties [11].

Transparent Exopolymer Particles (TEPs) are a type of EPS that are operationally defined as "*transparent particles that are formed from acidic polysaccharides and are stainable with alcian blue*" [21]. These specific gel-like particles are of interest as they have a high stickiness, play a role in aggregation (clumping together of particles) and in early biofilm formation [22].

1.1.2. Diatom biofilms

A biofilm can be defined as a "*collection of microorganisms and organic material embedded in a stationary 3D matrix*" [23]. This 3D matrix is usually made of EPSs excreted by the microorganisms. This

matrix helps in surface attachment, protects the cells and functions as a means to transport molecules from and to the substrate surface. The biofilm is often heterogeneous, which may or may not be substrate dependent. In nature, biofilms are often composed of multiple species, however, in this work the biofilm is made up of only one species of diatom as it was formed by a monoculture.

The stages of biofilm formation are schematically represented in Figure 1.4 [20]. The first step of biofilm formation is the formation of the *conditioning film*, this process starts as soon as the substrate is immersed in the liquid. During this phase, (macro-)molecules from the environment are absorbed in the substrate and form an initial layer. This layer has an effect on the microbial retention and the cell-substratum interaction. This film's composition is determined by the environment and may likely mask some of the substrate's properties [24]. After the conditioning film is formed, the cells will start to attach to the surface and produce EPS for the biofilm. More microorganisms will attach and the biofilm will mature until a certain point, after which it starts breaking down and components become dispersed again.

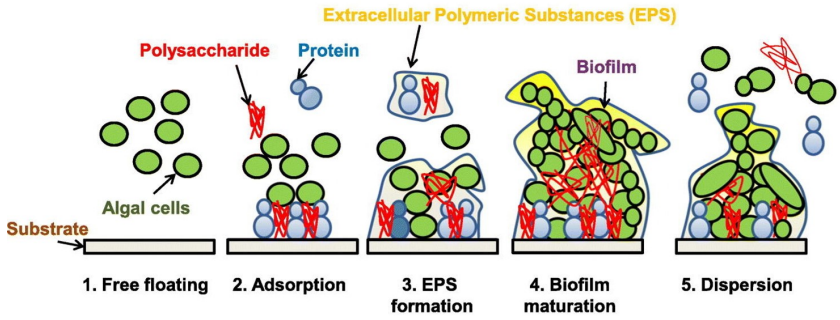

Figure 1.4: Schematic representation of diatom biofilm formation; adapted from [20]

The effect of substrates on diatom adhesion has mainly been studied in the context of preventing biofouling, for example on stainless steel [25] or on polymers [26], [27]. The hydrophilicity/hydrophobicity of the substrates plays a role, but the results are not consistent. This may be caused by the fact that EPS contains both hydrophilic and hydrophobic molecules, which may also vary over time and with different substrates [23], [26]. The physical properties of the substrate may also have an effect on initial adhesion and cell retention, but become less important as the biofilm matures [24]. Physico-chemical properties such as color, roughness or the formation of a passive layer may also affect diatom adhesion [7], [25], [28].

1.1.3. Diatom motility

Apart from forming biofilms, some diatom species are motile on a substrate. Two types of movement are discerned: *gliding* and *shunting* [27]. Gliding is the movement across the surface where there is a net change in position, while shunting is a movement in which the net position of the cell does not change. The current proposed model for raphid diatom motility (and adhesion) was proposed in 1984 [29] and is depicted in Figure 1.5 [13]. This system is composed of a myosin/actin system, transmembrane proteins and substrate adhesion molecules and is called the *Adhesion Motility Complex (AMC)*. The movement is caused by a force parallel to the substrate, causing the diatom to move in the opposite direction, leaving a trail of EPS behind [13].

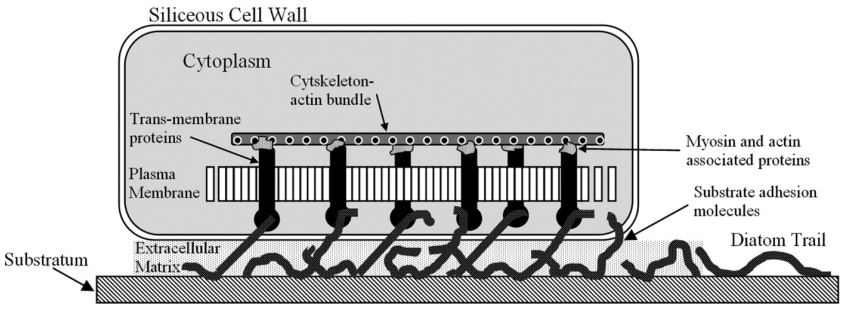

Figure 1.5: Schematic representation of diatom Adhesion Motility Complex [13]

These trails can be characterized by for example staining, SEM imaging, quartz crystal microbalance dissipation monitoring (QCM-D) and atomic force microscopy (AFM). The trails from diatom species *Amphora coffeaeformis* and *Craspedotauros australis* have been analyzed to better understand bioadhesives. The mucilage mainly consists of polysaccharides and proteins, but that no dihydroxyphenylalanine (DOPA) was present, which is responsible for the strong adhesion of mussels. They identified one of the components as *trans*Dihyp (2,3-cis-3,4-trans-dihydroxyproline), which is similar to DOPA [30]. In different research, the trails of the same species were also analyzed using QCM-D to determine their viscoelastic properties. It was observed that the trails were insoluble, suggesting some kind of curing taking place [12]. This property makes these trails interesting to further investigate for potential bioadhesives and surface treatments as in this thesis.

1.2. Aerospace aluminum alloys

Aluminum alloys are widely used in the aerospace industry, as they provide a good combination of a relatively low density and mechanical properties. They are categorized based on their main alloying element and are identified through four digits. In addition, a T may be added at the end which designates the temper treatment in heat treatable alloys [31]. The three alloys used in this projects were aluminum 99.5%, AA2024-T3 and AA7075-T6.

Aluminum 99.5% is a commercially pure aluminum with a low content of alloying elements. It is composed of 99.5% aluminum, the other 0.5% can be made up out of several elements such as Cu, Fe, Mg, Mn, Ti or Si. AA2024-T3 is part of the 2xxx series, meaning that the main alloying element is copper. The alloying elements for AA2024 are as follows: Cu (3.8-4.9%), Mg (1.2-1.8%), Mn (0.3-0.9%), Zn (0.3%), Si (0.5% max), Fe (0.5% max) and Cr (0.1%) [32]. The T3 designation means that the alloy is age-hardened, solution treated, naturally aged and cold-worked. AA2024-T3 can be used in structural components because of its good damage tolerance. AA7075-T6 has zinc as its main alloying element (5.1-6.1%), but also contains Mg (2.1-2.9%), Cu (1.2-2%), Si (max 0.4%), Fe (max. 0.5%), Mn (max 0.3%), Cr (0.18-0.28%) and Ti (max. 0.2%) [33]. The T6 designation means that it is solution heat treated and artificially aged. The weight of alloying elements in AA7075 (87.1 - 91.4 wt% Al) is higher compared to AA2024 (90.7 - 94.7 wt% Al) [34].

During the production of AA2024, particles known as intermetallic phase constituents or intermetallic particles (IMs) can form. These have a different composition than the matrix as they have a locally increased concentration of the alloying elements and can be seen as an alloy within the alloy. The size of these may vary from 0.5 - 500 µm [31]. While there are many different exact compositions, for this study the IMs of AA2024 have been divided into four macro-families following previous works [35]:

1. Al-Cu, the θ-phase
2. Al-Cu-Mg, the S-phase
3. Al-Cu-Fe-Mn phase
4. Al-Cu-Fe-Mn-Si phase

While copper as an alloying element increases properties such as strength and hardness, it reduces the

corrosion resistance of the material. In addition, due to the heterogeneous nature of AA2024 surface, it is susceptible to local corrosion, as the differing composition of the IM particles can lead to local galvanic couples. Except for the S-phase, which starts out anodic, these particles have a cathodic nature with respect to the Al matrix. The corrosion of AA2024 generally starts with a de-alloying of the anodic S-phase, turning it cathodic. This process can occur within the first minutes upon immersion [36]. After this phase, the trenching of various IMs starts. After prolonged exposure the trenching of the other IMs also starts. During this process, local physical (e.g. by pitting/trenching) and chemical (e.g. pH change, release of ions) changes take place [35].

Under normal environmental conditions, aluminum forms an Al_2O_3 layer, passivating the material and providing corrosion protection. This layer may be a combination of aluminum oxide and aluminum hydroxide ($Al(OH)_3$), which can form when it comes in contact with water. This layer may vary in thickness based on the composition of the substrate [37]. In addition, it was found for an AlCu alloy that the oxide layer also contained copper(I)oxide and that the oxide layer was thinner on the IM particles, meaning that this layer is physically and chemically inhomogeneous [38]. This layer becomes unstable in the presence of Cl^-, leading to dissolution of the oxide layer and ending the corrosion protection [39]. It is expected that the diatom cells will interact with these processes, which may influence their behavior or metabolism. Additionally, it might also be that the diatoms have an effect on the corrosion process (MIC).

1.3. Research objective and research questions

This thesis aims to combine the research field of material science with microbiology to investigate diatom-produced coatings on aluminum substrates by studying their surface interaction. This interaction was investigated by studying biofilm formation behavior and motility behavior. This leads to the following two research questions:

RQ1. *In what way does the aluminum alloy composition affect the biofilm formation by* Cylindrotheca fusiformis*?*

To answer this question, the biofilm formation of the diatoms was studied in relation to the three different factors: surface chemistry, surface preparation and growth medium.

RQ2. *Do the local composition variations in aluminum alloys affect the motility behavior of* Cylindrotheca fusiformis*?*

The diatoms' motility behavior was assessed in relation to three factors: surface chemistry, surface preparation and immersion time.

In addition to answering these questions, a key part of the project was to establish quantitative protocols for this study. Therefore a considerable part of this thesis comprises of the development of these methods.

1.4. Thesis structure

Chapter 2 contains the information on the culturing conditions of the diatoms, and the various materials and methods used during experimentation. In Chapter 3, the results of the various experiments are displayed and discussed. Chapter 3 is concluded with a general discussion about the interaction of the diatoms with the aluminum substrates. Conclusions and recommendations can be found in Chapter 4 and Chapter 5 respectively. Any supplementary information can be found in the Appendices.

2

Materials & Methods

This chapter contains the materials and methods used in the various experiments, as well as information on the basic maintenance of the diatoms. Section 2.1 and Section 2.2 contain information and techniques to work with diatom cultures. Section 2.3 discusses the setups for the growth curve. Section 2.4 contains the setup for the biofilm formation experiments. Section 2.5, Section 2.6 and Section 2.7 describe the setup and methods used for the motility experiments.

2.1. Species selection & culturing conditions

The species *Cylindrotheca fusiformis* was selected based on an initial pilot experiment on biofilm formation performed at the Royal Netherlands Institute for Sea Research (NIOZ) [16]. *Cylindrotheca fusiformis* cultures were kindly provided by NIOZ. They were cultured in a *Binder KBW 240 groeikast* (incubator) set to 15°C and 60% fan power. The cultures were kept in 25 cm^2 or 75 cm^2 polystyrene *Advanced TC ™ cell culture flasks* with filter caps to allow for gas exchange. The cultures were subjected to a 16h/8h light/dark cycle under *Osram TLD* (color: 965) lighting. They were cultured in a Mix Si medium, which is based on a combination of the f/2 medium and Adapted Enriched Artificial Seawater with added Si, also kindly provided by NIOZ [40]–[44].

As individual cultures follow a growth curve as in Figure 1.3, the cultures can be sustained through a procedure called *transferring*, in which a small amount of diatom culture is transferred to new medium. This is performed in the sterile field created by a flame to minimize the risk of contamination. A new sterile flask is filled with ±10mL of medium for the 25 cm^2 or ±20mL for the 75 cm^2 flasks, subsequently 1-5 mL of diatom culture is added. These cells form the basis for a new culture and can start growing again. *Cylindrotheca fusiformis* cultures were transferred every two weeks to sustain them. However, during the motility experiment, the cultures were transferred every week to keep them in the exponential growth phase.

2.2. Liquid sample processing

To create insight into the properties of the liquid cultures, the chlorophyll-a (chl-a) and TEP concentrations were determined. Aliquots or culture samples were always obtained using sterile equipment and working next to a flame unless otherwise mentioned. Solutions made with water were all made with type II water. The results for the liquid sample processing techniques can be found in Appendix D.

2.2.1. Chlorophyll-a (chl-a) concentration measurements

Chl-a is the green pigment in plants and some microorganisms such has diatoms responsible for their autothropic nature leading to photosynthesis. In addition, it may be used to estimate the biomass of phytoplankton in a liquid sample by measuring the autofluorescence. Chl-a molecules can be excited by 431 nm light (visible spectrum, violet), after which 671 nm light (visible spectrum, red) is emitted, which can be measured using a spectrophotometer. A spectrum of chl-a in acetone (extraction buffer) can be found in Section D.1. The method described here is based on [45]. Important to note is that during processing, samples should be kept in low light and cold conditions as much as possible to prevent premature breakdown of the chl-a. This can be achieved by working in dimmed lighting and limiting the time the samples are at room temperature. In addition, amino acids from human skin may break down chl-a, so it is advised to work with gloves and tweezers.

From the culture, a 1 mL aliquot was filtered over a *GF/F (Whatman ±0.7 μm) filter* placed on a glass Buchner funnel, using the filter setup as in Figure 2.1. The setup used a pressure regulator to ensure that the vacuum does not exceed -0.2 bar. The filter was then carefully removed from the funnel and stored in a scintillation vial, after which 20 mL of 90% acetone solution (from *Acetone ≥99.9%, ChromasolV®Plus*, Sigma Aldrich) was added as an extraction buffer. This was then left in the fridge (4°C) for at least 4 hours to extract the organic material from the filter. Once completed, the vials were sonicated in an ultrasonic ice bath for 2 minutes to loosen any leftover organic material from the filter. Subsequently, the acetone solution was poured in a centrifuge tube and centrifuged for 10 minutes at 1000 x g to separate any filter solids. The supernatant of the samples was collected for measurement. When it was not possible to do the extraction, the filters were stored in the freezer (-21°C) for later use. The 90% acetone solution should be stored in a 4°C fridge when not in use.

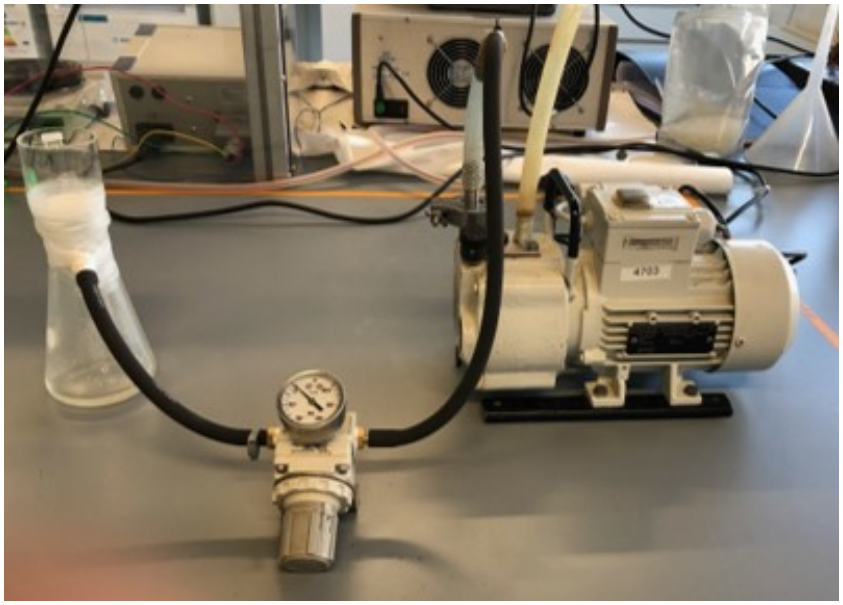

Figure 2.1: Filter setup used for the filtering of TEP and chl-a; left the glass filter, right is the vacuum pump with a pressure regulator in between

Chl-a cannot be measured directly due to other pigments creating a fluorescence signal at the same wavelength, therefore, two measurements are required. The supernatant was placed in the *Quartz Suprasil High Precision Cell (light path 10 mm, Hellma Analystics)* cuvette and measured on the *Jasco J815 spectropolarimeter* (kindly facilitated by TU Delft's Faculty of Applied Sciences) at the excitation wavelength of 431 nm. After which a couple of drops of 10% HCl were added to the sample. This causes the chl-a to be broken down into its degradation products (pheophytin-a), which do not give a signal at the same wavelength. The sample was then measured again, and the difference in the signal can be linked to the chl-a concentration. The relationship is defined by Equation 2.1, in which $chla$ is the concentration chl-a in the sample [µg/L], R_b and R_a are the emission intensity signals measured before and after adding the HCl respectively [V], $V_{extraction}$ is the volume of the acetone extraction

buffer [mL] (20 mL), V_{sample} is the volume of the filtered sample [mL], d is the dilution (=1, in case no dilution is used) and *C* is a constant determined by the analyzing a standard concentration series.

$$chla = (R_b - R_a) \cdot \frac{V_{extraction}}{V_{sample}} \cdot d \cdot C \tag{2.1}$$

The standard concentration series was made by preparing 90% acetone samples with a known chl-a concentration and measuring these on the spectrophotometer. C was then determined using Equation 2.2, in which $chla_{st}$ is the concentration of the standard sample [µg/L], R_b and R_a are the signals measured before and after adding the HCl respectively. The $\frac{chla_{st}}{R_b}$ and $\frac{R_a}{R_b}$ ratios should be relatively constant. The average of the values found in the standard series is used in Equation 2.2, which results in a value for constant C.

$$C = \left(\frac{chla_{st}}{R_b}\right)_{av} \cdot \frac{1}{\left(1 - \left(\frac{R_a}{R_b}\right)_{av}\right)} \tag{2.2}$$

The chl-a standard samples were prepared using chl-a from *Anacystis nidulans* (*C6144-1MG, Sigma Aldrich*) and from *Acetone ≥99.9%, ChromasolV®Plus (Sigma Aldrich)*. 1 mg of chl-a powder is slowly dissolved in 100 mL 90% acetone, to create a solution of 10 mg/L. This solution was divided in aliquots for ease of use and stored in darkened containers at -21 °C.

The concentration of the standard was verified using absorbance spectroscopy. The standard was measured in a *Quartz Suprasil High Precision Cell (light path 10 mm, Hellma Analystics)* cuvette on the *Perkin Elmer Lambda 35* spectrophotometer at a wavelength of 662 nm. Subsequently, the concentration of the standard was calculated using the Lambert-Beer equation (see Equation 2.3), in which E is the measured absorption, ϵ is the specific absorption of chl-a (87.62 L/g cm), c is the concentration of chl-a [g/L] and l is the path length in the cuvette [cm].

$$E = \epsilon \cdot c \cdot l \rightarrow c = \frac{E}{\epsilon \cdot l} \tag{2.3}$$

2.2.2. Transparent Exopolymer Particle (TEP) concentration measurements

TEP can be quantified based on a method from [46], [47], by measuring absorbance at 787 nm using UV/vis spectroscopy. The TEP was first made visible by adding Alcian Blue (AB) solution to the aliquot. The AB binds to -COOH and -O-SO_3 groups and stains the acidic polysaccharides. The AB solution was prepared by measuring 100 mL distilled water and adding drops of *Acetic acid 99-100% (Sigma Aldrich)* until a pH of 2.5 was reached. A magnetic stirrer was added to the beaker to ensure proper mixing of the water and acetic acid. After acidification, 40 mg of AB was added to the acidified water and gently shaken to dissolve. To ensure a homogeneous solution, the AB solution was filtered over a *PES 0.2 µm syringe filter* and stored in a new container. The AB solution has to be stored at 4°C and can used for around a month, after which a new solution needs to be made because AB slowly precipitates.

A 1 mL aliquot was taken from the culture to extract the TEP from. Subsequently, 0.5 mL of the AB solution was added to this sample. The sample was gently inverted a couple of times to ensure that a homogeneous solution was formed. This solution was filtered over a *0.4 µm Nuclepore PC* filter placed over a glass Buchner funnel using the filter setup as in Figure 2.1. The vacuum should not exceed -0.2 bar, as this could cause the TEP to be sucked through the filter. This filter was then extracted using tweezers and placed in a scintillation vial.

Extraction was done by adding 6 mL of 80% sulfuric acid (from *Sulfuric adic, ACS reagent 95-98%, Sigma Aldrich*) to the filter and leaving it for a minimum of 2h and a maximum of 20h. During this

time, the vials were gently shaken 3-5 times to remove small bubbles. A ”blank” filter which was only exposed to 1 mL of distilled water and 0.5 mL AB solution was also prepared to serve as a reference sample. After extraction, the sulfuric acid was placed in *Quartz Suprasil High Precision Cell (light path 10 mm, Hellma Analytics)*. Subsequently, the absorbance at 787 nm was measured using a *Perkin Elmer Lambda 35* spectrophotometer. The sulfuric acid sample from the blank sample served as the reference fluid. Similar to chl-a filters, the TEP filters can be stored in the freezer (-21°C) to be measured at a later time before adding the extraction buffer.

In order to translate the absorbance value to a TEP concentration, a calibration curve is required. This curve was generated using a Xanthan Gum (XG) solution (from *Xanthan Gum from Xanthomonas campestris G1253, Sigma*) as a TEP equivalent. The XG solution was made by adding 7.5 mg of Xanthan Gum to 100 mL of distilled water, creating a solution of 75 mg/L. Subsequently, this was used to prepare samples as in Table 2.1. These samples were then processed in the same way as other liquid samples for TEP measurements. This calibration curve resulted in a relation between the TEP concentration and the absorbance value which differs for each AB solution. Based on this relation, the concentrations of unknown samples can be calculated. A calibration curve can be found in Section D.2.

Table 2.1: Preparation and final concentration of TEP calibration samples

XG solution [mL]	Distilled water [mL]	Sample concentration [mg/L]
0.000	1.000	*0.000 (blank)*
0.125	0.875	*9.370*
0.250	0.750	*18.75*
0.500	0.500	*37.50*
0.750	0.250	*56.25*
1.000	0.000	*75.00*

2.3. Generating growth curves for *Cylindrotheca fusiformis*

A growth curve was made to serve as a guide for determining the growth phase of cultures based on their cell concentration. The growth curves were generated from three individual cultures of 75 mL, all kept under the aforementioned culturing conditions. Daily counts were taken using optical microscopy, and two daily 1 mL samples were taken to measure the chl-a and TEP concentrations. The cultures were inoculated at a relatively low concentration of 1.0×10^4 cells/mL to ensure a complete growth curve.

Cell counting was done manually by means of a *Sedgewick Rafter counting chamber*, which is a microscope slide with a grid and a chamber that holds exactly 1 mL (see Figure 2.2). To ensure that the concentration obtained using this method is reliable, several counting rules were set up. These counting rules were also followed for any subsequent counts unless otherwise mentioned:

1. The cultures were homogenized by gently swirling them before taking an aliquot for counting
2. The entire counting chamber was visually checked under low magnification to ensure that the cells are homogeneously distributed
3. A minimum of 10 squares or 100 cells was counted (see Figure 2.3)
4. Cells on the border of a square are only counted if they are more than halfway inside the square
5. Cells were counted from images, as shown in Figure 2.3

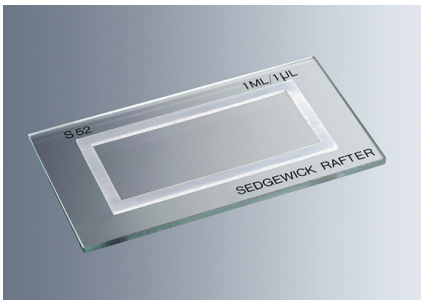

(a) A Sedgewick Rafter counting chamber

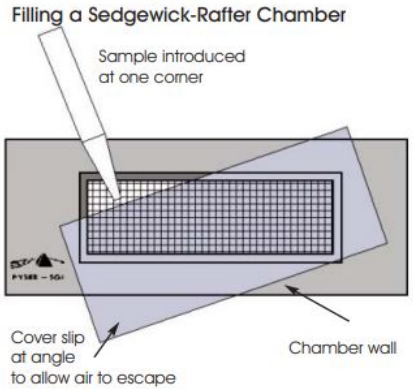

(b) Filling procedure; the volume of the sample is 1mL

Figure 2.2: The Sedgewick Rafter counting chamber [48]

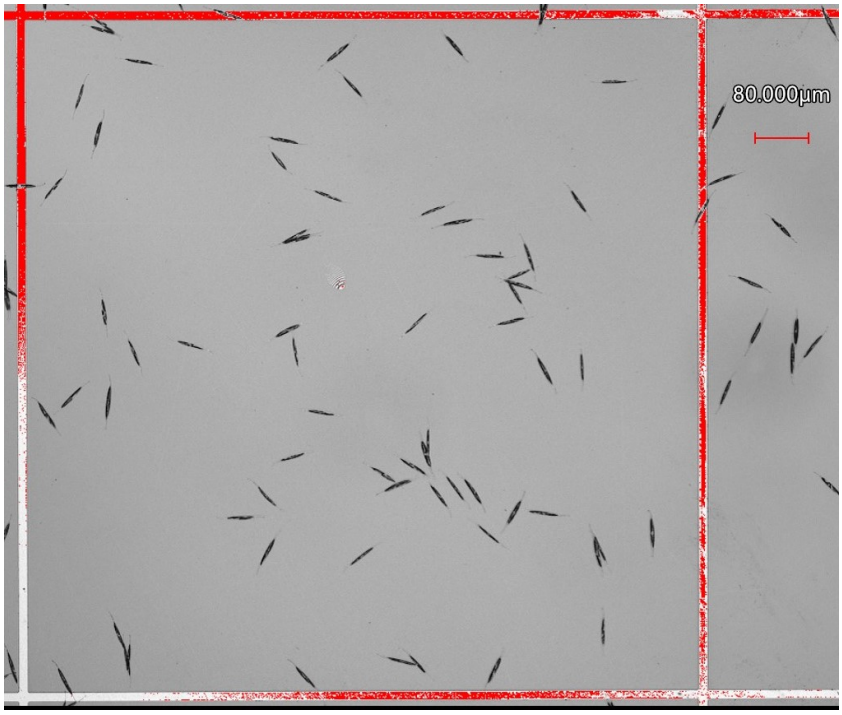

Figure 2.3: Example of a counting square under the *Keyence Laser Scanning Confocal microscope* in laser mode (mag: 10x)

2.4. Biofilm formation

2.4.1. Biofilm formation on various materials

Metal sheets of 20x20 mm^2 of Al99.5, AA2024-T3 and AA7075-T6 were immersed in 100 mL medium with 10 mL of diatom culture for 14 days. In this case samples were not pre-treated other than being cut to the right dimensions and degreased with ethanol. This experiment was used to found out if *Cylindrotheca fusiformis* would form films on different aluminum alloys. In this case all samples were kept together in the same beaker, but they were not in physical contact with each other.

After a 14 day immersion, the plates were taken out carefully and imaged using the *Keyence Wide-Area 3D Measurement System Controller, VR-5000*. Images were taken in ”wet” condition, immediately after removal from the liquid and ”dry” condition, after the samples were placed in a desiccator for 24h.

After imaging the ”wet” and ”dry” conditions, the biofilm was removed gently using a wet tissue to reveal the underlying layer attached to the metal surface, which was both imaged using the *Keyence Wide-Area 3D Measurement System Controller, VR-5000* and the *Keyence Laser Scanning Confocal microscope*.

Fourier-transform infrared spectroscopy (FTIR)

FTIR was used to chemically characterize the biofilms before and after the removal of the biofilm. The analysis was performed using a *Perkin Elmer Spectrum 100 FT-IR Spectrometer*, setting the spectrum from wavenumbers 4000-650 cm^{-1}. Before each measurement, a background spectrum was taken to account for the background signal caused by the IR crystal. The samples were screwed as tight as possible onto the diamond/ZnSe crystal to ensure good contact.

2.4.2. Biofilm formation in various media

Another biofilm experiment was set-up to investigate the influence of the medium on the substrate surface and biofilm. Four samples of *AA2024-T3 by Kaiser Aluminum* (*ASN-A3010, thickness 2mm*) were cut into 3mmx3mm samples. The samples were wet grinded on a turntable using SiC grit paper in the following order: P320 (46.2 µm grit size), P800 (21.8 µm), P2000 (10.3 µm), P4000 (5 µm). After grinding, the samples were cleaned using ethanol to remove any metal shavings or other contamination. Subsequently, the samples were dry polished for 2 minutes at 250 rpm using a water-based diamond paste to obtain 3 µm and finally 1 µm roughness. Between each polishing, the sample was cleaned using ethanol to remove the excess diamond paste. After polishing, the samples were cleaned in an ultrasonic bath filled with ethanol for 2 minutes and dried with compressed air.

Next, the samples were each submerged in different solutions in separate beakers for 14 days, see Table 2.2. It should be noted that either filtered natural seawater (NSW) or Adapted Enriched Artificial Seawater (ESAW) is present in all solutions. After 14 day immersion, the plates were imaged using the *Keyence Wide-Area 3D Measurement System Controller, VR-5000* in ”wet” conditions.

Table 2.2: Starting conditions for the biofilm formation experiment in various media

Sample	Solution	Cell concentration [cells/mL]
1	NSW	-
2	Mix Si medium	-
3	Mix Si medium + diatoms	2.15×10^4
4	NSW + diatoms	2.21×10^4

2.5. Setting up the motility study

In preparation of the motility study, several tests were set up to find the right experimental conditions. Three different variables were selected to vary: immersion time, material and topology. The specific experimental conditions for these can be found in Table 2.3. The measuring times are the times after immersion when the motility was monitored. The roughness is the finest grain used for grinding/polishing. The volume is the volume of cell suspension to which the aluminum substrates were exposed. Table 2.3 shows two cell concentrations: mother-line concentration and cell suspension concentration. The mother-line is the culture from which this cell suspension was made. The cell suspension is the suspension to which the aluminum substrates were exposed. Note that the concentration of the cell suspensions used in the motility experiments is considerably lower than the concentration used for the biofilm formation experiments. In addition to these parameters, factors such as settling time, volume, cell suspension concentration and imaging technique were also explored.

Table 2.3: Experimental conditions for the various motility trials

Effect of:	Measuring times [h]	Material	Roughness [µm]	Volume [mL]	Conc. cell suspension [x10^4cells/mL]	Conc. mother-line [x10^5cells/mL]
Immersion time	1; 4; 21; 24; 28; 96	Al99.5	1	2	4.65	6.90
Material	0	Al99.5; AA2024; AA7075	1	1	3.35	5.03
Topology	0	Al99.5	10; 82; 200	0	2.28	9.10

2.5.1. *In-situ* motility monitoring

The aluminum samples were placed in a custom made 3D printed cell, which has a circular hole with a diameter of 20 mm, leading to 314.2 mm^2 exposed area (see Figure 2.4b). This cell was placed under a *Dino-Lite High Magnification* (AM7515MT4A) digital microscope as in Figure 2.4a. All experiments were performed on a pneumatically stabilized table to minimize disturbance by vibrations. In addition, the setup was shielded from light coming from any other sources than the microscope using curtains.

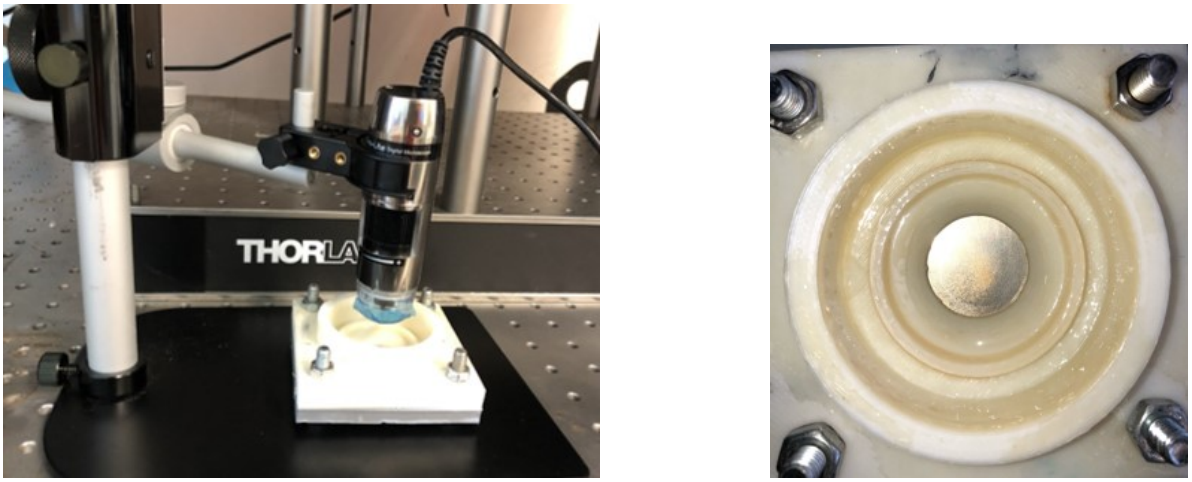

(a) Setup of the cell and the digital microscope

(b) Top view of the cell

Figure 2.4: The experimental setup for monitoring diatom motility

It was found that the action of moving the sample from the incubator to the measurement setup caused flows within the suspension. Leading to cells being re-suspended in the liquid, rather than attach and glide over the substrate. Therefore, after the measurement cell had been placed under the microscope and focused on the substrate, the setup was left to settle for 30 minutes before starting the measurement. Motility was observed using the DinoCapture software for a duration of 10 minutes with a frame rate of 10 seconds.

2.5.2. Quantifying general cell motility

As a measure for general cell motility, an analysis method previously used to monitor corrosion was used, adapted from [49]. The protocol consists of various macros in ImageJ. The first step converts all images in the stack to gray-scale (”*8 bit*”) and performs a recursive repositioning through planar rigid body rotation and translation. The coordinates are mapped according to Equation 2.4, in which the first

image in the stack serves as a reference for all other images.

$$x, y = \{\{cos\theta, -sin\theta\}, \{sin\theta, cos\theta\}\} \cdot \mathbf{u} + \Delta\mathbf{u} \tag{2.4}$$

The next step calculates the ”difference” between two subsequent images by subtracting the pixel intensities from each other, see Equation 2.5. This generated a ”difference” figure in which the unchanged pixels were black (0) and changed pixels were lighter, subsequently, the black pixels were taken as background by setting a lower threshold (minimal change). Choosing the correct lower threshold allowed for filtering out the noise, in this case the threshold was set to 20. By subtracting the background, an image was generated in which the changed pixels were black.

$$i_{difference}(x, y) = |i_{n-1}(x, y) - i_n(x, y)| \tag{2.5}$$

For the next step, the Look-Up Table (LUT) was inverted so that the background was black and the changed pixels were white. From this image, it was possible to extract the affected area (AA, see Equation 2.6). N is the number of changed pixels, while N_{total} is the total number of pixels. An example of an AA graph based on the pixel variation between frames can be seen in Figure 2.5. In this research the affected area was used as a quantification for movement.

$$AA = \frac{N(t)}{N_{total}} \cdot 100\% \tag{2.6}$$

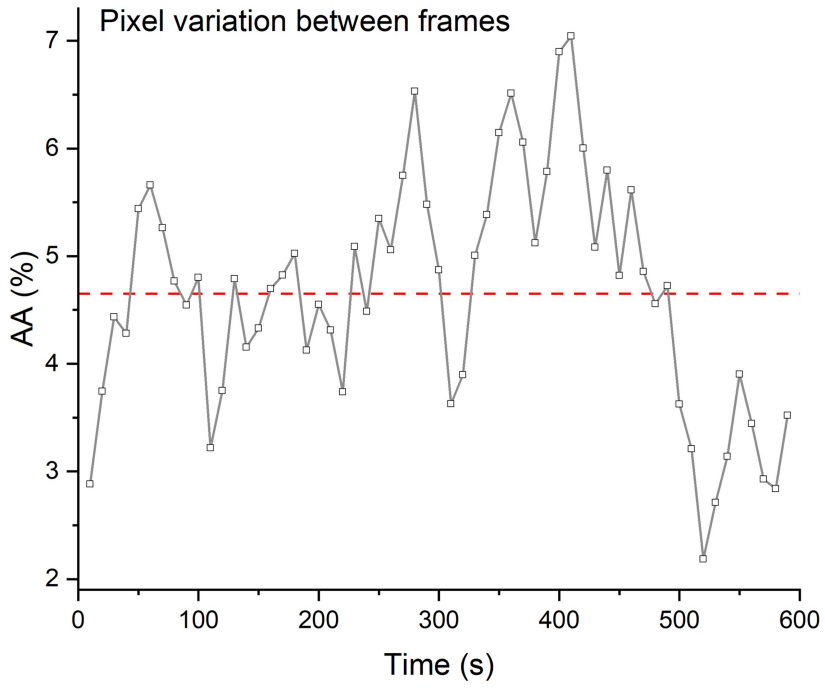

Figure 2.5: An example of the percentage of affected area over 600 seconds with a measurement rate of 10s; the red line is the average

Finally, the degree of change was also visualized by implementing a color-gradient (Fire-LUT). In this color plot the unchanged pixels are white and the changed pixels are colored, in which a darker color signifies a larger pixel change. This also allows to distinguish whether a registered movement is caused by cell motility on the surface or other causes such as cells floating in the medium. The final outcome of the software is visually represented in Figure 2.6.

Figure 2.6: Frame from the image sequence produced by the general motility software; left shows the original picture in gray scale; the middle shows the changed pixels with respect to the previous image; the right shows the changed pixels with the color applied, a darker color implies a greater intensity change

2.5.3. Quantifying individual cell motility

In addition to general motility, the motility of single cells was also tracked using a plugin for ImageJ called ”*MTrackJ*”. This plugin allows to track individual cells and record various parameter such as their coordinates, velocity, distance traveled and pixel value. The plugin can also generate several views to illustrate the path traveled, which looks like Figure 2.7. This tool is used to analyze the tracks both quantitatively and qualitatively.

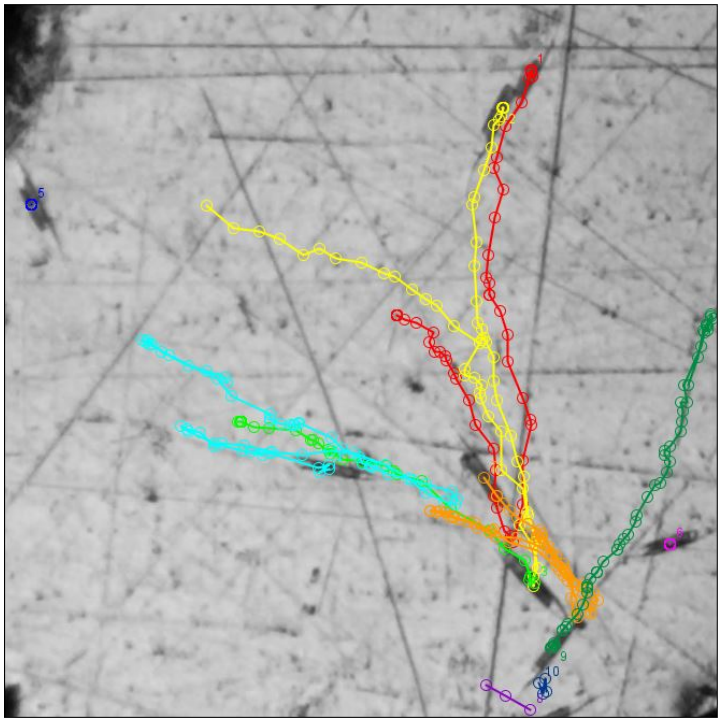

Figure 2.7: Image showing paths of several individual cells tracked using MTrackJ

2.6. Motility study on Al99.5 and AA2024-T3

The aim of this experiment was to investigate the potential influence the IMs and their varying composition have on diatom motility. To this aim a motility study on Al99.5 and AA2024 was designed. Prior to exposure to the diatom cells, a SEM/EDS mapping of the AA2024 samples and their intermetallics was performed. Next, the surface of the aluminum sample was exposed to 1 mL of cell suspension extracted from an exponential phase mother-line. The cells present in this suspension were monitored *in-situ* using the setup as in Figure 2.4. After 24h, the cell suspension was removed and the surfaces of the samples were analyzed using a AB stain and Raman spectroscopy. From the initial experiments as described in Section 2.5, the parameters were set to 24h monitoring, exposure to 1 mL cell suspension with a concentration between $2.0x10^4$ - $3.0x10^4$ cells/mL and polishing the surface to 1µm to ensure data quality.

The experiment was done in linear triplicates for each material, designated as A, B and C. All samples were exposed to the cell suspension for 24h, however, the times at which their motility was monitored, differed per sample. A schematic of the timeline can be seen in Figure 2.8. The samples can be identified based on a combination of a letter and number, e.g. B-99.5 which indicates the Al99.5 sample B that was measured at 1h, 16h and 20h after immersion.

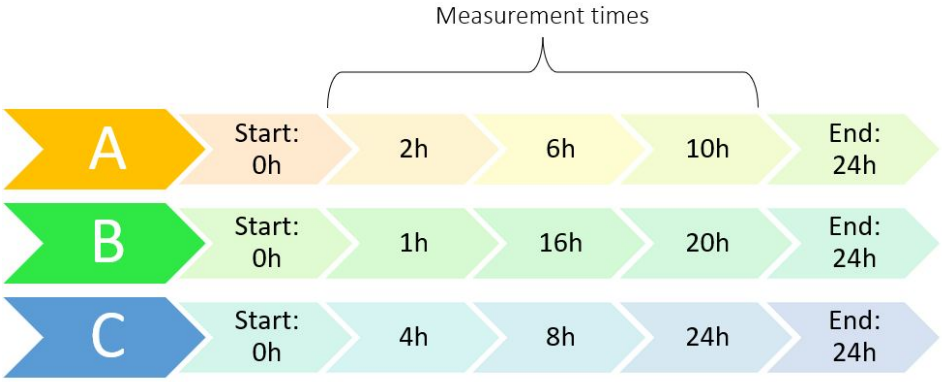

Figure 2.8: Schematic overview of the timeline for the motility study

2.6.1. Material preparation

The material samples used in for this study were made from a 2 mm thick sheet of commercial bare AA2024-T3 by Kaiser Aluminum (ASN-A3010) and a 1.5 mm thick sheet of Al99.5 from Salomon's Metalen B.V. The samples were cut to a size of 30x30 mm^2 and grinded and polished as in subsection 2.4.2. The samples were kept in a desiccator for the time between the preparation of the samples and time they were used for the motility study (1-2 weeks).

With the current setup as in Figure 2.4, it was not possible to monitor the entire exposed surface, so a region of interest (ROI) was defined. The ROI was marked to be easily identified using a micro-indenter to create a minimalist pattern. The markers were made using a *CSM micro-scratch tester* in indentation mode using a Berkovich diamond tip with the settings as in Table 2.4. The pattern is an asymmetrical pattern to ensure that the right orientation is used when matching the SEM images with the images taken with the digital microscope. The indents were placed at a spacing of 0.3 mm, meaning that a rectangle of 0.09 mm^2 is created, which is referred to as the region of interest (ROI), see Figure 2.9. It should be noted that due to the inaccuracy of the machine, the indents are not exactly 0.3 mm apart. To account for this, the exact distance between all indents was measured during the imaging on the SEM. The region of interest has to be circled using a permanent marker to shorten the process of locating the indents under the SEM. This circle is later removed using ethanol, to prevent interference with the diatoms' motility.

Table 2.4: Settings for the CSM micro-scratch tester for indentation

Loading type [-]	Linear
Acquisition rate [Hz]	10
Maximum load [mN]	1000
Loading rate [mN/min]	2000
Unloading rate [mN/min]	2000

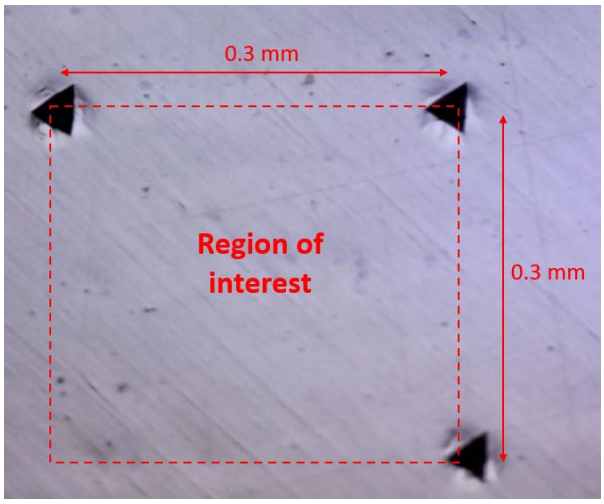

Figure 2.9: Indents marking the ROI on an AA2024 sample

2.6.2. Intermetallics localization and identification

The SEM/EDS imaging and IM identification in the ROI was done using a *JEOL JSM-840-EDS*. To obtain the desired resolution, the images are taken at magnification 500x, which means that the ROI was mapped in six individual images, which were later stitched together. The images were taken in SEM backscattered electron (SEM-BSE) mode with the following settings: 15 keV, 10 µA, compo, RBEI, LM. This mode causes areas with different compositions to show up in different shades of gray. Between images, the settings should not be changed and the emission current should be stable to ensure good quality images. The horizontal steps were 0.120 µm and the vertical steps were 0.100 µm, this ensures enough overlap for Adobe Photoshop to stitch the images together.

The IMs were visually identified based on a color difference, subsequently, the EDS spectra of the IMs were obtained using point analysis. These spectra were used to classify the different IMs according to their composition. As identification of the IMs is a time consuming process, only the compositions of the largest IMs were analyzed.

2.6.3. Image analysis

The six individual SEM images of the AA2024 samples were stitched together using ”*photomerge*” in ”*reposition*” mode in Adobe Photoshop, resulting in an image of the region of interest, see Figure 2.10. The merged SEM-BSE image was then overlaid on the optical image collected with the DinoCapture during immersion, using the ”*free transform*” and ”*warping*” options in Adobe Photoshop to transform the SEM-BSE image.

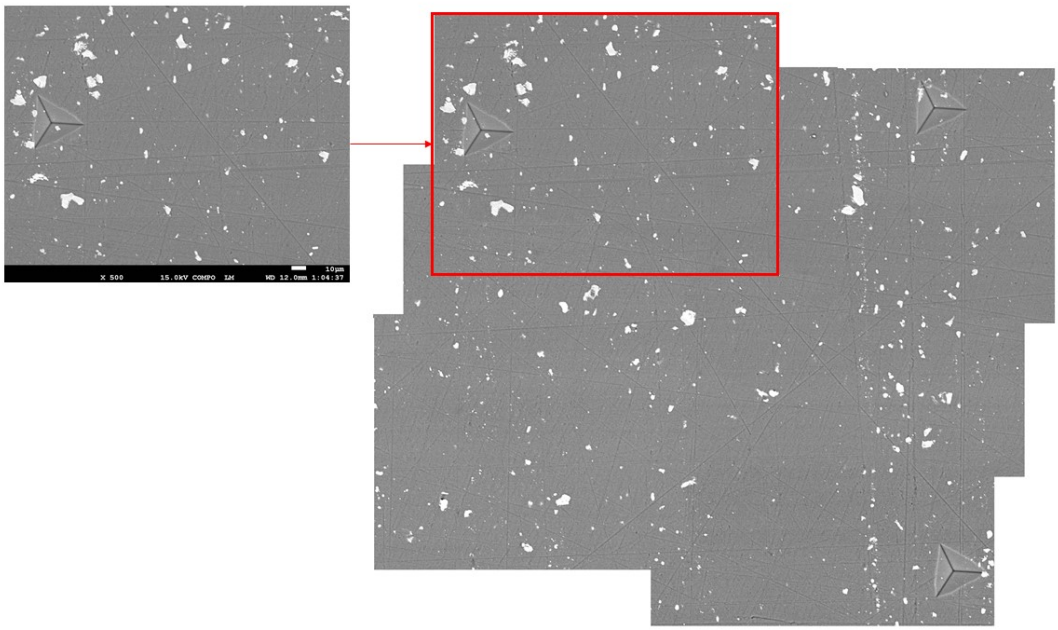

Figure 2.10: The stitching procedure for the SEM-BSE images; left: a single SEM-BSE figure. Right: region of interest stitched together using 6 individual SEM-BSE images (mag 500x)

Subsequently, this warped image was imported into ImageJ to generate a mask. The image was first converted to gray-scale (*8-bit*). Because of the clear contrast between the IMs and the matrix, it was possible to generate a mask using the "*Threshold*" option. The threshold was adjusted until all intermetallics are black and the matrix is white, see Figure 2.11a. To exclude extremely small particles and find the coordinates of the IMs, the "*analyze particles*" function was used with the settings as in Figure 2.11b. In addition, the plugin "*nnd*" (Nearest Neighbor Distances) was applied to find the inter-particle distance. The generated mask of the ROI was then imported back into Adobe Photoshop and adjusted to generate an image as in Figure 2.12, where the IMs are overlaid on the optical image taken during immersion.

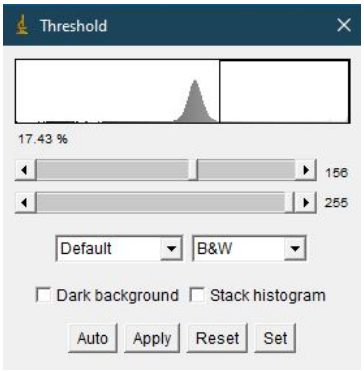

(a) Thresholding in ImageJ

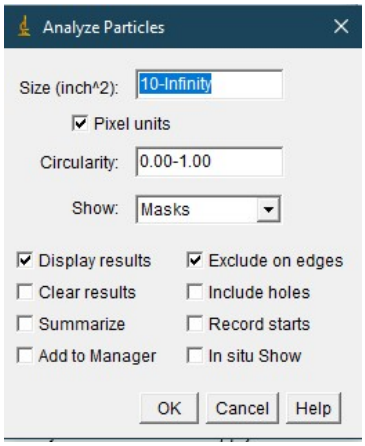

(b) Settings for "*analyze particles*" in ImageJ

Figure 2.11: Settings for particle analysis in ImageJ

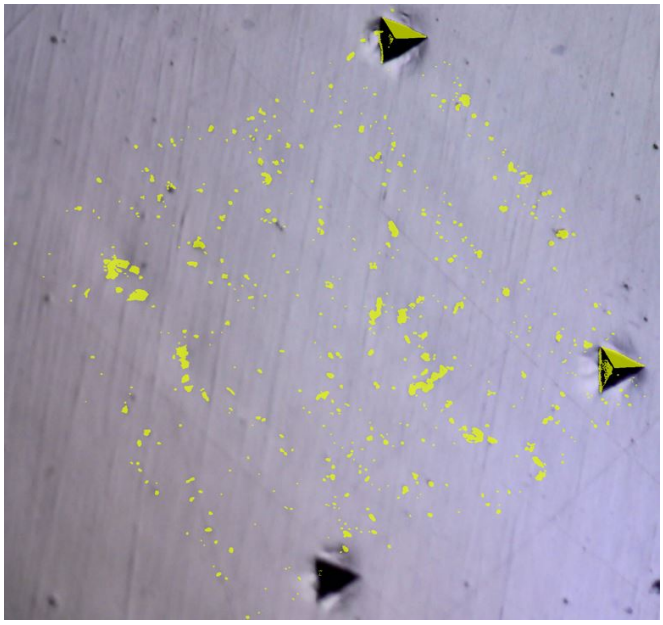

Figure 2.12: The optical image overlaid with the mask generated from the SEM-BSE images

2.6.4. UV treatment

During SEM analysis, a carbon build-up may occur on the target surface. UV/Ozone treatment is a technique that removes organic contamination by causing chain scissions by UV light and simultaneously causing decomposition by generating ozone gas and reactive atomic oxygen [50]. Therefore, after the SEM/EDS procedure, the samples were exposed to a 10 minute UV/ozone treatment to remove any carbon build-up that may have occurred. The UV light was generated using three 30 Watt UV-light tubes with the samples placed at a distance of 5 cm. Prior to treating the samples, the lamps were allowed to warm up for 10 minutes. An experiment was performed to verify the UV treatment, the results can be found in Section C.2.

2.6.5. Making of the cell suspension

The cell suspensions to which the aluminum plates were exposed in the motility study, were made from mother-line cultures in the exponential phase. Based on the results of the previously performed growth curve, this would be between $6.1x10^4$ and $6.7x10^5$ cells/mL for *Cylindrotheca fusiformis* under these conditions. To achieve a manageable number of cells in the ROI, the desired cell dilution was made to have a concentration between $2x10^4$ and $3x10^4$ cells/mL. Dilutions were made with medium to ensure an abundance of nutrients. Approximating the cells as boxes of 400 μm^2, 7.86 x 10^5 cells would be required to cover the whole surface in cells, however, this most likely not required to cover the whole substrate in EPS as the cells are motile. In case all cells in a 1 mL suspension with a $2.0x10^4$ - $3.0x10^4$ cells/mL sink to the substrate and are distributed homogeneously, this would lead to a cell density of 64-95 cells/mm^2 and around 6-9 cells in the ROI.

Due to logistical restrictions, a new cell suspension was made for each sample. A sample from the mother culture was taken and counted on the day the cell suspension was made to ensure that the cells were indeed in exponential phase and that the correct dilution for the cell suspension could be made. An aliquot of the made cell suspension was also counted to ensure the concentration of cells was indeed in the desired range. In addition, two 1 mL samples were taken from both the mother culture and the cell suspension to determine the chl-a and TEP concentrations. These samples were processed as described in subsection 2.2.1 and subsection 2.2.2 respectively.

2.6.6. *In-situ* motility monitoring

The same setup as described in subsection 2.5.1 was in the motility studies. Before exposing the aluminum samples to the diatom cell suspension, the substrates were degreased using ethanol, and subsequently rinsed with Mix Si medium to remove any residue ethanol. Once the metal plate was securely in place and the setup was tested for leaks, 1 mL of cell suspension was pipetted on top. All samples were exposed to the cell suspension for 24h, but measured at different exposure times. In between measurements, the setups were kept in the culturing incubator in a large plastic bag, to prevent CO_2 depletion, but to create a closed environment.

The samples were taken out of the incubator some time before the measurement to allow for settling time. Similar to Section 2.5, all measurements were preceded by a 30 minutes settling period. The digital microscope was set to darkfield mode to create the best contrast between the cells and the substrate. The imaging was done using the DinoCapture software, which was set to take an image every 10 seconds for 10 minutes. The lighting was kept constant during the measurement.

2.6.7. Processing of the samples post-mortem

In order to determine whether *Cylindrotheca fusiformis* leaves trails during motility, various methods were explored. After 24h exposure to the diatom cell suspension, the cells suspension was poured off the aluminum samples. Next the samples were rinsed gently 3x with distilled water, to remove any remaining medium or unattached cells as this may interfere with the trail detection.

Fluorescence microscopy

Fluorescence microscopy was performed using a *Nikon A1R laser-scanning confocal microscope*, with a *Nikon Plan Apo Lambda 20x/0.75NA* lens. The excitation laser has a wavelength of 488 nm and operated at 10% power. Furthermore, the fluorescence emission filter was set to 525/50 nm, the pinhole size to 1.5 AU and the photomultiplier gain to 90. All samples were gently rinsed and left in a desiccator to dry before imaging. Because the samples were not treated before imaging, the imaging relied on the principle of autofluorescence.

The samples that were imaged included the plates used in the motility study. For comparison, two additional conditions were added: a 5 day low concentration (LC, 2-3 x10 ^{4} cells/mL) 2 mL diatom cell suspension exposure and 5 day high concentration (HC, ±4x10^4 cells/mL) 2 mL diatom cell suspension exposure. All samples were rinsed with distilled water and dried in a desiccator before observation.

Raman spectroscopy

Raman spectra were obtained for the B and C samples used in the motility studies, using a *Renishaw inVia confocal Raman microscope* using the settings as in Table 2.5. The locations for the spectra were selected and focused visually and subsequently measured using the mapping function. The spectra were compared to those of plates exposed to 24h medium exposure and no exposure to any solution.

Table 2.5: Settings for obtaining the Raman spectra for aluminum samples

Range [cm^{-1}]	400-4000
Exposure time [s]	300
Laser [nm]	532
Laser power [%]	1
Accumulations [-]	2

Staining followed by optical microscopy

Two different stains were used: *Stains-All* (Sigma-Aldrich) and Alcian Blue. The various trials done with Stains-All did not yield any interpretable results, therefore the method and results can be found in Section B.3.

The AB solution was prepared as in subsection 2.2.2. After rinsing, the samples were fully immersed into a petridish filled with AB solution. After 30 minutes, the samples were again gently rinsed three times with distilled water to remove any residue of the AB solution. Subsequently, the plates were imaged using the *Keyence Wide-Area 3D Measurement System Controller, VR-5000*.

2.7. Direct motility comparison between Al99.5 and AA2024-T3

In order to eliminate biological variability between samples, an experiment was designed to directly compare the affinity of the diatoms to both substrates. A sample was especially designed in which both samples could be exposed to the same diatom cell suspension, see Figure 2.13.

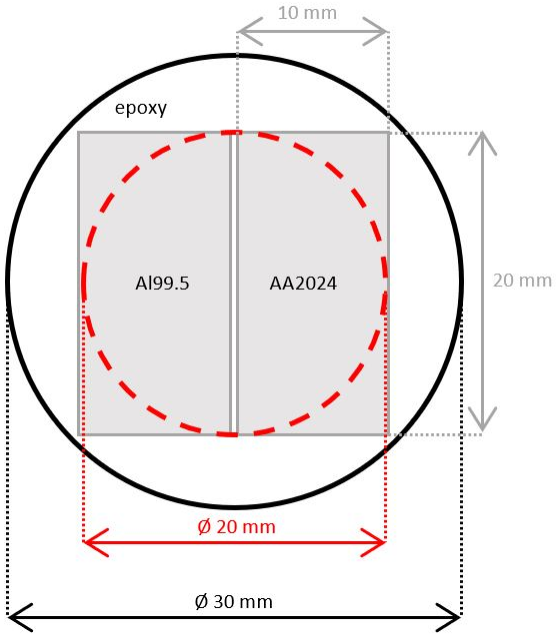

Figure 2.13: Sample design for a direct comparison between Al99.5 and AA2024, the red circle indicates the area that will be exposed to the diatoms

2.7.1. Sample preparation

From the same plates as used for the motility study, pieces of 10 mm x 20 mm were cut. These were embedded in an epoxy resin, by placing them in the molding cup and pouring the resin on top. The resin made used was *EpoFix Resin* and *EpoFix Hardener*, which was prepared by mixing 35 g resin with 4.2 g hardener. The samples poured in the *Struers CitoVac* vacuum impregnation unit for 45 min to remove any bubbles. After degassing the plates were positioned in the still liquid resin using a needle. Subsequently, the samples were left to cure overnight (min. 10h).

The samples were removed and automatically polished rather than manually polished which was done for the motility study. This was more practical considering the geometry of the sample. The final of level of polishing was the same for as in the motility study (1 µm). The automatic polishing was done using the *Struers Tegramin-20* polishing machine on the following program: P180, 20s; P320, 1 min;

P1000, 1 min, P2000, 1 min; P4000, 1 min; 3 µm DiaPro polishing, 4 min; 1 µm DiaPro polishing, 3 min. Between grinding steps, the samples were cleaned using water, and between the polishing steps, the samples were cleaned using water, soap and ethanol. In order to fit in the observation cell, the sample was cut down to a ±3 mm thickness using the *Struers Secetom 10* precision cutting machine. Similar to the samples in the motility study, the samples were cleaned 2 min in an ultrasonic ethanol bath and exposed to the same UV treatment as in subsection 2.6.4. To ensure that the samples were level in the observation cell, a small amount of mounting clay was placed underneath the epoxy disk and was pressed to be level.

2.7.2. *In-situ* motility monitoring

Two experiments were setup, one with the same conditions as the motility experiment and one trial with a higher cell concentration to monitor preference on a larger scale. The setup was the same as for the motility study, using the *Dino-Lite High Magnification* (AM7515MT4A) digital microscope, using a cell suspension with a concentration of 2.98 $x10^4$ cells/mL obtained from a mother-line in the exponential phase (1.53$x10^5$ cells/mL), 1 mL cell suspension and allowing for 30 minutes settling time before measuring. The motility was observed at 0h, 2h, 6h and 24h. Because of the high magnification required to monitor motility, the Al99.5 and AA2024 sides of the sample were monitored in turn, rather than simultaneously. The high concentration trial was done in a similar way, but with 1 mL cell suspension with a concentration of 7.24 x 10^5 cells/mL, which was only observed at 0h.

3

Results & Discussion

In this chapter, the growth curves are discussed in Section 3.1. Next the biofilm formation and motility study experiments are analyzed in Section 3.2 and Section 3.3, Section 3.4 and Section 3.5 respectively. The chapter is concluded with a general discussion based on all obtained results in Section 3.6.

3.1. Growth curves

A growth curve allows for identification of the different growth phases. This curve allows selection of aliquots from a certain growth phase e.g. the exponential phase, based on the cell concentration. The growth curve was generated by taking daily aliquots and counting them using optical microscopy. The growth curve of *Cylindrotheca fusiformis* can be found in Figure 3.1. From this figure, the different growth phases were determined based on growth rate. This is important for future experiments, as cells from different growth phases may show different behavior.

The exponential growth phase was determined by plotting the growth curves on a logarithmic scale and identifying the linear region. It was found to be between 6.1 x 10^4 cells/mL and 6.7 x 10^5 cells/mL based on the average of the three cultures. For the motility study it was decided to use cultures in the exponential growth phase. When these cultures were prepared, the cultures were inoculated at a concentration aimed in the early exponential phase and left for 24h at least to accumulate to the new circumstances.

Section D.1 contains the growth curve compared to the chl-a concentration. These curves should look very similar, as chl-a concentration may be used as an alternative method of determining the biomass. In addition, Appendix E contains the growth curve for alternative species *Chaetoceros calcitrans*.

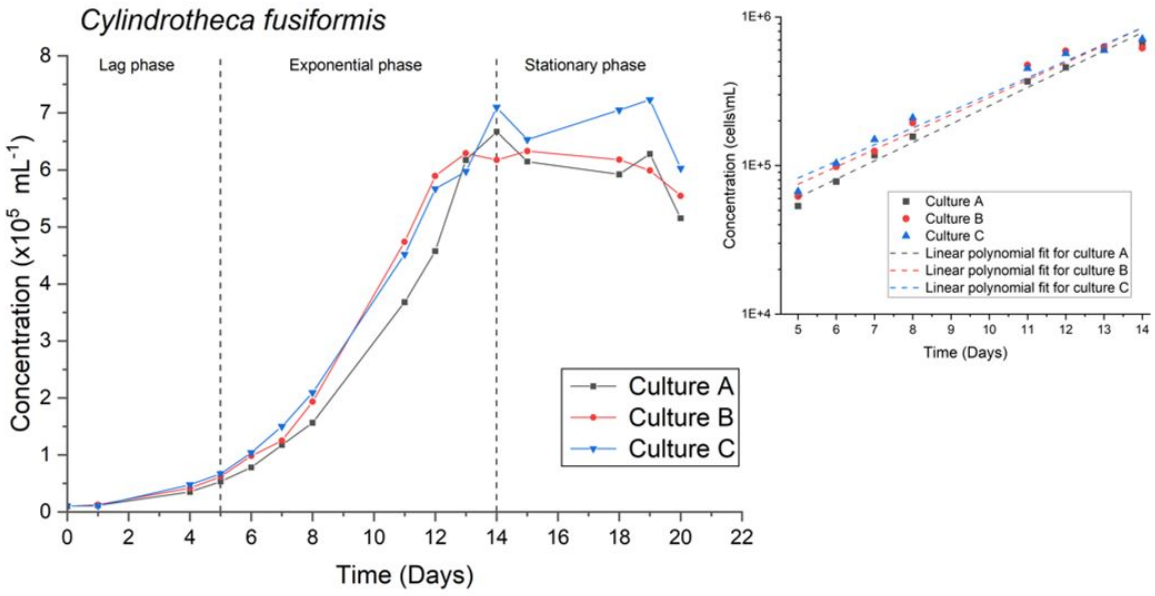

Figure 3.1: Growth curve of *Cylindrotheca fusiformis* under culturing conditions

3.2. Biofilm formation

Several biofilm formation experiments were done to observe *Cylindrotheca fusiformis'* biofilm forming capabilities under different circumstances.

3.2.1. Influence of alloy composition

As can be seen from the top row in Figure 3.2, biofilms formed on all three alloys. The top row shows the substrate immediately after removal from the diatom culture (”wet”), the middle row shows them after they have been left to dry in a desiccator overnight (”dry”), and the bottom row shows the substrates after the top layer was carefully removed using a wet tissue.

There appear to be precipitates, which are expected to have formed from components from the medium reacting with the metal at those locations. This reaction appears on the edges for Al99.5 and AA7075, but is located on the surface of AA2024. These precipitates have been marked with cyan rectangles in Figure 3.2. Another interesting observation is that the corrosion appears to be considerably less than what would be expected of aluminum alloys 2024 and 7075 in a saline solution exposed for 14 days. An example of a polished AA2024 surface exposed to a 0.05M NaCl solution for 14 days can be seen in Figure 3.10.

The biofilms have a different appearance on each of of the alloys, but upon first glance, the biofilm seemed to have formed most uniformly on AA7075. This is somewhat unexpected as AA7075 has multiple alloying elements (8.6-12.9 wt%, [33]) and has a chemically inhomogeneous surface. It might be expected that the most (chemically) uniform surface (Al99.5) leads to the most homogeneous biofilm formation. After the removal of the top layer of the biofilm, a remaining EPS layer appears to cover the whole substrate for AA7075 homogeneously. While there are several uncovered spots appear on the Al99.5 sample. Interestingly, some of these spots seem to coincide with darker spots on the biofilm itself, which could suggest that the cells were still trying to cover the entire substrate but were unable to form an EPS layer there. Several of these spots are marked with red circles in Figure 3.2.

The AA2024 sample shows some discoloration, however, it is unclear whether this is caused by a difference in the EPS layer or by corrosion of the underlying substrate. Two of these areas of dis-

coloration are indicated with dark blue ovals in Figure 3.2. This could be indicative of a difference in EPS composition or amount or perhaps a reaction with the material. This would be consistent with a biofilm study for *Cylindrotheca fusiformis* on PVDF, polyethylene plastic, polypropylene fabric and plain drawing paper [23]. The authors found that the biofilm EPS (bEPS) was different in amount as well as composition for the different polymeric substrates with lower elemental differences than the alloys studied here. The difference in appearance of the biofilms and EPS layers means that the biofilm formation is influenced by the substrate, this could be caused by composition differences. It should be noted that it cannot be ruled out that the difference in appearance of the EPS layers is caused by the wiping.

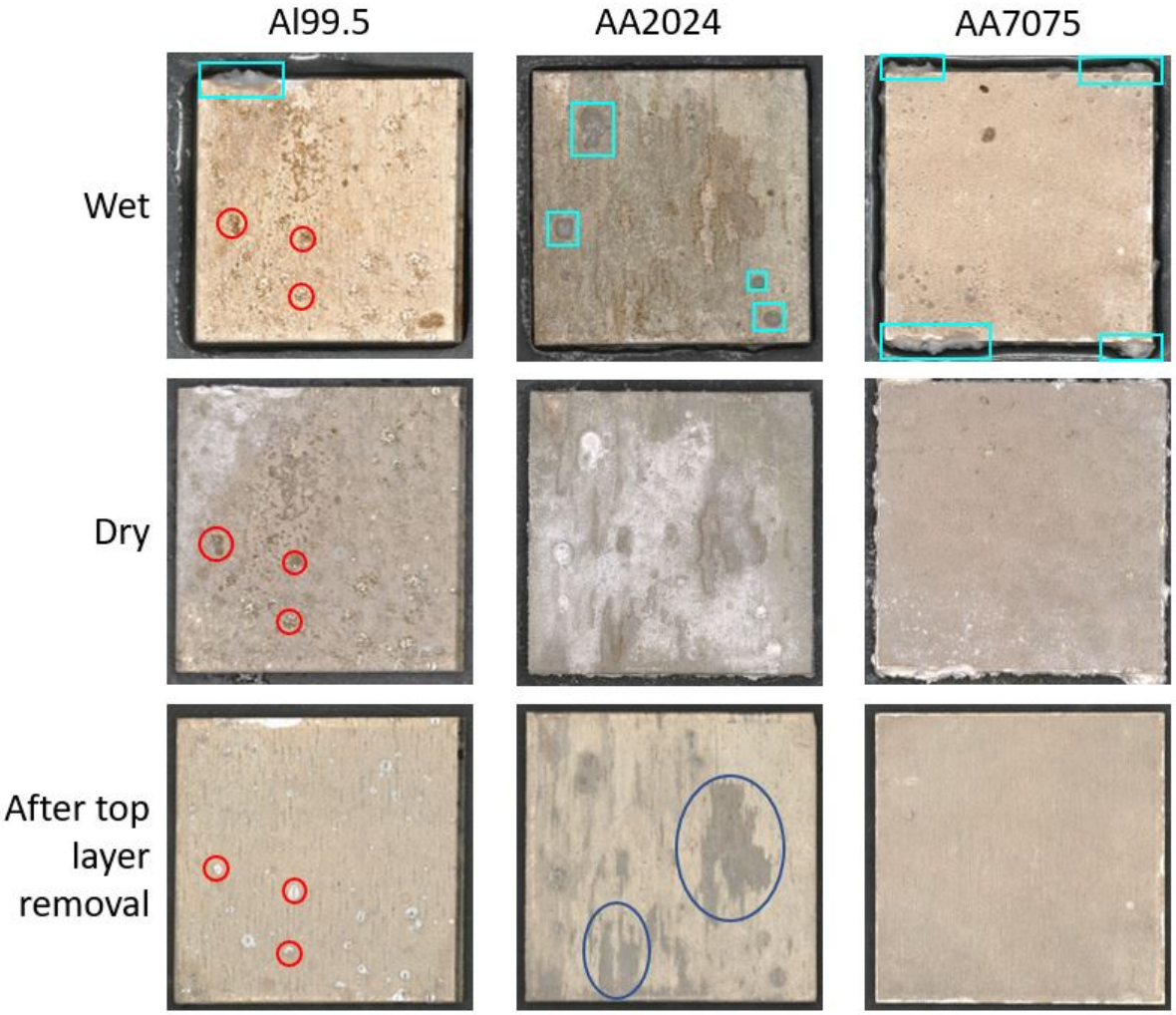

Figure 3.2: Biofilm formation on degreased only Al99.5, AA2024-T3 and AA7075-T6 after a 14 day immersion in a diatom culture; the top row shows the samples immediately after they have been removed from the culture, the middle row shows the samples after they have been dried, the bottom row shows the samples after the top layer of biofilm has been gently removed using a wet tissue; the read areas indicate the inhomogeneity on the Al99.5 substrate; the cyan rectangles indicate the locations of the precipitates; the dark blue ovals indicate the regions of discoloration on AA2024

The surfaces were also observed on the microscopic scale, see Figure 3.3. Interestingly, it shows that the coverage of the AA7075 sample is not as homogeneous as it appears on macroscale as there are clear color differences. This could mean these areas are not covered with EPS or that the EPS has a different composition in these areas. The covered areas on the Al99.5 appear to be homogeneous, save for the spots where there appear to be no coverage. The AA2024 sample also shows a clear color difference in the micrograph. This may again be caused by a difference in composition or amount of EPS. Additionally, the EPS layers were observed using SEM, the results can be seen in subsection B.2.1.

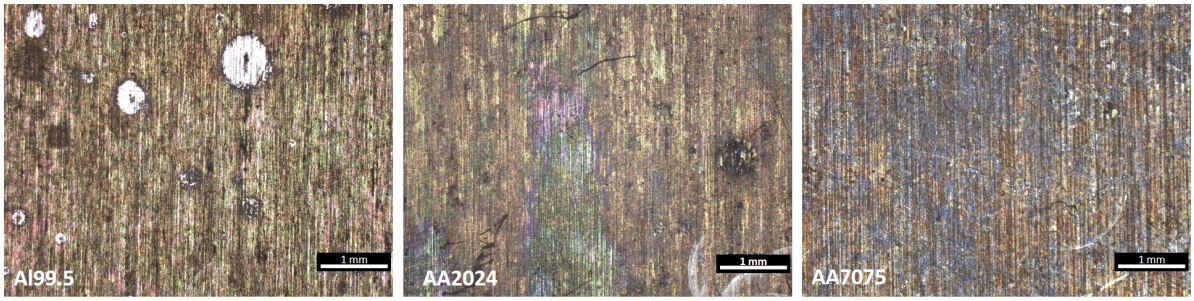

Figure 3.3: The EPS layer as observed by the *Keyence Laser Scanning Confocal microscope* (mag: 2.5x); from left to right Al99.5, AA2024 and AA7075

In conclusion, *Cylindrotheca fusiformis* was able to form covering biofilms on all the alloys. In addition, an EPS layer appeared to have formed on all alloys. This is a promising result from a coating perspective, as a relatively uniform adhesive coating is already formed without further optimization. This is consistent with earlier biofilm tests performed at NIOZ with *Cylindrotheca fusiformis* biofilms on PMMA and titanium plates (unpublished results, [16]). In this case the biofilm was removed straight after being taken out of the liquid culture using a toothbrush and it was observed that it was impossible to remove all organic material using this method.

Fourier-transform infrared spectroscopy (FTIR) on biofilms

FTIR was performed on the biofilms to see whether it was possible to detect them and if so, if it could reveal something about the composition. Measurements on the bare substrates and of the liquid medium were also performed and can be found in section B.1. The spectra for the biofilms on the various substrates can be found in Figure 3.5. Several peaks can be distinguished: (1) a broad peak centered around 3350 cm^{-1} ranging from 3650 cm^{-1}-2750 cm^{-1}, (2) a sharp peak at 1640 cm^{-1}, (3) a peak between 1510-1550 cm^{-1}, (4) a peak around 1430 cm^{-1} and finally (5) a sharp peak around 1100 cm^{-1}. The peaks discussed in this section were all absent on the FTIR spectra obtained for the metals, the spectra for the metals can be found in Figure B.2.

Peak (1) is identified as $\mathrm{O}-\mathrm{H}$ stretching, most likely caused by the $\mathrm{O}-\mathrm{H}$ bonds in polysaccharides in combination with water left in the biofilms [20]. Even though the biofilms are dried, there is likely still residual water present. The $\mathrm{N}-\mathrm{H}$ stretch is also located at 3500 cm^{-1}-3300 cm^{-1}, which may also contribute to peak (1) [51].

Peak (2) and peak (3) are indicative of proteins as they are located in the amide I and amide II/amide III bands respectively [20], [52]. The locations of these bands and the main vibrational modes of the peptide bond can be seen in Figure 3.4. FTIR analysis of the adhesive pads of the pennate marine diatom *Toxarium undulatum* revealed peaks at 1638 cm^{-1} and 1545 cm^{-1} [53], which could be consistent with what is observed here. The peak at 1638 cm^{-1} was identified to be from $\mathrm{C}=\mathrm{O}$ stretching in secondary amides (amide I). Alternatively, peak (2) is associated with imine $\mathrm{C}=\mathrm{N}$ stretching or alkene $\mathrm{C}=\mathrm{C}$ stretching [51]. Peak (2) is also observed in the spectrum of the liquid Mix Si medium (see Figure B.1), meaning it is not necessarily caused by proteins excreted by the diatoms. Peak (3) around 1545 cm^{-1} can be attributed to $\mathrm{C}-\mathrm{N}$ stretching and $\mathrm{N}-\mathrm{H}$ bending from amides (amide II) [53].

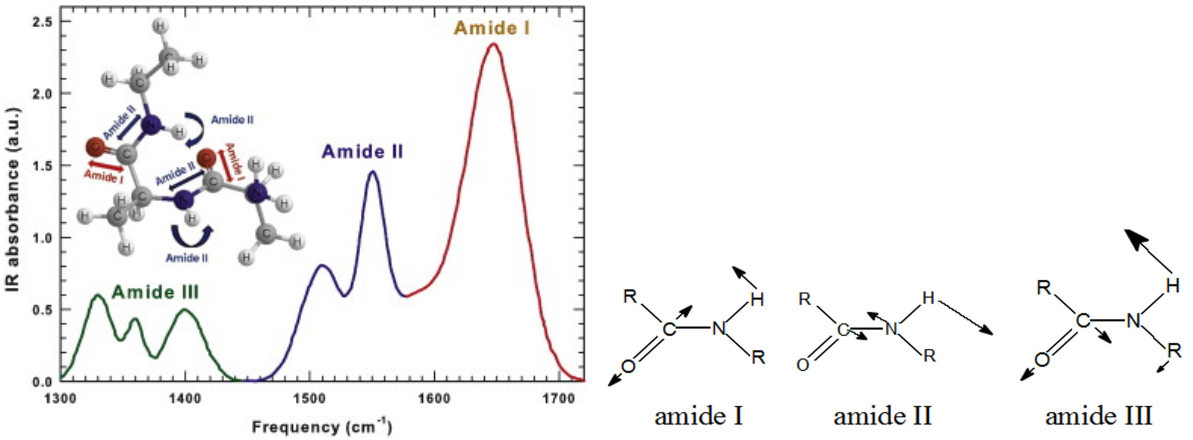

(a) The different amide regions in an FTIR spectrum [54]

(b) The main vibrational modes for amides; adapted from [55]

Figure 3.4: The FTIR vibrational modes and locations in the FTIR spectrum for amides

Peak (4) and peak (5) are located in the fingerprint (single bond) region, making it more challenging to identify them. Peak (4) is could caused by an amide III vibration. Peak (5) is could be caused by C—O vibrations, which are associated with carbohydrates [52]. In Figure 3.5 a substrate dependent difference is observed between peaks (3) and (4). The difference between these amide peak ratios could indicate a difference in the biofilm, and could be interesting to explore in future research.

The observations made here are consistent with literature, stating that diatom biofilm EPS mainly comprises of polysaccharides and proteins. It is also similar to a spectrum taken of a biofilm formed by *Cylindrotheca fusiformis* on polyvinylidene fluoride membrane (PVDF), see Figure 3.6 [20]. In which peak A at ±3300 cm^{-1} (peak (1) in Figure 3.5) is associated with O—H stretching in polysaccharides and peak B around ±1650-1640 cm^{-1} (peak (2) in Figure 3.5) is linked to C=O and C—N stretching in primary amides which indicate proteins.

FTIR was also tried on the EPS layers that remained after the top layer of the biofilm was removed with a wet tissue and also on samples that were exposed to a low concentration diatom culture (max. $3x10^4$ cells/mL) for 24h, but this did not produce usable results probably due to the detection limit of the machine. This led to exploring other techniques for detecting organic material: fluorescence microscopy, Raman spectroscopy and various stains, see subsection 3.4.3.

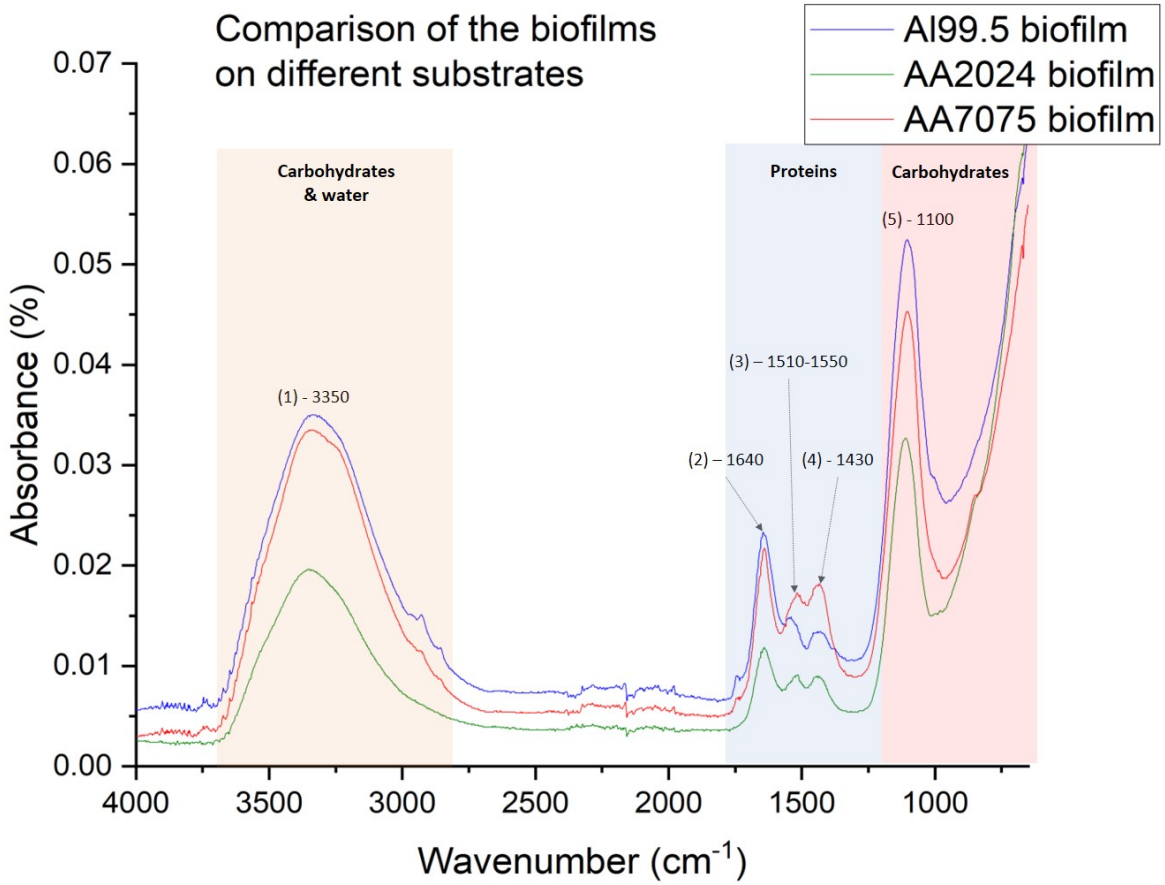

Figure 3.5: FTIR spectra of the dried biofilm on various aluminum alloys

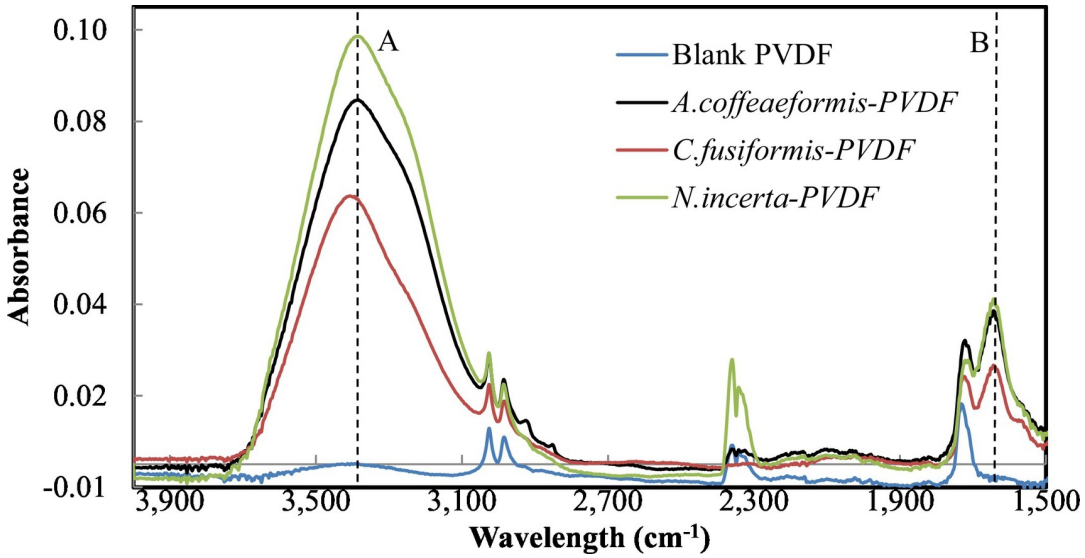

Figure 3.6: FTIR spectra of biofilms formed on PVDF by various diatom species; peak A being attributed to polysaccharides and peak B attributed to proteins [20]

3.2.2. Influence of the medium on the substrate

To investigate the protection potential and the white precipitation that were observed in the experiment in subsection 3.2.1, an experiment with natural seawater (NSW) and mix Si medium with and without diatoms was devised, the results of which can be found in Figure 3.7. Several observations can be made from this image. The first being that the white precipitation that was observed previously, is also present in the beaker with only medium and to a lesser extent in the one with only NSW, meaning that the precipitation does not require diatom cells. This white precipitation is not observed in the NSW or medium kept in storage conditions (glass or polystyrene flasks without metal in them), indicating that it is formed by a reaction between the medium and the metal.

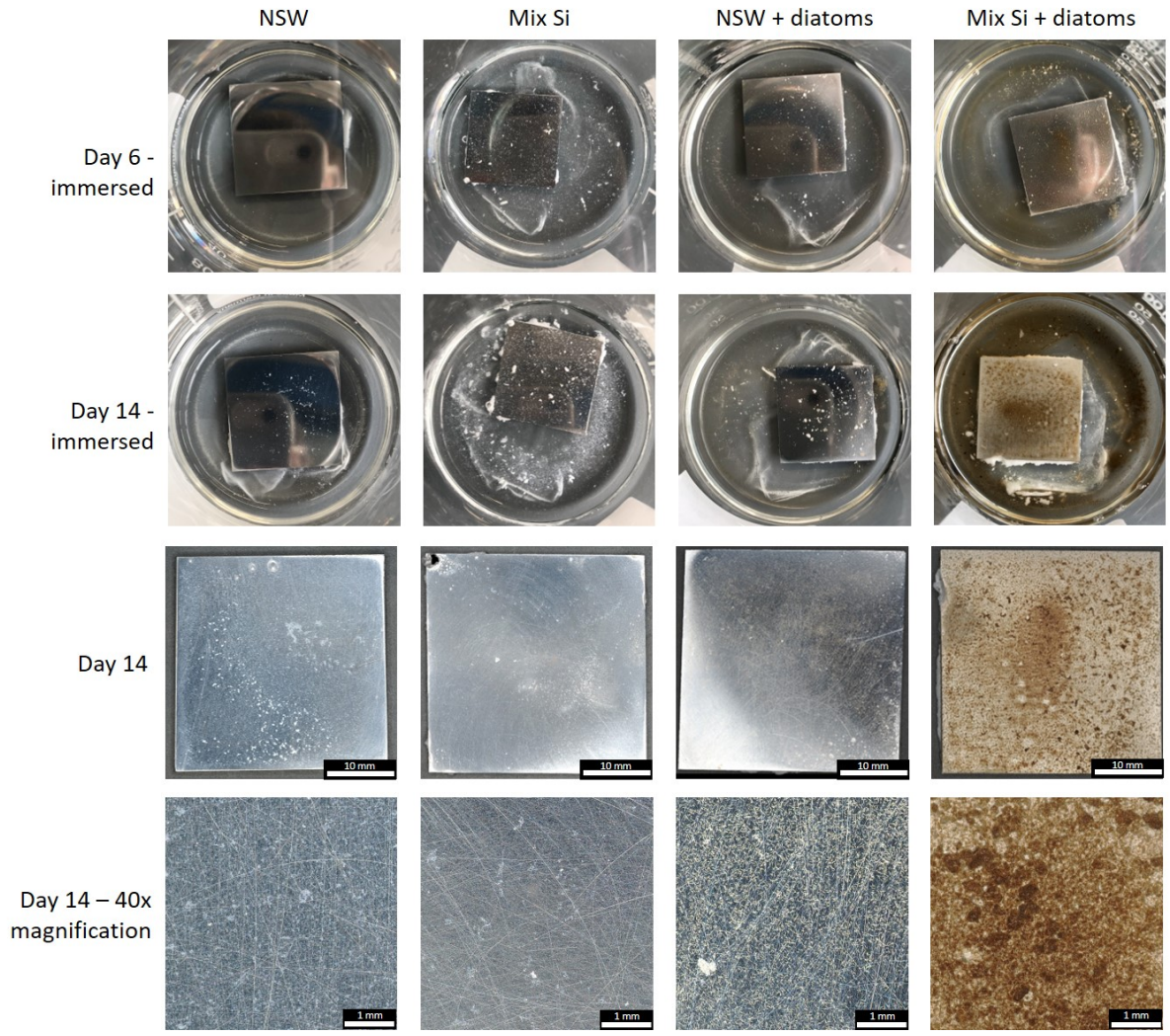

Figure 3.7: The results of AA2024 plates immersed in various media; the top row shows them after 6 days, the other rows show them after 14 days

Table 3.1: Concentrations of the cells suspensions used in the biofilm formation experiment, measured at the start of the experiment (day 0) and the end (day 14); it should be noted that the cell count was most likely underestimated, as the solutions were not homogenized before taking the counting samples

Sample	**Cell concentration day 0 [x10^4 cells/mL]**	**Cell concentration day 14 [x10^4 cells/mL]**
Medium + diatoms	2.15	23.2
NSW + diatoms	2.21	8.44

A second observation is that the biofilm forms best in an environment in which the diatoms grow

best, i.e. the mix Si medium. On the sample exposed to the NSW + diatoms, a very thin layer of cells has formed, suggesting that they started to colonize the surface, but simply did not have the resources to continue growing. This is consistent with the cell count that was performed on day 14, see Table 3.1. This clearly shows that the cells did grow in the NSW, but considerably less compared to the suspension with medium. This is also clearly visible in the bottom row of Figure 3.7 (the 40x magnification images). In the Mix Si medium, the diatoms were able to reproduce and produce sufficient EPS to form a covering thick biofilm. In the culture with diatoms and NSW, the individual cells seems to have attached to the substrate, but they were unable to form a thick biofilm. However, it is known that diatoms can create EPS under stressful conditions. So there may be a covering film on the plate immersed in the NSW + diatoms solution, but it may not be visible.

The difference is also clearly seen in the post-mortem SEM images. Figure 3.8 shows a network of cells that is linked together through EPSs. Figure 3.9 only shows single cells or small groups of cells which have settled on the surface surrounded by some EPS and meaning that the substrate was not fully covered in EPS. For more SEM images of these surfaces, see subsection B.2.3 and subsection B.2.4.

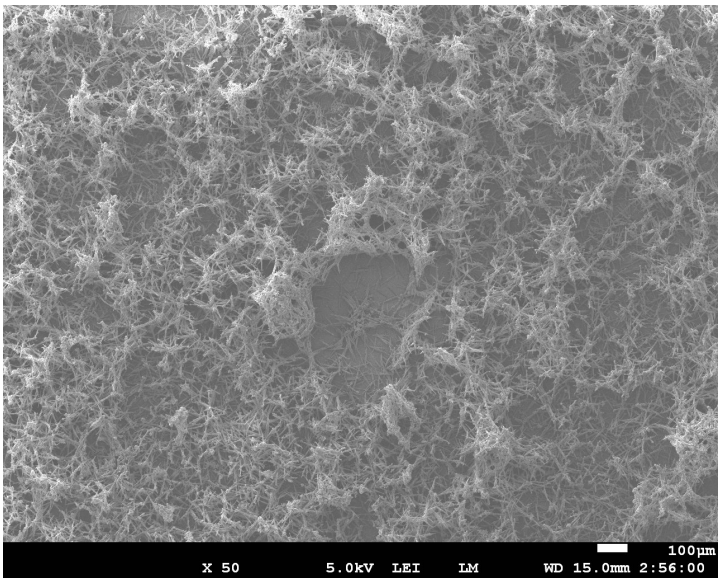

Figure 3.8: Biofilm on polished AA2024-T3 exposed to diatoms in medium for 14 days (mag:50x)

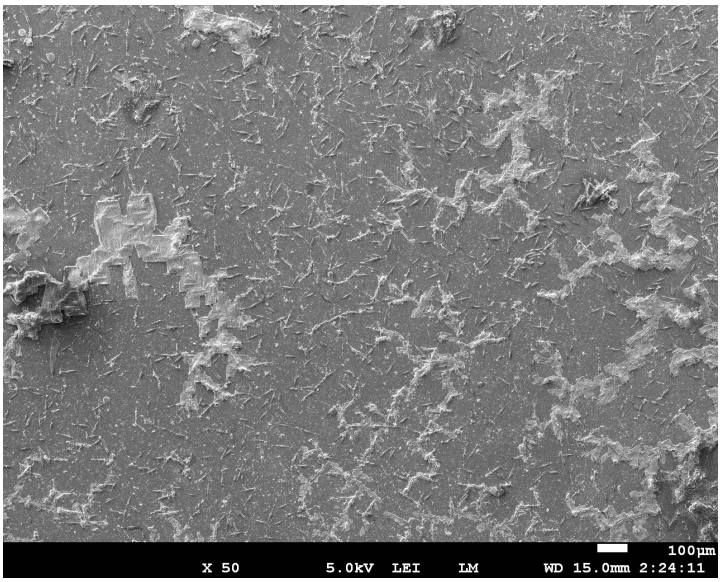

Figure 3.9: Biofilm on polished AA2024-T3 exposed to diatoms in NSW for 14 days (mag:50x)

Comparing the samples in Figure 3.7 with sample that has been exposed to a 0.05 molar NaCl solution (Figure 3.10), it can be clearly seen that corrosion is considerably more present in the latter. This would mean that some corrosion slowing/inhibiting mechanism is activated in the tested NSW and medium in spite of the higher salt concentration. The mix Si medium contains Adapted Enriched Artificial Seawater (ESAW) with a salinity of 3.55 %, which is similar to the NSW, which has an assumed salinity of 3.5%. This is corrosion behavior is contrary to what was expected, as generally salinity increases corrosion rates up until 3%, after which is gradually decreases again [56]. Both the NSW and the ESAW also contain other substances besides NaCl (e.g. phosphates), one of which may be responsible for the corrosion inhibition/protection. Independently of this, the diatoms did not increase corrosion.

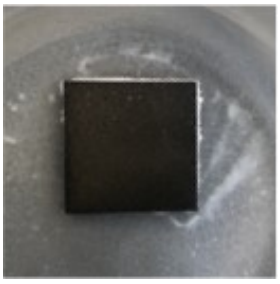

Figure 3.10: A sample of polished AA2024 exposed to a 0.05 molar NaCl solution for 14 days

3.3. Effect of immersion time, topology and metal surface composition on motility

In order to get an idea of diatom motility behavior, several experiments were set-up with a range of immersion times, materials and topologies. The results from these experiments formed the basis for the experimental setup for the later motility study in section 3.4.

3.3.1. Influence of immersion time on motility

The immersion time was tested using an Al99.5 sample to determine the time frame during which motility can be observed. The general motility results were analyzed using the ”overall motility” method from subsection 2.5.2. As can be seen from Figure 3.11, the average general motility increased for the first 28h. Somewhere between 24h and 96h, cell had stopped moving and any detected motility was caused by background noise. During this experiment, it was noted that the number of cells in the field of view could vary considerably. This could bias the results, as it stands to reason that more cells result in more general motility.

To compensate for this and to make the result more comparable, the average general motility was normalized with respect to the average number of cells in the frame. The average number of cells was computed by counting the number of cells in the field of view for one frame per minute (t=0 s, t=60 s, t=120 s etc.). This was averaged to get an estimate of the average number of cells present in the field of view during the experiment. For example, the 109 cells denoted for the 1h measurement in Figure 3.11, means that there were on average 109 cell in the field of view based on 10 out of the 60 frames.

The general motility as in Figure 3.11 was then divided by the average number of cells in the field of view for that measurement (i.e. the numbers in the bars in Figure 3.11), resulting in a motility % per cell, see Figure 3.12. The normalized result shows a similar trend to the non-normalized result as it also shows an increase in motility for the first 24h. Other than the non-normalized result, the normalized result shows a slight decrease at 28h. At 96h there was no motility the normalized result appears to be considerably higher than the non-normalized result. The relatively high normalized motility is caused by the background noise and the fact that there are few cells (33) in the frame, as no cell

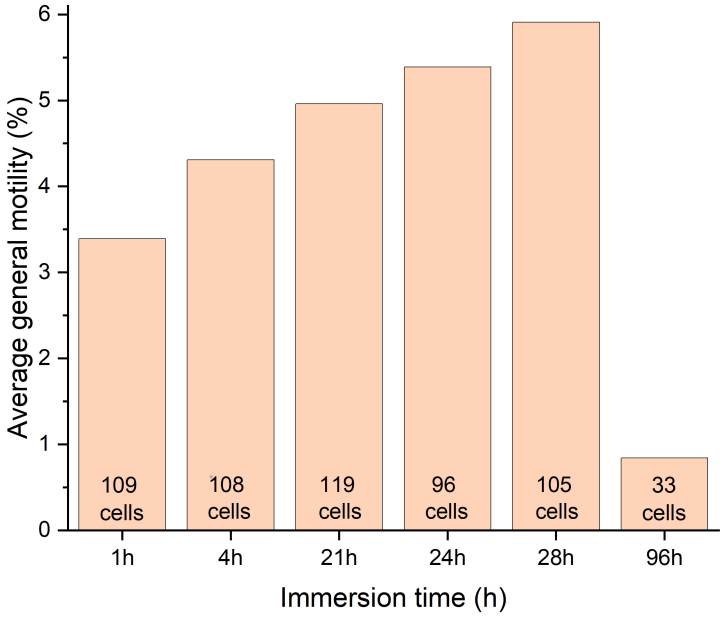

Figure 3.11: General motility as a function of immersion time on Al99.5; the numbers in the bars represent the average number of cell in the field of view for that measurement

motility was observed in the raw image data. Another observation was that at 96h, no film was formed and the cell suspension turned opaque white, suggesting that the cells were incapable of growing and most likely died or were dying. This may be caused by the relatively low concentration and low volume, as *Cylindrotheca fusiformis* was able to form a biofilm on Al99.5 during the biofilm experiment (subsection 3.2.1).

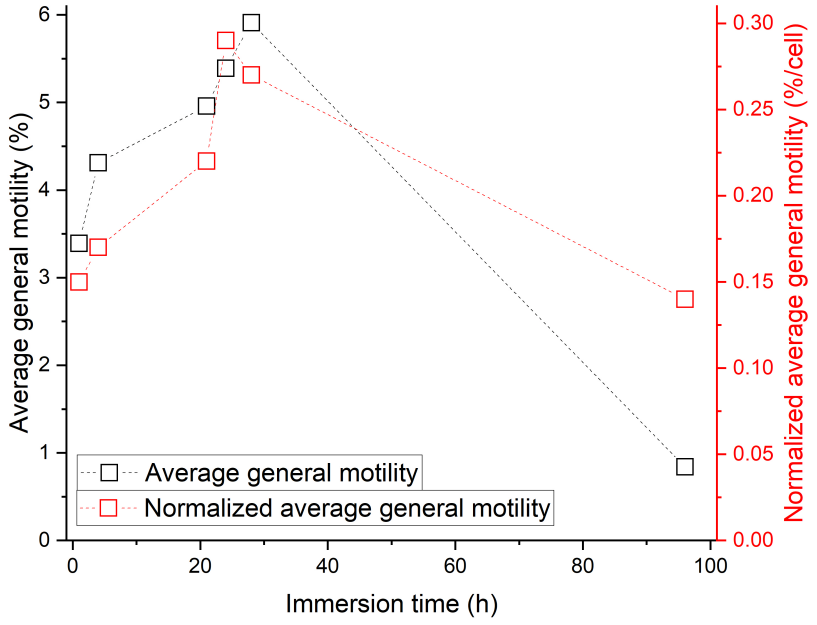

Figure 3.12: The average general motility and the normalized average general motility as a function of immersion time

The results from this experiment show that 24h is a reasonable time frame for motility observations. In addition, it was discovered that the cells are easily re-suspended into the liquid during logistical operations. Which led to a settling time of 30 minutes, before starting observation. This experiment was performed using 2 mL of cell suspension, however, this resulted in significant background movement caused by cells floating in the suspension, therefore it was decided to work with 1 mL in future.

3.3.2. Surface topology influence on motility

Similar to subsection 3.3.1, the general motility for different topologies for an Al99.5 substrate was also measured, of which the results can be found in Figure 3.13. Due to the roughness, the contrast between the cells and substrate was decreased, making it impossible to accurately count the number of cells present in the frame. However, it can be observed that the general motility is similar for the tested roughnesses, but that slightly more motility was observed on P180 which is in the same size range as the diatoms (±60-75 µm). Another observation is that the diatoms are able to move parallel and perpendicular to the grooves that were created during the grinding process, see Figure 3.14. It does appear as if the cells can get stuck in a groove, which can be seen in the blue track in Figure 3.14a, but the cell was able to maneauver itself out of the groove again, suggesting that the grooves are not insurmountable.

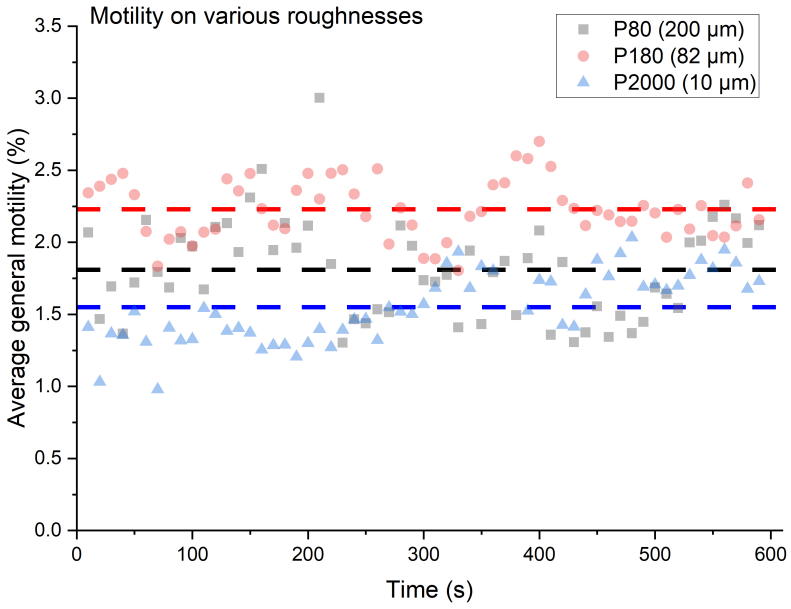

Figure 3.13: General motility on Al99.5 samples with variable roughnesses; P80, P180 and P2000 have microstructures of 200 µm, 82 µm, and 10 µm respectively; the dashes lines represent the averages; the immersion time was between 0h-1h; the samples were exposed to a cell suspension with a concentration of 2.28×10^4 cells/mL

While it can be concluded that *Cylindrotheca fusiformis* shows good motility on substrates with different roughnesses, it was decided that future testing would be done on polished samples (1 µm). This way the cells do not have to physically overcome the topology, as it is considerably smaller than the cell size (60-75 µm). This also yields the best quality data as there is a clear contrast between the cells and the substrate, making the individual tracking of the cells easier.

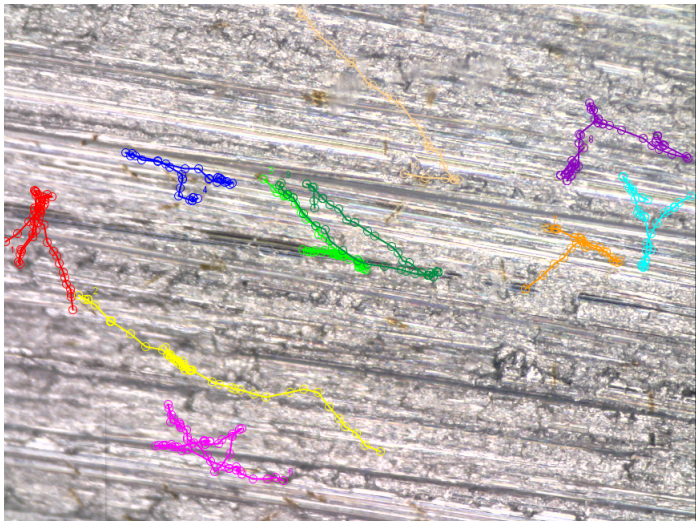

(a) Tracks on P80 (mag: 472.0x)

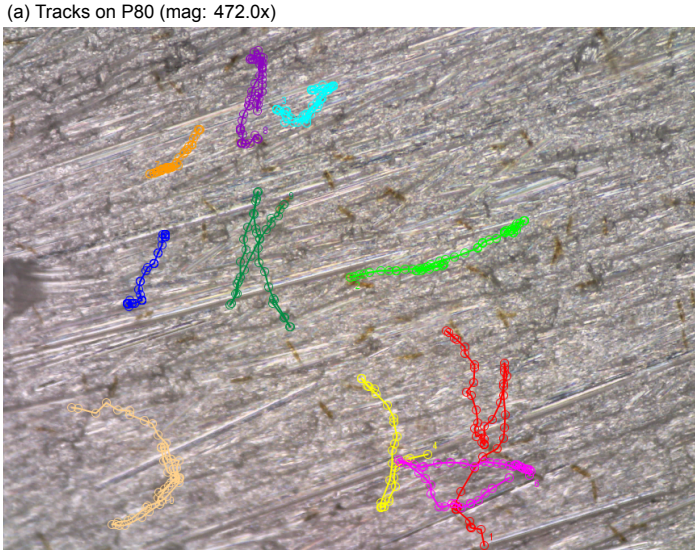

(b) Tracks on P180 (mag: 470.5x)

(c) Tracks on P2000 (mag: 470.0x)

Figure 3.14: Overview of the traveled paths of 15 randomly chosen cells for Al 99.5 with various topologies

3.3.3. Motility on three different aerospace alloys

Three different alloys were used to see whether the cells would stay motile on substrates that contain potentially toxic elements. The main alloying element for AA2024 is copper, which has been reported to be especially toxic for aquatic biota [57]. The motility was computed in the same way as for the subsection 3.3.1. The results and normalized results can be seen in Figure 3.15. Motility ranges from 1.7% to 2.1%, showing the most motility on AA7075, see Figure 3.15a. This effect disappears upon normalizing the results, see Figure 3.15b. The normalized results shows that the cells are most motile on Al99.5, while it had the fewest cells in the ROI. The main observation of this experiment is that the cells show motility on all the different substrates, but that there could be substrate related differences.

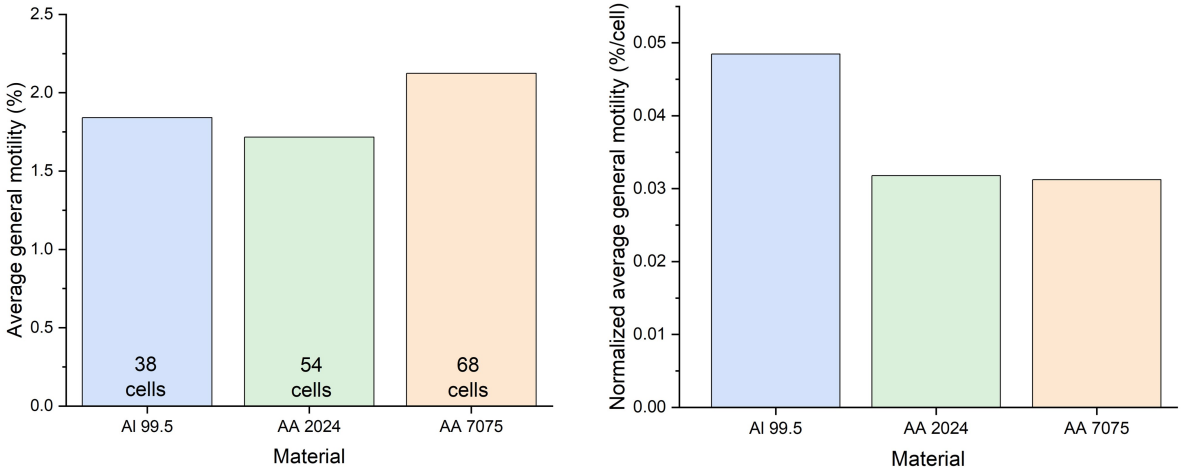

(a) Average general motility as a function of material

(b) Normalized average general motility as a function of material

Figure 3.15: General motility variations as a function of material; the immersion time was between 0h-1h; the samples were exposed to a cell suspension with a concentration of 3.35×10^4 cells/mL

The motility was examined in greater detail by analyzing 15 cell paths using the MTrackJ plugin for ImageJ, resulting in the tracks as in Figure 3.16. The first thing to note it that the quality of the surface treatment is considerably less for the Al99.5 sample, as can be seen from the many scratches on the substrate compared to the AA2024 and AA7075 samples. Looking at the tracks, it appears that they are shorter on the Al99.5 compared to the other two . However, when analyzing these tracks it is important to note the difference between the *distance traveled*, which is the length of the track, and the *distance from the start*, which is the distance between the first and last point in the track. Interestingly, there does not seem to be a considerable difference between the average traveled distance (Figure 3.17a), but there is a difference between the distance from the start (Figure 3.17b) between the alloys and the commercially pure Al99.5. Meaning that the cells on Al99.5 mainly move back and forth on their own trail. This may be caused by the chemical composition of the substrate. It might also be that they want to minimize contact with the substrate by traveling back and forth over their own path of excreted EPS. The spread of the data is quite large, suggesting that there is a considerable difference between individual cells.

In addition, in the raw video data the cells appeared to be moving faster on the AA7075 sample, however, this could not be concluded from the current data as the analysis showed no substantial difference in the average velocities, which were 1.64, 1.60 and 1.50 pixels/s for Al99.5, AA2024 and AA7075 respectively. One should also take into account that the images were not taken at exactly the same magnification, but varied slightly, which might result in a significant difference for the velocity values as these are relatively small and thus sensitive to small scale variances.

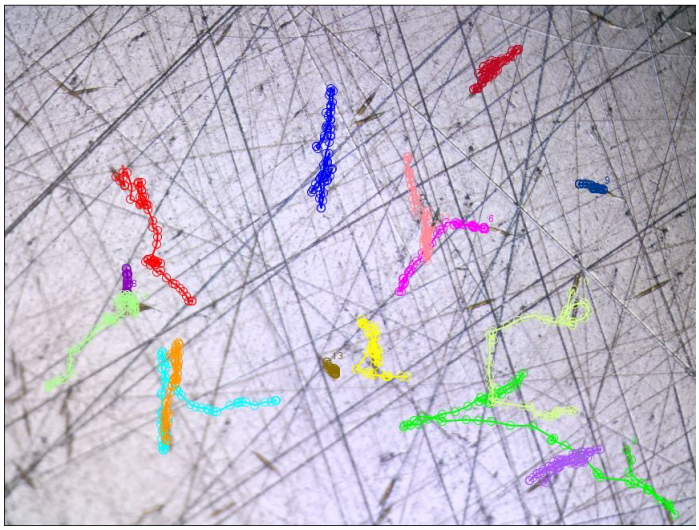

(a) Tracks on Al99.5 (mag: 471.5x)

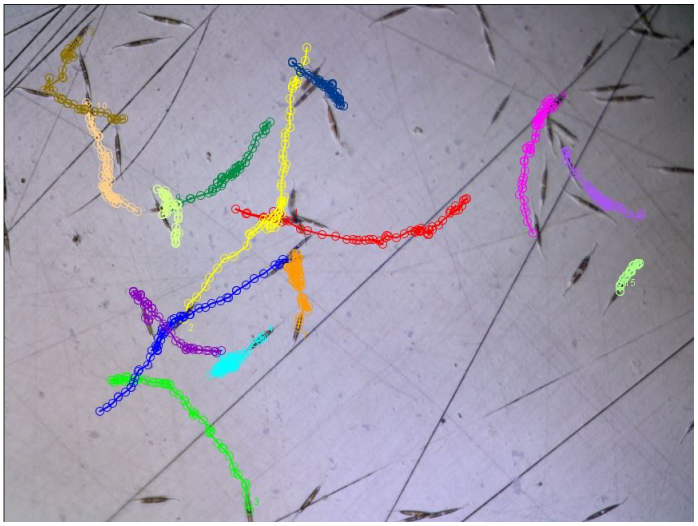

(b) Tracks on AA2024 (mag: 471.0x)

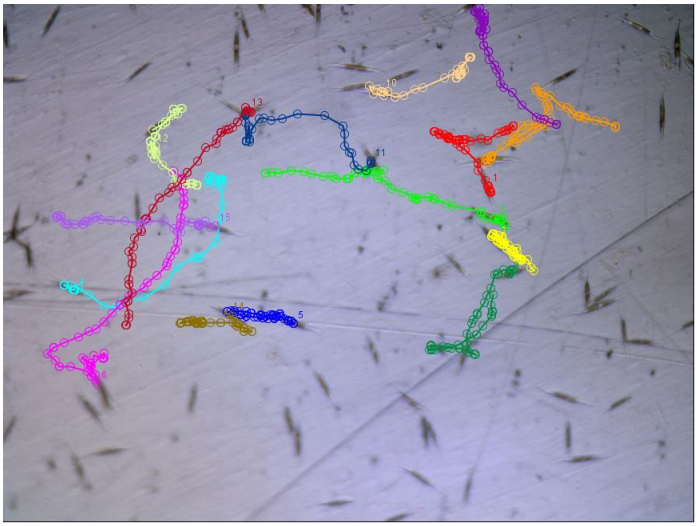

(c) Tracks on 7075 (mag: 470.5x)

Figure 3.16: Overview of the traveled paths of 15 randomly chosen cells for various materials

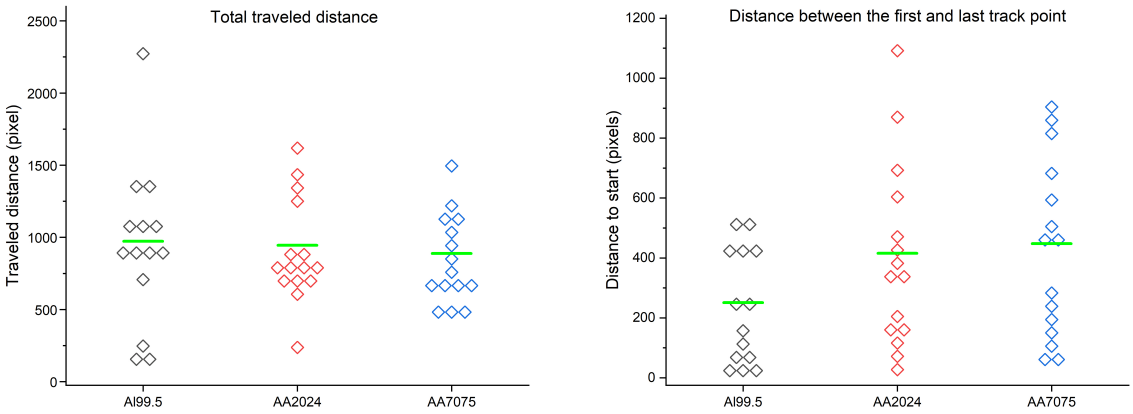

(a) Average traveled distance on the different substrates

(b) Distance to starting point on the different substrates

Figure 3.17: Average distance traveled and distance to the starting point on the different substrates; each diamond represents an individual track; the green line represents the average

3.4. Effect of local composition on cell motility

Based on the results from section 3.3, the parameters for a motility study were set. To eliminate (macro) topology influence and to generate the best quality data, the samples were polished to 1 µm and exposed to a volume of 1 mL cell suspension. Furthermore, based on the increasing motility for the first 24h (see Figure 3.12), the monitoring time was set to 24h. To study the effect of the diatoms, an Al99.5 and AA2024 sample were also observed when they were exposed to just medium for 24h. These results can be found in section C.1.

3.4.1. General motility

The first step was to analyze the average general motility as described in subsection 2.5.2 for all samples and time points. The results of this analysis can be seen in Figure 3.18, in which the x-axis depicts the time after inoculation. There is a clear difference between the Al99.5 and AA2024 samples.

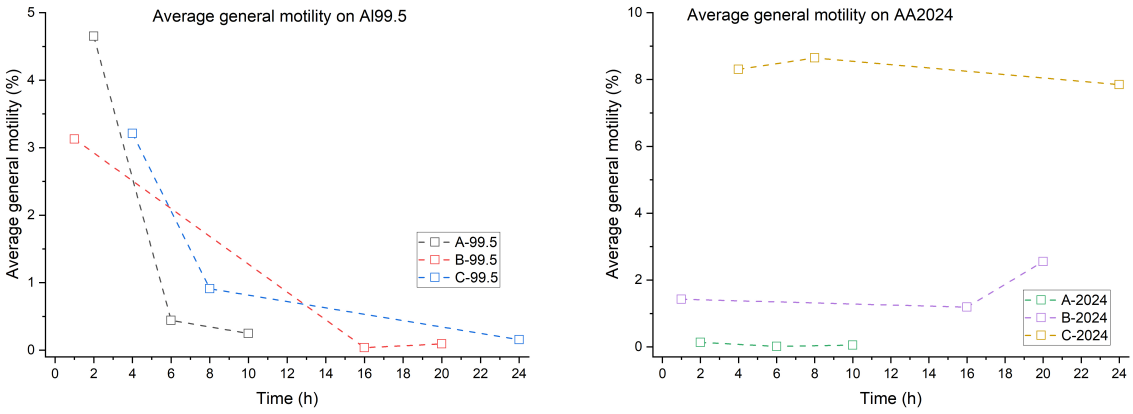

(a) Average motility for the Al99.5 samples

(b) Average motility for the AA2024 samples

Figure 3.18: Average general motility for 3 samples of Al99.5 and AA2024-T3

Sample C-2024 stands out because it appears to be more motile compared to all other samples, with an average general motility of 8.3%. On the other hand, sample A-2024 stands out because there appears to be almost no movement at all, with an average pixel change of only 0.07%. This was confirmed with the raw visual data, showing that there does not appear to be any motility by the cells on sample A-2024. This could be caused by the cells prematurely dying, however, this is unconfirmed. For sample C-2024, the motility remains relatively constant, while sample B-2024 does show a slight increase in motility after 16h. The averages for the Al99.5 samples show considerably less spread compared to the AA2024 samples. It could be that the large variation between the AA2024 is related to the composition, but that was not proven during this experiment. The compositional breakdown of the AA2024 samples can be found in section A.2.

All three Al99.5 samples show a similar trend in which the motility decreases over time, resulting in none or almost no cell motility after 10h. This is contrary to what was observed earlier in subsection 3.3.1, where the motility increased during the first 24h. During the initial experiment the volume was 2mL rather than the 1mL used in this motility study. In addition, the concentration was higher in initial experiment ($4.65x10^4$ cells/mL) compared to the concentrations used for this motility study ($2.37\text{-}2.90x10^4$ cells/mL), which may be related to the difference observed.

During experimentation, it became clear that there were noteworthy differences in the number of cells in the ROI. Therefore, the normalization process as described in subsection 3.3.1 was applied, the results of which can be seen in Figure 3.19. Several trends can be noted from this figure, the first being the decrease in motility over time for the Al99.5 samples can still be observed. The peak that appears in sample B-99.5 at 20 hours is caused by the extremely low number of cells (2). This was confirmed with the raw image data, that showed that the only movement is caused by background movement and not by cell motility. For the AA2024 samples, the same trends hold as for the non-normalized average general motility. The normalized motility stays more constant on AA2024 when compared to Al99.5 and there is a larger variation between the AA2024 samples than between the Al99.5 samples. The results are presented as a function of immersion time in Figure 3.20. Figure 3.20a shows that for Al99.5 the general downwards trend over time still holds. Figure 3.20b does not show a clear trend, which is caused by the considerable differences between the samples. The variation in the number of cells in the ROI indicates that the assumption that the cells will distribute homogeneously on the surface may not be valid, as this would mean that there are between 6-9 cells in the ROI.

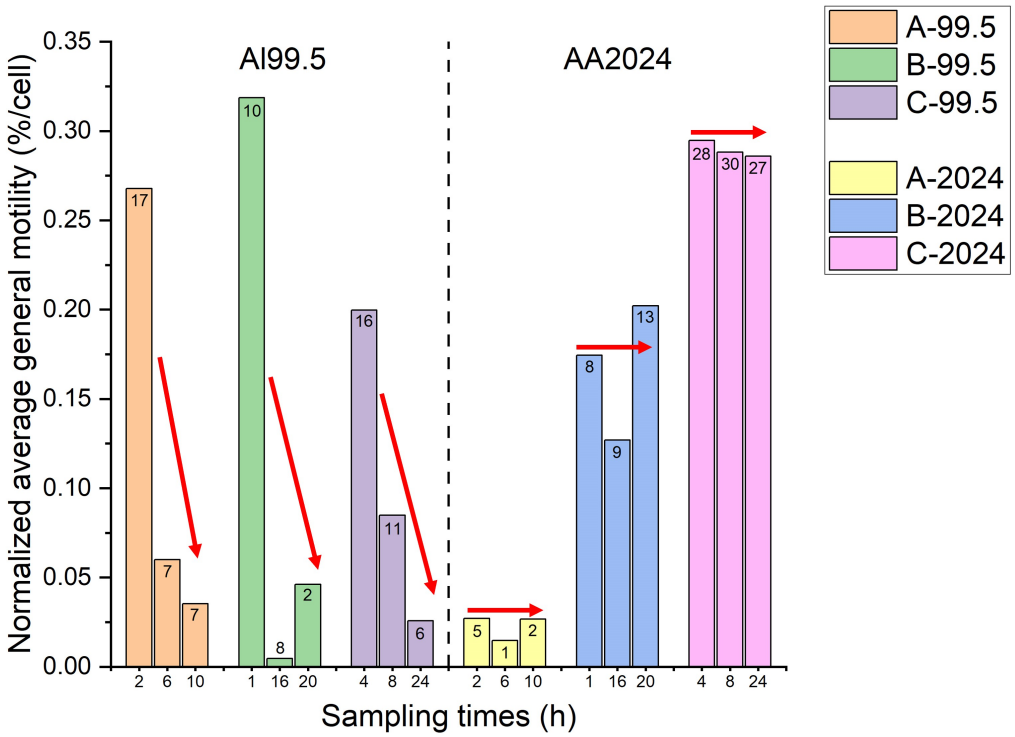

Figure 3.19: Normalized average general motility of the *Cylindrotheca fusiformis* cell suspension on the different samples; the numbers in the bar denote the average number of cells in the ROI for that measurement; the red arrows indicate the general trend

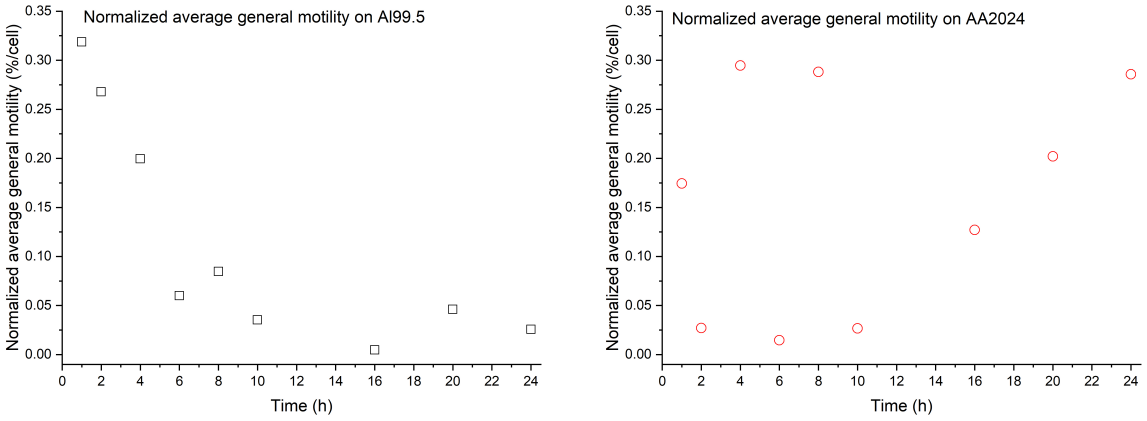

(a) Normalized motility on Al99.5 as a function of immersion time

(b) Normalized motility on AA2024 as a function of immersion time

Figure 3.20: Average general motility for Al99.5 and AA2024-T3 as a function of immersion time

Another feature to note is that the average number of cells in the ROI ranges from a single cell up to 30 cells. This does appear to be directly related to the concentration of either the cells suspension or the mother-line, see Table 3.2. This leads to question the assumption that the cells suspension will be homogeneously distributed on the scale of the ROI on the substrate when pipetted on. This difference could be caused by cell migration, but this remains unconfirmed as no measurement was done at 0h.

Table 3.2: Cell concentrations for the cell suspensions and mother-line cultures

Sample	Concentration cell suspension ($x10^4$)	Concentration mother-line ($x10^5$)
A - 99.5	2.37	1.36 (A21.1)
B - 99.5	2.90	0.65 (A21.1)
C - 99.5	2.76	4.53 (A21.1)
A - 2024	2.57	2.08 (A21.1)
B- 2024	2.80	3.46 (A20.1)
C - 2024	2.90	2.17 (A20.1)

Diatom behavior

To quantify diatom behavior several parameters were assessed: the number of motile cells, the average velocity and the average track length. A cell was defined to be motile in case the mean velocity was at least 0.1 µm/s, this corresponded well with the qualitative data. In case there were too many cells to track individually, 15 or 16 tracks were selected and analyzed, otherwise all tracks were analyzed.

Due to the fact that for Al99.5 no motility was observed for measurement points after 8h, a distinction can be made between ”short term” (0-8h) and ”long term” (8-24h) behavior. For the long term, all investigated parameters show a similar trend to the general motility. For the AA2024 samples, they stay relatively constant over time. For the Al99.5 samples, there is a decrease in time, which is consistent with overall decrease motility and number of cells in the ROI. Considering the short term, a different phenomenon can be observed, see Figure 3.21. While the parameters of the Al99.5 samples all decrease over the first 8 hours, their values for the first two hours do not appear to be lower than those for the AA2024 samples. For the first 2 hours, all cells on the Al99.5 are motile, with an average velocity and track length that is higher than for the AA2024 measurement. After 4 hours the average velocity and the average track length decreases, meaning that the motile cells become less motile. A further decrease is observed for the 8h point, after which motility completely ceases. A large variation was observed both on the Al99.5 and the AA2024 samples.

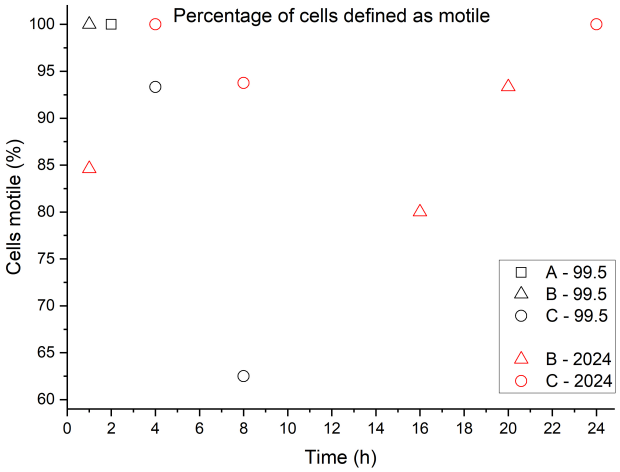

(a) The percentage of cells considered motile on Al99.5 and AA2024

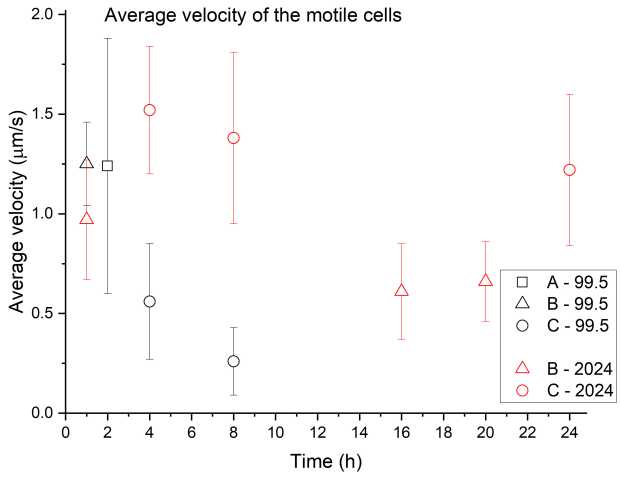

(b) The average velocity of the motile tracks on Al99.5 and AA2024

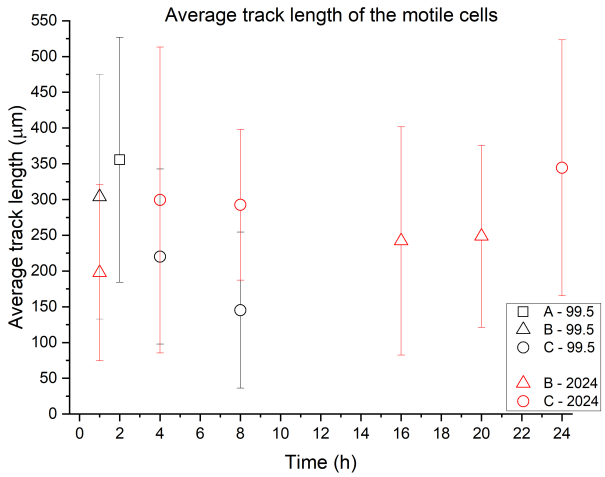

(c) The average track length of the motile cells

Figure 3.21: Motility and velocity on Al99.5 and AA2024-T3; the whiskers represent one standard deviation

As can be seen from Figure 3.21b there is a considerable variability in the average velocity of the tracks. Which is consistent with the observation that cells move at different speeds. Additionally, there is also a large variability in the velocity for each individual track. This is consistent with the observation that cells move intermittently and can remain stationary for a period of time before moving again. The maximum velocity observed was 7.47 µm/s, however, this may be caused by the cell (temporarily) detaching and flowing in the liquid rather than gliding over the surface. Nevertheless, maximum speeds of around 2.5-3.0 µm/s were observed for gliding cells, see Figure 3.22.

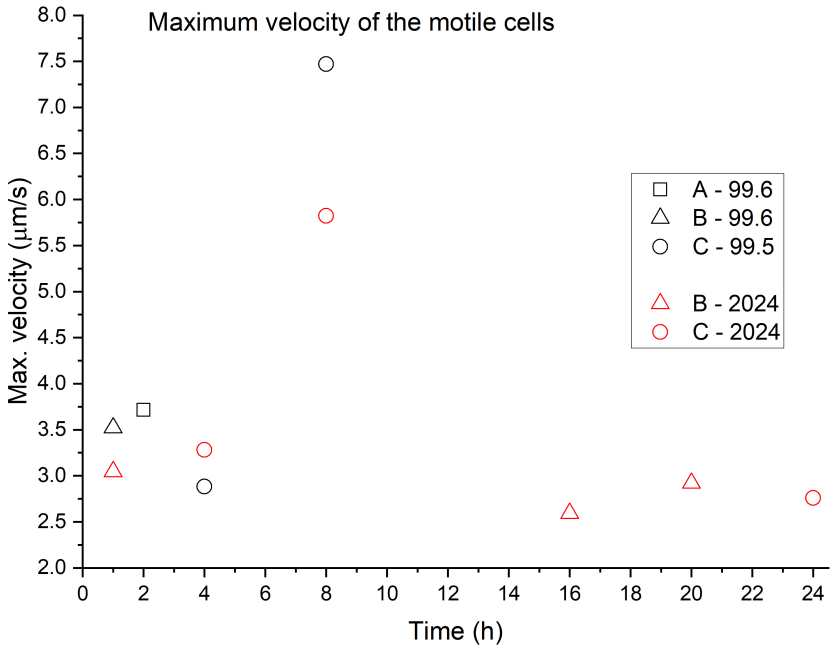

Figure 3.22: Maximum velocity measured on polished Al99.5 and AA2024-T3

Cells were able to move both forwards and backwards (bidirectionality), meaning they were able to change direction 180°, without having to turn around. Which is consistent with earlier observations for raphid diatoms, albeit on different substrates [13], [58]. In addition, it was decided to loosely classify tracks into categories: straight lines, circles, random, shunting or stationary (non-motile). Most of the tracks on both substrates could be sorted in either the straight lines or random category. Movement along a curve was classified as circles, these tracks occurred less, but were observed on both substrates. Shunting behavior (the cell moving backwards and forwards but with no net change in position) was also observed. While this behavior was observed on both substrates, it was the dominant type of movement for the observation done on Al99.5 at 8h, see Figure 3.23. This behavior is somewhat similar to which was observed earlier on Al99.5 in Figure 3.16a. During this experiment, however, this behavior was only observed after 8h, while in subsection 3.3.3 the behavior was observed immediately upon immersion. For *Amphora coffeaeformis* it was observed that their random movement was ellipsoidal, but that cells were capable of traveling in a straight line when reacting to a chemical gradient [27], [59]. During this research, no baseline random measurement was done, making it not possible to determine whether their behavior is coordinated.

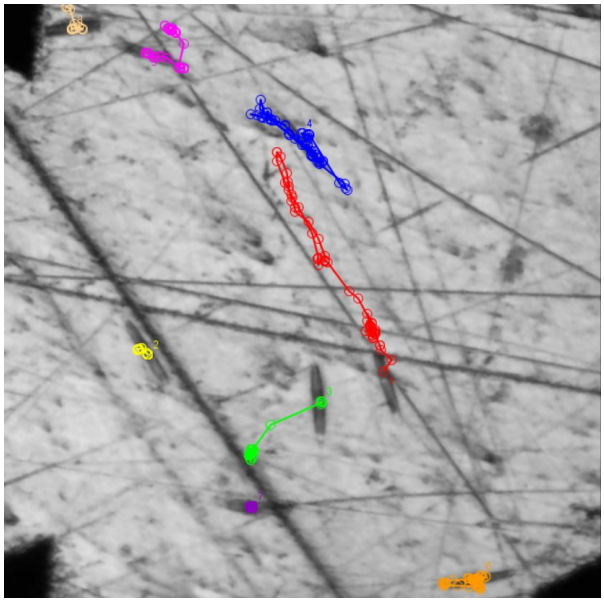

Figure 3.23: Shunting behavior as observed on sample C-99.5 after an immersion time of 8h

3.4.2. Interaction of the diatoms with IM particles

The diatoms' travel paths were also reviewed with regards to the IM particles, an example of these results can be seen in Figure 3.24. From these results, no definitive conclusions could be drawn on avoidance/attraction behavior of the diatoms with regards to the IMs. All types of IM particles were crossed by diatom paths. In addition, cells did not appear to linger on certain IMs. Cells that did linger, did not necessarily do this on a location with an IM particle. However, there were several regions in the were the diatoms did not appear to cross through (the orange oval in Figure 3.24). These regions were generally low in IMs, however, more research is required to draw solid conclusions. For additional information on the identification of the IMs and all the IM maps with diatom tracks, see Appendix A.

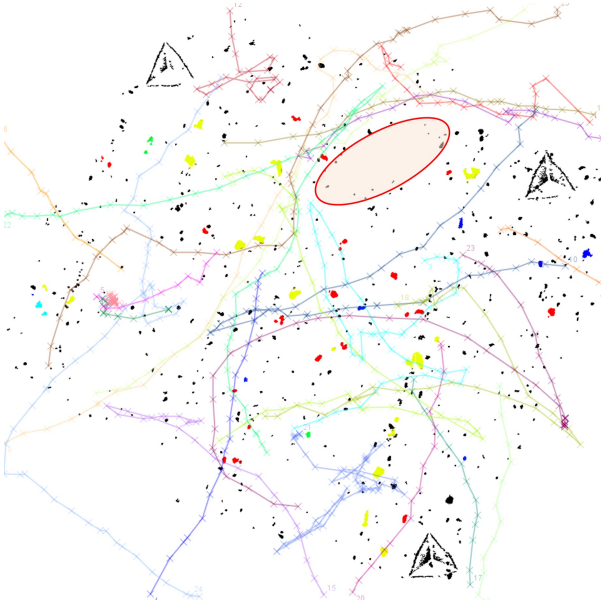

Figure 3.24: Example (C-2024) of a color coded IM map with the diatom tracks overlaid; green = AlCu, red = AlCuMg, blue = AlCuFeMn, yellow = AlCuFeMnSi, cyan = other; immersion time was 4h; the orange oval shows a region that the diatoms did not appear to cross and is low IMs

There are several factors apart from the chemistry of the surface that may be of influence. One phenomenon that was observed when studying the raw data and that clearly influenced the diatoms' path, but not related to the chemical characteristics of the substrate, was the mechanical interaction between cells. Cells were observed to collide with each other and to stay interlocked for a while before separating again. In addition, some diatoms are able to react to chemical concentration gradients and to local cell concentrations [27]. The surfaces were prepared to have a roughness of 1 µm, but it was visually observed that there were imperfections, which may result in a physical barrier for the cells. However, this is unlikely, as the results in subsection 3.3.2 indicate that relatively large topologies can be overcome. Finally, it is important to note that the substrate also undergoes chemical and physical changes upon exposure to an electrolyte. Corrosion processes may locally release ions and create a concentration gradient or locally cause a pH change. Additionally, physical changes such as the creation of holes or accumulations of corrosion products can change the topology of the surface.

3.4.3. Post-processing

Based on literature, it is plausible that during motility, *Cylindrotheca fusiformis* secretes organic material in the form of trails. Although it has not been reported for this diatom species. Whether this organic material adheres to the surface and what the chemical and physical characteristics are, is unknown. AB staining, fluorescence microscopy and Raman spectroscopy were used to post-mortem investigate the samples used for the motility study. In addition, post-mortem SEM images of sample C-2024 can be found in subsection B.2.2.

Alcian Blue (AB) staining

The results of the staining with AB to detect organic material can be seen in Figure 3.25. For this technique, the A samples form the motility study were used, meaning that they have been exposed to a relatively low concentration cell suspension for 24h. There appears to be a difference between the Al99.5 and AA2024 sample. The AA2024 shows a clear blue hue, which becomes even more pronounced on the magnified image, this blue hue is absent on the Al99.5 sample. This indicates that there is a difference in the organic matter that is secreted on both substrates. It could be that more EPS is secreted on the AA2024, or perhaps that the organic matter is more adhesive on the AA2024, meaning less of it is washed away during rinsing. One should keep in mind that AB is used to stain a specific type of EPS, namely acid polysaccharides (TEP), meaning the difference could also be in the composition of the EPS.

This method was used to indicate whether there is organic material left on the surface after diatom motility, and it appears to be successful. Comparing it with samples only exposed to medium (see Figure 3.26), there appears to be stained material on the diatom exposed AA2024 sample, which is absent on the medium only sample.

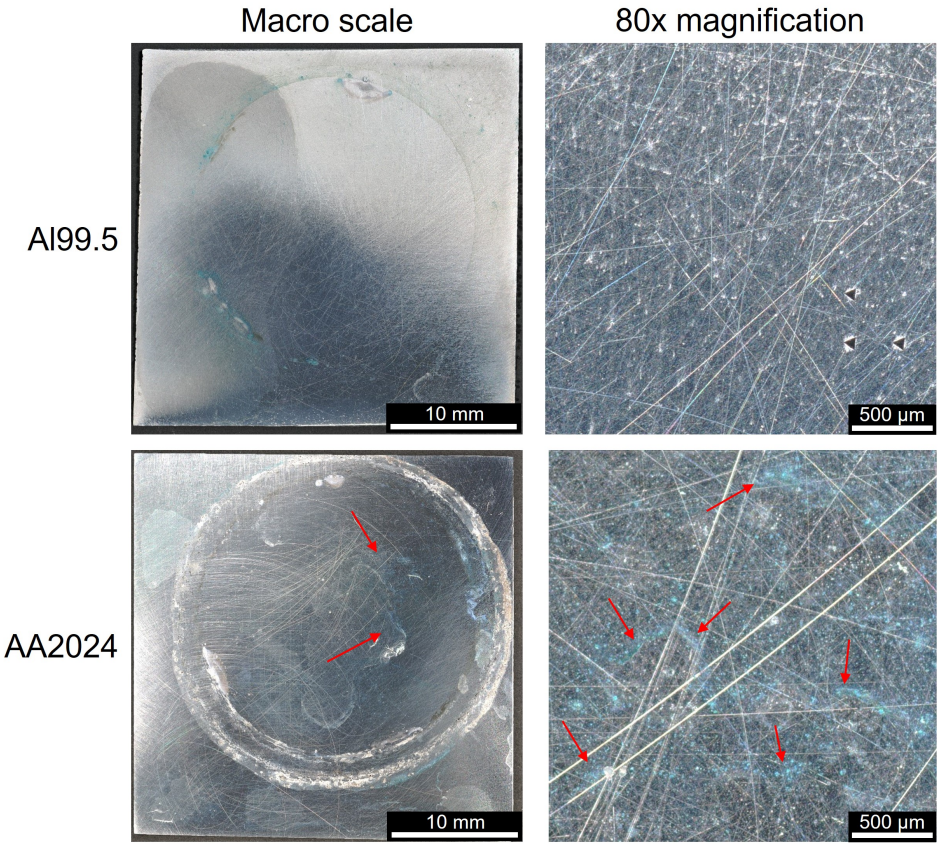

Figure 3.25: Images of an Al99.5 and AA2024 sample stained with AB after 24h exposure to a diatom cell suspension; the red arrows indicate the blue hue on the AA2024-T3 sample

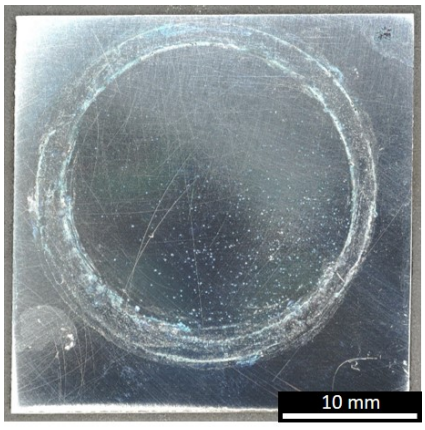

Figure 3.26: Image a AA2024-T3 sample stained with AB after 24h exposure to only mix Si medium

Raman spectra

An attempt was made to detect potential motility trails using Raman spectroscopy. The samples used for this technique, were the B & C samples from the motility study, meaning that they have been exposed to a relatively low concentration cell suspension for 24h. An advantage is that the Raman setup allows for mapping, meaning it is possible to get an overview of a small specific region. For ease of comparison, one representative spectrum for each of the investigated samples was chosen, the results can be seen in Figure 3.27 and Figure 3.28. The bands of interest are the same as for FTIR, so the amide I, II and III regions (1700 cm^{-1} - 1200 cm^{-1}), the carbohydrate region (<1200 cm^{-1}) and the O—H stretch around 3350 cm^{-1}. The spectra as displayed here have been processed by subtracting the baseline, filtering out cosmic rays and have been smoothed for clarity.

The Raman spectra for Al99.5 can be seen in Figure 3.27. When analyzing the Al99.5 spectra it is clear that there are peaks on the diatom exposed samples, which are not on the medium only exposed sample. Most noticeable are the larger peaks that appear in the region of 800-1850 cm^{-1}. A peak that is present on both diatom exposed substrates is the peak around 890 cm^{-1}, which is in the fingerprint region, meaning it is difficult to identify the exact cause for this peak. However, it is notably absent in the sample that has been exposed to medium only and it lies in the region that indicates carbohydrates. Another prominent peak which remained unidentified but is present on the diatom exposed samples but absent on the medium only exposed sample is around 1830-1850 cm^{-1}. There are several peaks in the region of 1700 cm^{-1} - 1200 cm^{-1}, these can be indicative of proteins as they correspond to amide groups. A peak that is noticeably absent, is the broad one around ±3350 cm^{-1} which indicates the O—H stretch. The spectra obtained from the Al99.5 samples indicate that there is organic material left on the substrate after 24h exposure.

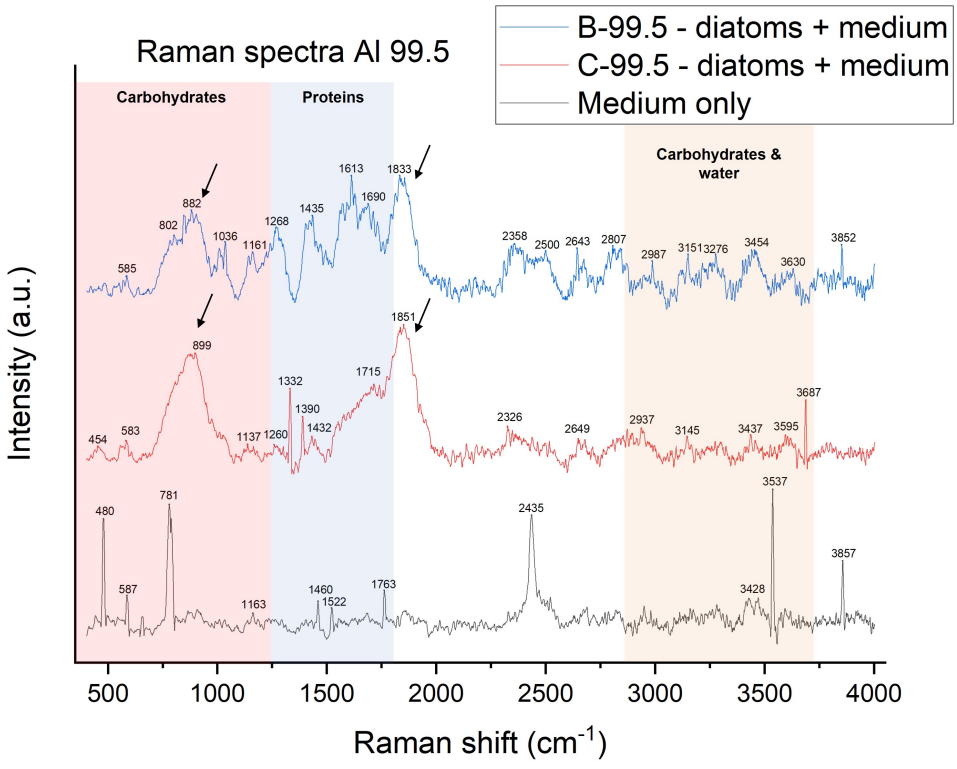

Figure 3.27: Raman spectra for Al 99.5 samples exposed to diatoms suspension or medium only for 24h; sample B & C are those used in the motility study

The Raman spectra for 2024 show some interesting results, as can be seen in Figure 3.28. Several peaks appear on the medium exposed sample, these are located at 585 cm^{-1}, 885 cm^{-1}, 1431 cm^{-1}, 1735 cm^{-1} and 1853 cm^{-1}. These are assumed to be caused by the underlying substrate and the

medium. The next result to note is the difference between both the diatom exposed samples: sample B shows almost no signal, while sample C shows some clear peaks. This could be caused by the fact that the EPS coverage may not be homogeneous, meaning that there could be parts of the substrate which are not covered with EPS. On sample C, peaks to note are located around 900-1150 cm^{-1}, 1300-1450 cm^{-1}, 1600-1860 cm^{-1} and two large ones around 2900 cm^{-1} and around 3500 cm^{-1}. Similar to the FTIR spectra, the broad peak on sample C around 3500 cm^{-1} is likely caused by $\mathrm{O}-\mathrm{H}$ bonds. The peaks around 2889 cm^{-1} and 2937 cm^{-1} are consistent with research done on the mucilage of *Navicula sp.* [60]. In this research, two Raman peaks were found at 2882 cm^{-1} and 2936 cm^{-1}. These were identified as the $-\mathrm{CH_2}-$ and $-\mathrm{CH_3}$ asymmetric and symmetric stretches, which could be indicative of carbohydrates. In addition, the peaks between 1700-1200 cm^{-1} could be prescribed to either the amide I, II or III regions, which could indicate the presence of proteins. Finally, some peaks can be found in the region indicative of carbohydrates on sample C-2024, which are also absent on sample B-2024.

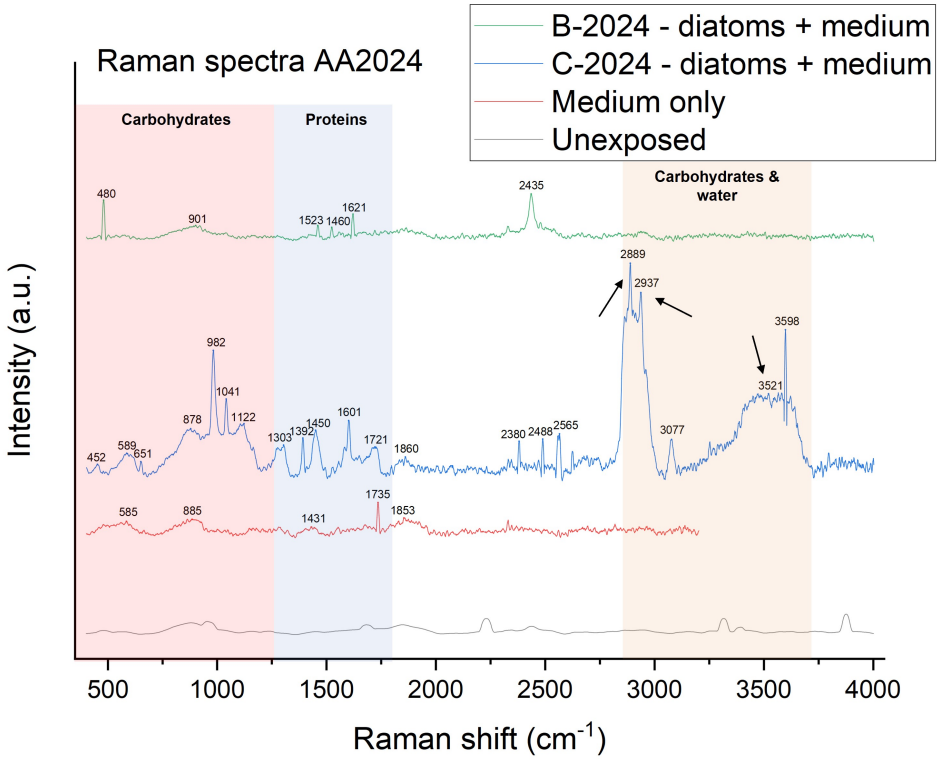

Figure 3.28: Raman spectra for AA2024 samples exposed to diatoms suspension or medium only for 24h and one sample that has had the same pre-treatment of polishing and UV-treatment but no exposure

Several points should be taken into account when analyzing these Raman spectra. The signal is not very strong, making it difficult to distinguish the exact location of the peaks. This may be tweaked by altering the settings on the machine or by post-processing. However, too rigorous smoothing may result in information being lost. It might be that the material left by the diatoms is simply too little to give a strong signal and is limited by the detection limit of the machine. Secondly, the surface of AA2024 is not homogeneous which can result in different Raman spectra for different locations, this was not accounted for in these analyses. Additionally, it was not investigated how corrosion products could potentially influence the spectra.

The main objective of taking these spectra, was to see whether it was possible to determine whether there was organic material on the substrates after 24h exposure to a low concentration cell suspension. These spectra show clear indications that there is indeed organic material on the surface in the form of peaks in the carbohydrate and amide (protein) regions, which corresponds with what would be expected in *Cylindrotheca fusiformis* motility trails.

Fluorescence microscopy

The results from the fluorescence microscopy can be found in Figure 3.29. Several things can be observed from this image, the first being that the negative control (medium exposure only) also shows fluorescence. This may be caused by the settings of the microscope. Alternatively this may be caused by something on the aluminum substrate or the conditioning layer exhibiting fluorescence. Another observation is that the positive control (visible biofilm) shows the least fluorescence. Which could mean that the layer of biofilm is blocking the signal from underneath. However, on the Al99.5 sample with the visible biofilm, several fluorescent clouds can be seen, which are suspected to be some kind of EPS. In addition, a fluorescent signal can be seen from the cells on both the biofilm samples and the AA2024 5-day LC exposure sample.

This method was intended to see whether it was possible to detect if there are trails left during *Cylindrotheca fusiformis* motility. From the image it becomes clear that either this method of detection or sample preparation is not suitable or that *Cylindrotheca* does not leave trails during motility, as no trails were detected. However, the latter is unlikely, as both the AB staining and the Raman spectra indicate the prescence of organic material on the surface after 24h low concentration diatom exposure.

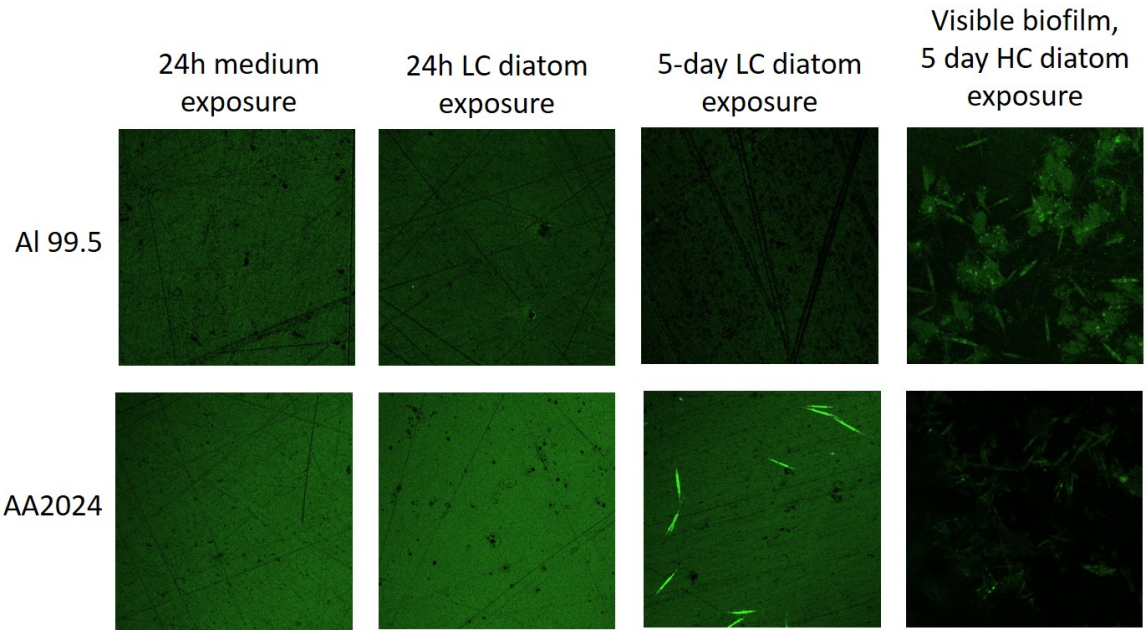

Figure 3.29: Fluorescent images taken of various substrates under various conditions; LC indicates low concentration, HC indicates high concentration

3.5. Direct comparison of Al99.5 and AA2024-T3

In order to eliminate biological factors between samples and to confirm the potential preference for AA2024 over Al99.5, a direct comparison was made between a Al99.5 and AA2024 sample exposed to the same cell suspension.

3.5.1. High concentration trial

Figure 3.30 shows an image taken of the two materials. From this image it is not directly clear whether the cells have a preference as both substrates have cells on them. However, from visual inspection of this high concentration trial, it appears that there are more cells on the AA2024 substrate. In addition, there are also cells that settled on the epoxy gap and an agglomerate can be seen at the bottom of the image. Which could mean they could prefer the epoxy over either metal. The average general motility was also monitored immediately after immersion, resulting in similar averages of 3.1% and 2.9% motility for Al99.5 and AA2024 respectively.

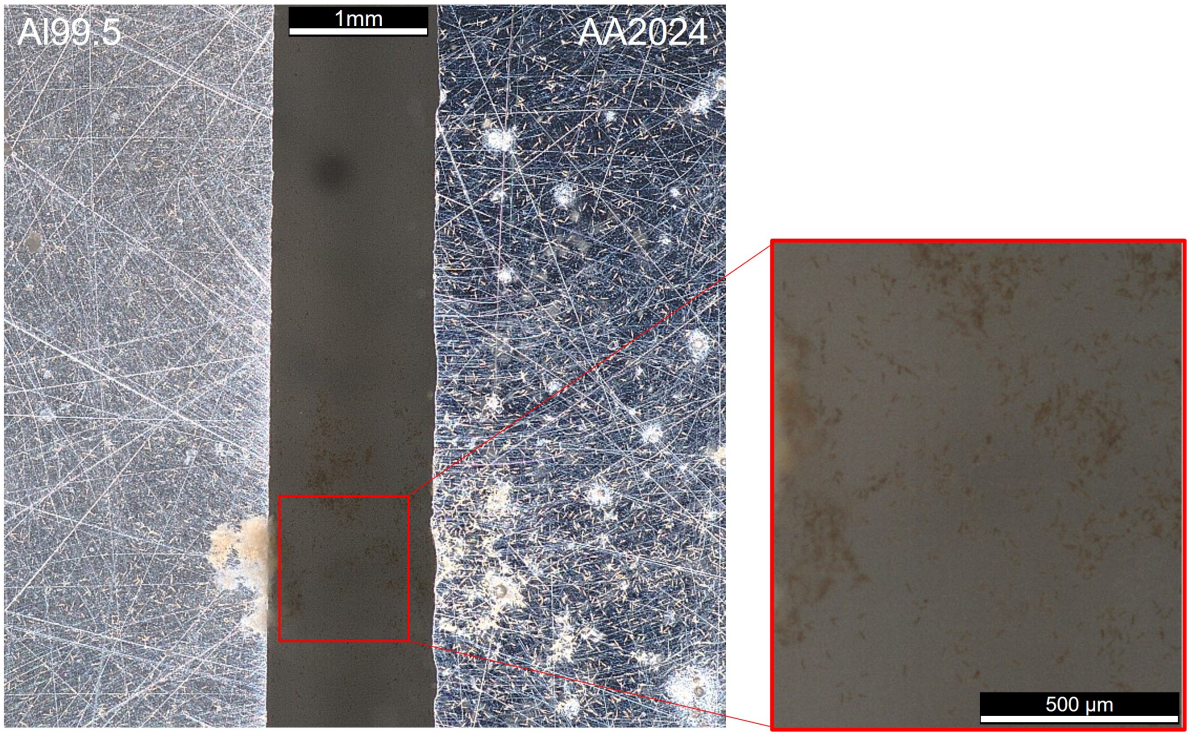

Figure 3.30: Image of the Al99.5, AA2024 and the epoxy, taken with the *Keyence Wide-Area 3D Measurement System Controller, VR-5000* at 40x magnification after about 1h of immersion; left is the Al99.5 substrate, middle is the epoxy resin, right is the AA2024 sample; the closeup is taken at 160x magnification

3.5.2. Direct comparison of the diatoms' motility

A direct comparison experiment was done using the same conditions as the motility study, the results of which are displayed in Figure 3.31. Initially, there is more motility on the Al99.5 substrate, but this decreases rapidly. The motility of the AA2024 also decreases over time, but less steeply than for Al99.5. This is only partly in agreement with earlier measurements.As in previous experiments it was observed that the motility stayed constant or even increased over 24h on AA2024 (except for sample A-2024 from section 3.4), while in this direct comparison it decreases to essentially no movement over the course of 6h. Figure 3.31 shows that the motility of the Al99.5 decreases more rapidly than for AA2024. In addition, the starting general average motility on Al99.5 is less than observed in section 3.4 and more decreases rapidly.

This could potentially be explained by the fact that the Al99.5 and AA2024 are exposed to the same cell suspension. This means that any (toxic) products that are released in the electrolyte can diffuse throughout the entire electrolyte, affecting cells on both substrates. In addition, it should be noted that effect of the epoxy was not further investigated, but this may also influence the cells' behavior, as the agglomerates as in Figure 3.30 might suggest.

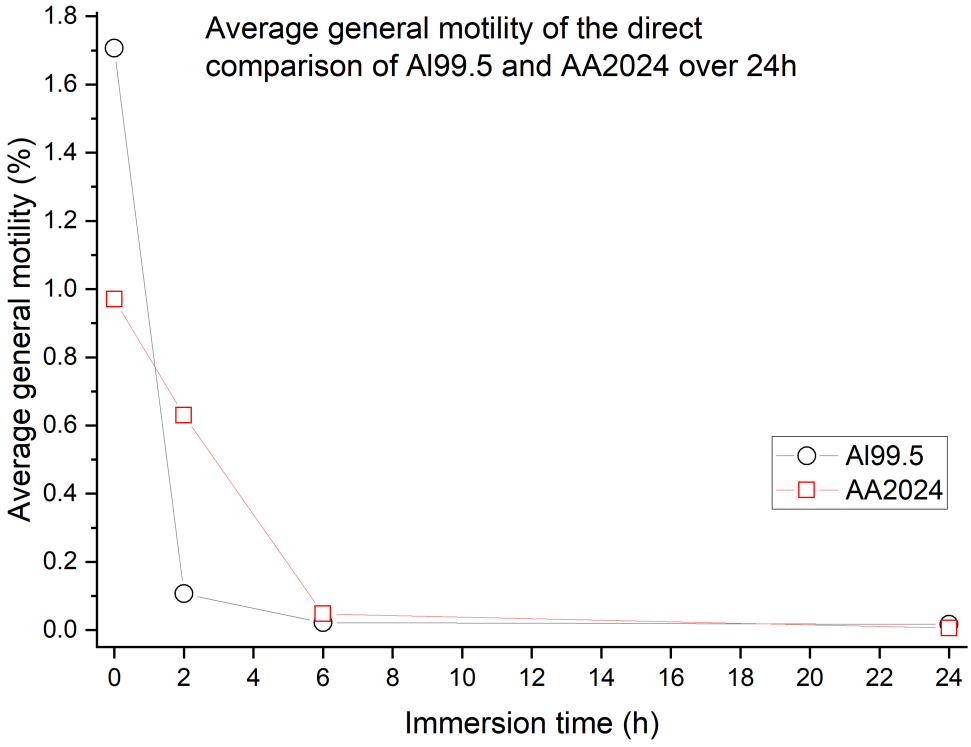

Figure 3.31: The average general motility of Al99.5 and AA2024-T3 over 24h in a direct comparison

3.6. General discussion

This section contains some general discussion points regarding the relation between motility and biofilm formation and the diatoms' interaction with the substrate that came up during the course of this project.

3.6.1. Motility vs. biofilm formation

During this research, the diatoms' motility and biofilm forming capabilities were investigated separately. It was observed that the combination of the low volume (1 mL) and the relatively low concentration (<3 x 10^4 cells/mL) used in the motility studies did not cause a biofilm to grow, independently of the surface composition and topology. This combination of factors was required due to several limitations of the setup used to observe motility. During the motility trials, it was found that the low volume was required to get good quality data for motility observation. Additionally, the low concentration was required to be able to study the motility of individual cells on a substrate. It was also observed that increasing the volume and the concentration, does lead to biofilm formation.

Rather than forming biofilms, it was observed that white aggregations formed over time for the low volume, low concentration samples. These aggregates are suspected to contain (dead) diatoms, as the cells were not observed to be on the surface anymore. These aggregates most likely also contain EPS as cells under nutrient stress or during cell lysis excrete high concentrations of TEP, which plays a role in aggregation [20]. Finally, it likely also contains precipitates from the medium. These precipitates also formed when there were no diatoms present in the medium, but does not form in the bottles the medium is kept in. This suggests that the medium and the metal undergo some kind of interaction to form these precipitates. However, it was not possible with optical microscopy to discern individual components. Additional chemical analysis could perhaps determine the individual components.

An important step into unraveling diatom motility and their interaction with the substrate is to understand why diatoms move. From a biological point of view, it would be logical that it is part of a survival strategy. For example, to be able to migrate to a region with a more beneficial climate for survival and reproduction. In nature, benthic diatoms' motility serves to move towards the light during daylight hours, while settling back into the nutrient rich sediment at night [61]. Experiments have shown that diatoms are capable of chemotaxis, for example as reaction to concentrations of certain sugars [62] and dissolved silicic acid [58]. The authors suggest that dSi-directed movement may be the cause of the patchy nature of biofilms. This is an important aspect to investigate, as this may be a key factor in forming homogeneous biofilms. Another key factor in creating homogeneous biofilm is the cell concentration. In a study using *Amphora coffaeaformis*, it was reported that cells moved away from cell aggregates [27]. The effect of cell concentration on motility and on biofilm formation should be investigated for *Cylindrotheca fusiformis*.

3.6.2. Interaction with the substrate

Interestingly, in this study, the motility trend appears to be substrate related, while in an earlier motility study on glass and PDMSE, the motility trend appeared to be mainly species specific, see Figure 3.32 [63]. Also note, that for this study the motility became equal on glass and PSMSE after 5h. This is partly contrary to what was observed during this thesis, as the motility between Al99.5 and AA2024 diverged more over time when investigated separately in section 3.4. When investigated in the same cell suspension as in section 3.5, the Al99.5 and AA2024 showed a similar equalizing effect at 6h. It should be noted that the number of cells tracked in [63] were significantly higher (1074-2474 cells) compared to this project (max. 30 cells).

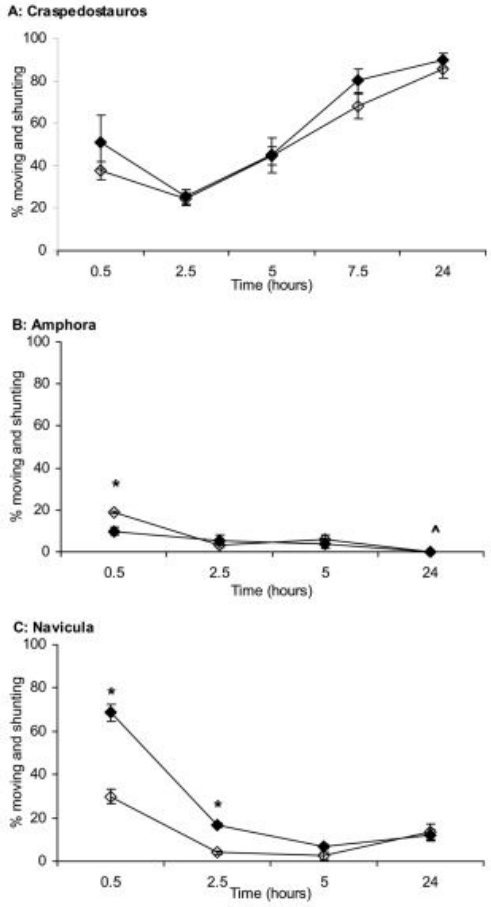

Figure 3.32: The motility of three diatom species monitored on acid washed glass and PDMSE over the course of 24h; ♦ = glass, ◊ = PDMSE [63]

It is expected that there is an interaction between the materials' corrosion processes and the diatoms (MIC). However, the alloys did not corrode as fast as expected in the medium. This effect was observed both with and without the diatoms present for AA2024, suggesting that it there is a buffer effect caused by (a component of) the medium and the alloy. One thing that was observed with regards to corrosion, is that the cells avoided a relatively large corrosion spot that originated in one of the indents in sample B-2024, see Figure 3.33a. Cells have been observed moving to the edge of the spot and either staying there or continue moving in a different direction, this may be caused by chemical and/or physical changes in this area. Post-mortem SEM imaging of that location shows a clear deposit which may have been a physical barrier for the diatoms, see Figure 3.33b. However, additional research is required to unravel the exact interaction between *Cylindrotheca fusiformis* and AA2024 corrosion.

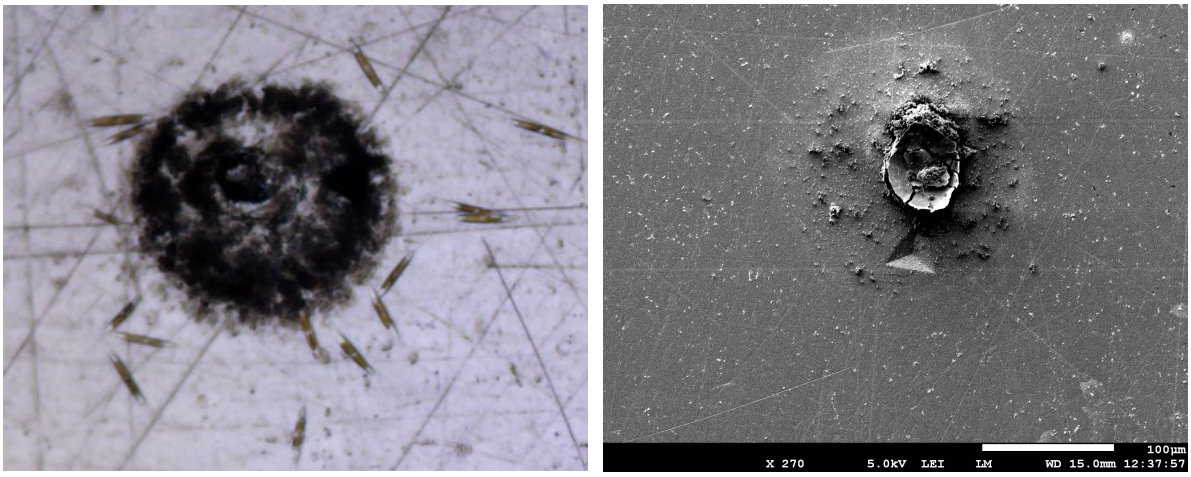

(a) Optical image of the corrosion spot on sample B-2024

(b) SEM image of the corrosion spot on sample B-2024 (mag:270x)

Figure 3.33: Corrosion spot located near the indent on sample B-2024; the cells appear to avoid the location

The effect of aluminum in seawater and diatoms has been studied in the context of seawater contamination. It was found that different diatom species have different sensitivities for aluminum toxicity. In addition, a species dependent effect was discovered with respect to the roles of dissolved aluminum and precipitated aluminum [64]. During this project, the tests were performed on solid aluminum substrates, but over the course of exposure it is possible dissolved aluminum was released in the medium, see Figure 3.34. As toxicity is concentration related, this may explain why the cells appeared to have died in the motility studies conditions. The motility study was performed with a very low volume (1 mL), leading to a very high substrate/liquid ratio. This may have caused the concentration of dissolved Al to be high enough to kill the cells. This would also be consistent with the observation that the cultures used for the biofilm formation experiment did not collapse, as these were performed at higher cell concentrations and volumes.

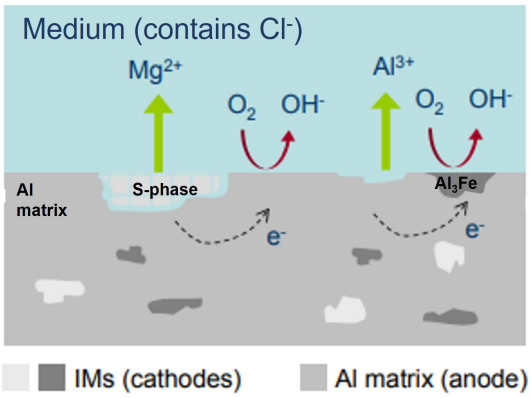

Figure 3.34: Corrosion on AA2024 could lead to Al being released into the medium; adapted from [65]

It has been reported that a higher starting cell density led to an increased sensitivity to aluminum toxicity in diatoms *C. closterium* and *P. triconutum* [64]. This is contrary to other studies done for microalga *Selenastrum capricornutum* for copper, zinc and cadmium [57]. In this particular study the a higher cell concentration led to a decrease in sensitivity. The latter would be consistent with what was found during this project: that a low cell concentration in combination with a low volume did not lead to biofilm formation because of Al toxicity, while biofilm formation was possible at higher concentrations (and volumes). This decrease in toxicity was hypothesized to come from lower metal accumulation rates or by less metal bound per cell [57]. While an increase in sensitivity with cell concentration was thought to come from nutrient depletion, which stresses the cells and could have led to increased sensitivity [64]. It should be noted that the volume and concentration effect have not been investigated separately during this project, meaning it might be either one or a combination of both.

While not investigated, the authors of the aforementioned study stress the possible effect the metal speciation may have [64]. This could be a reason for the difference observed between Al99.5 and AA2024. Al99.5 might cause the Al to be in a more toxic speciation than AA2024, causing a more rapid decline of motility. This would also be consistent with the observation during the test where the two metals were exposed to the same cell suspension (section 3.5), in which the cells on AA2024 followed a similar decline in motility as those on Al99.5, as in this case they were connected through the liquid allowing molecules to diffuse throughout. Aluminum (III) speciation in seawater is partly pH dependent, see Figure 3.35 [66]. The pH of the medium is ±7, and can rise for growing diatom cultures, e.g. a randomly sampled culture was found to have a pH of ±8. In addition, local corrosion processes can also cause the pH to locally rise up to 9.5 above AlCu IMs [35]. However, this is less likely as only limited corrosion was observed during the motility studies. Nevertheless, a (locally) varying pH may cause a change in Al speciation.

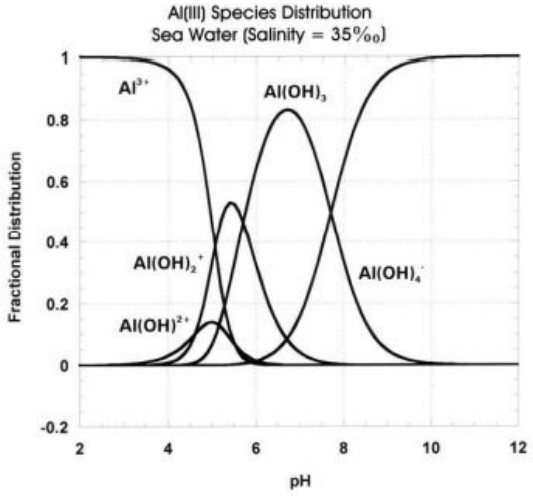

Figure 3.35: The Al(III) species distribution in seawater; adapted from [66]

Previous research showed that different species interact differently with substrates, which can result in different biofilms. It is also known that different species excrete different EPS, which has an effect on coating properties. In recent research it was shown that *Cylindrotheca fusiformis* had a very rapid growth rate compared to *A. coffeaeformis* and *N.incerta*, two other biofilm forming species. This may cause the biofilm to be unstable, due to the fact that a nutrient-limited environment is created which leads to the internal nutrient transport rate to increase. In addition, the TEP production of *C. fusiformis* was less after 70h compared to two other marine species [20]. As it is suspected that TEP plays an important role in biofilm formation, it might be useful to investigate other species on aluminum alloys. While disintegration of the biofilm was not observed in this study, it is advised to keep this in mind for future studies. Fouling species such as *A. coffeaeformis* and *C. australis* have both been researched in the context of adhesion, their adhesive material and motility, albeit on different substrates and could perhaps serve as a good reference.

4

Conclusions

The research objective of this project was to assess the potential of using diatoms for coating purposes on aerospace aluminum alloys by investigating the interaction between the cells and the aluminum alloy substrate. The following questions with various aspects were formulated to serve as a guideline:

RQ1. *In what way does the aluminum alloy composition affect the biofilm formation by* Cylindrotheca fusiformis?

To answer this question, the biofilm formation of the diatoms was studied in relation to the three different factors: surface chemistry, surface preparation and growth medium.

Based on microscopical inspection, it is observed that *C. fusiformis* exhibits different biofilm formation behavior on aerospace aluminum alloys with different compositions. The most homogeneous biofilm was formed on AA7075 compared to Al99.5 and AA2024. The reason for this may be the compositional difference. In addition, a relatively adhesive EPS film was formed on three different aluminum alloys, which could not be removed easily from either Al99.5, AA2024 or AA7075. The EPS layer had a different appearance on the different alloys and showed inhomogeneity on all tested alloys. A covering biofilm grew on degreased-only as well as on polished samples, leading to conclude that *C. fusiformis* can form films on various surface topologies. Finally, the growth medium was also investigated as a non-substrate factor. It was found that a growth medium is required for the cells to form a thick visible biofilm, but that the cells were able to adhere to a polished AA2024 surface even in low nutrient and low silica conditions.

RQ2. *Do the local composition variations in aluminum alloys affect the motility behavior of* Cylindrotheca fusiformis*?*

The diatoms' motility behavior was assessed in relation to three factors: surface chemistry, surface preparation and immersion time.

Cylindrotheca fusiformis exhibited motility on all tested substrates and all topologies, demonstrating a good capability of interacting with different aerospace alloys. The motility of *C. fusiformis* showed a decrease over time on the Al99.5 substrate, while it remained constant on AA2024, leading to conclude that aluminum alloy composition variations have an effect. Diatoms on Al99.5 also showed a decrease in velocity and traveled distance over time. As the surfaces were given the same pre-treatment, and all other conditions were kept equal and constant, it can be concluded that this effect is due to composition variations. When an Al99.5 and AA2024 substrate were immersed into the same cell suspension at the same time, the motility trend on both substrates showed a decrease over time. This effect could be caused by aluminum species being released into the cell suspension, which may be toxic to diatoms at high concentrations. The aluminum speciation and/or amount may be different for Al99.5 than for

AA2024, which would be consistent with a substrate related difference. The effect of local composition variations was also investigated by means of an analysis of the diatom tracks with regards to the IMs, but this did not produce any conclusive results yet.

This research proved that *Cylindrotheca fusiformis* is able to form covering biofilms on various aluminum alloys. This behavior is dependent on the aluminum alloy substrate. In addition, the biofilm formation was found to be dependent on cell concentration and volume, as low volumes and/or low concentrations did not lead to biofilm formation on either Al99.5 or AA2024. These findings may be used to as a factor to improve film formation for coating purposes. As an overall conclusion, this work demonstrated that diatom-produced coatings on aerospace aluminum alloys are promising and deserve further evaluation.

5

Recommendations

This project was exploratory research into the interaction between diatoms and aerospace alloys with the future intent of using diatoms to generate coatings and/or pre-treatments. This work has laid the base by demonstrating that *Cylindrotheca fusiformis* can form biofilms and shows motility on various aluminum alloys with different topologies. In order to further explore their potential, the following recommendations for future work are made.

Considering the intent to use diatom-produced films as pre-treatments or coatings, their coating properties should be analyzed. This work proved that relatively adhesive homogeneous biofilms and EPS layers can be formed. A key component for a coating is sufficient adhesion to the underlying substrate. This may be evaluated by for example a pull-off test. In order to test the properties of these biofilms as coatings, it is important that they form a cohesive and homogeneous film, therefore it is recommended to analyze the cohesiveness of the film. In case the cohesiveness and homogeneity is insufficient for mechanical testing, it is recommended to study the effect of growth-related conditions such as light, temperature, and nutrients. Alternatively, hybridizing the films with other polymers can potentially improve their quality.

In order to properly assess the role diatoms may play in corrosion protection of aluminum alloys, it is necessary to link their behavior to the alloys' corrosion processes. During this work, the corrosion seemed less than expected after a 14 day immersion in the Mix Si medium with and without diatoms present. To further investigate this phenomenon, the time frame of an immersion experiment may be extended until corrosion is observed. It is also recommended to test the corrosion protection of the films, by immersing a substrate with a biofilm in a NaCl solution and compare it to a non-coated alloy. The corrosion process can be monitored visually using the same software as in subsection 2.5.2 and by electrochemical measurements. In an investigation into the use of bacterial EPS for corrosion, three criteria were formulated: (1) low intrinsic corrosiveness, (2) sufficient adhesiveness and (3) low biodegradability by other microorganisms [67]. These criteria can serve as a starting point for further evaluation of the corrosion protection performance. Alternatively, a pre-corroded substrate may be exposed to a cell suspension to study the interaction between the cells and the corrosion products. SEM/EDS may be used to identify the different corrosion products, to determine if the interaction is alloy composition dependent. It would be interesting to see whether *Cylindrotheca fusiformis* is still able to form a biofilm on corrosion affected areas.

With the current setup, the diatoms had to be taken out of the incubator for observation, causing the cells to become re-suspended in the liquid and causing a change in lighting and temperature. The temperature was measured for a 1 mL medium sample which was taken out of the incubator and left out at room temperature for 1h. The temperature was found to rise from 14.5 °C to a stable 19.5 °C over the course of the measurement. While it did not appear to kill the diatoms, the frequently changing circumstances may have an effect on their behavior. In order to minimize these effect, it is recommended

to build the observation setup in a controlled environment such as in the incubator or a climate chamber, allowing for constant observation without disturbances. The experimental setup can be further optimized to enable monitoring of the motility behavior prior to biofilm formation. As during this work, the biofilm formation and motility behavior had to be investigated in separate experiments. A biofilm formation experiment in such controlled conditions can shed some light on where the diatoms decide to settle to start forming the biofilm. This information can be combined with SEM/EDS to potentially relate the colonization behavior to the chemical composition of the surface. This experiment can provide crucial information on the diatoms' preferences, and subsequently its results can be valuable input to the improvement of the biofilm formation process.

To investigate the hypothesis that the cells are unable to form a biofilm due to aluminum toxicity, an post-aluminum-exposure analysis of the cell suspension is recommended. This may for example be done using inductively coupled plasma-mass-spectroscopy (ICP-MS), which enables the detection of low concentrations of elements (parts per billion). It can confirm the presence of dissolved aluminum in the suspension and whether there is a difference between suspensions exposed to Al99.5 compared to suspensions exposed to AA2024. In addition, the sensitivity of *Cylindrotheca fusiformis* to Al toxicity can be evaluated by performing an experiment using dissolved aluminum. The combined results should be able to show whether the Al toxicity hypothesis is plausible.

Interesting to explore would be a motility experiment under Si depleted conditions. As Si is also present in IMs in AA2024, this experiment could indicate whether the diatoms are able to sense the Si when it is bound into a solid and not in the chemical compound of silicic acid, which is the source for diatom silica formation [58]. It has been reported that Si depletion has an influence on the motility behavior. In a Si-poor environment, *Seminavis robusta* exhibited a sort of "searching behavior" whereby the gliding speed of the diatoms increased. The cells also displayed directed motility towards dSi sources when introduced [58]. It is interesting to investigate if this chemotaxis could possibly be used to guide cells across a substrate, ensuring that the whole surface is covered in EPS/biofilm.

While the corrosion software and MTrackJ are able to quantify motility behavior, there are several factors to take into account when analyzing the results. The first being that cells may have moved out of the ROI making it impossible to track them. If they subsequently moved back into the frame, they were considered as as a new cell track, leading to an overestimation of the number of cells that are motile. Another limitation of the applied method is the inability to confirm whether cells actually are attached to the substrate or floating above it. Cells may float just above the surface if excreted polymers are unable to attach to the substrate properly. In addition, detach/re-attach behavior can also be initiated by diatoms. This behavior was previously observed for motile species *Amphora coffeaeformis* on a hydrophobic substrate [27]. And while the aluminum substrates in this work are hydrophilic, this behavior was very likely also observed during the motility studies. The diatoms showed rapid orientation changes, sometimes combined with the cell becoming out of focus, which suggests that the cell (temporarily) detaches from the surface and later re-attaches. It might also be possible for diatoms to pivot around a point of contact, rather than being fully attached to the substrate. In order to analyze this hypothesis, it is recommended to enhance the test setup, enabling cell tracking in 3D.

The techniques for quantifying TEP and chl-a are established, but the existing protocols had to be tailored for the labs at TU Delft. For example, the filter setup used for the extraction of TEP and chl-a from liquid cultures was custom built for this project. This setup was not functioning optimally, resulting in inconsistent outcomes. Therefore, not all TEP and chl-a results are included in this thesis. However, in order to link liquid culture characteristics to biofilm formation, it is advised to further analyze and optimize these techniques.

Another technique that did not produce the intended results was the staining of the motility trails using Stains-All (by Sigma-Aldrich). In literature, this carbocyanine dye was used to visualize the trails left by the diatoms [12], [60]. However, this was done on glass and silica and not on a metallic substrate. Attempts to use this dye on aluminum substrates during this project were unsuccessful. It is most likely that *Cylindrotheca fusiformis* leaves trails during motility, however, different methods of visualization and quantification are required. Trails have been successfully visualized using atomic force microscopy [19], quartz crystal microbalance with dissipation monitoring [12] and using a combination of staining,

freeze-drying and SEM [60]. These alternative techniques can serve as a basis to explore and further develop methods for visualizing the trails on aluminum substrates.

A final recommendation is to increase the sample size as there was a considerable difference observed during the motility study for the three samples of AA2024. While all three samples showed a somewhat similar trend, the absolute numbers were quite different. Even if sample A-2024, the sample which did not show any motility, is disregarded, there is still a considerable difference between samples B and C, as average general motility was around 4x higher on sample C than on sample B. Whether this is due to biological factors, the method or perhaps the differences between the aluminum alloy samples remains unknown. Increasing the sample size can reduce this variation and uncertainty and can perhaps also explain the differences between individual samples.

A

Appendix

A.1. Intermetallics identification

The intermetallics were identified based on their EDS spectra. See Figure A.1 for the four different types of intermetallics and their spectra.

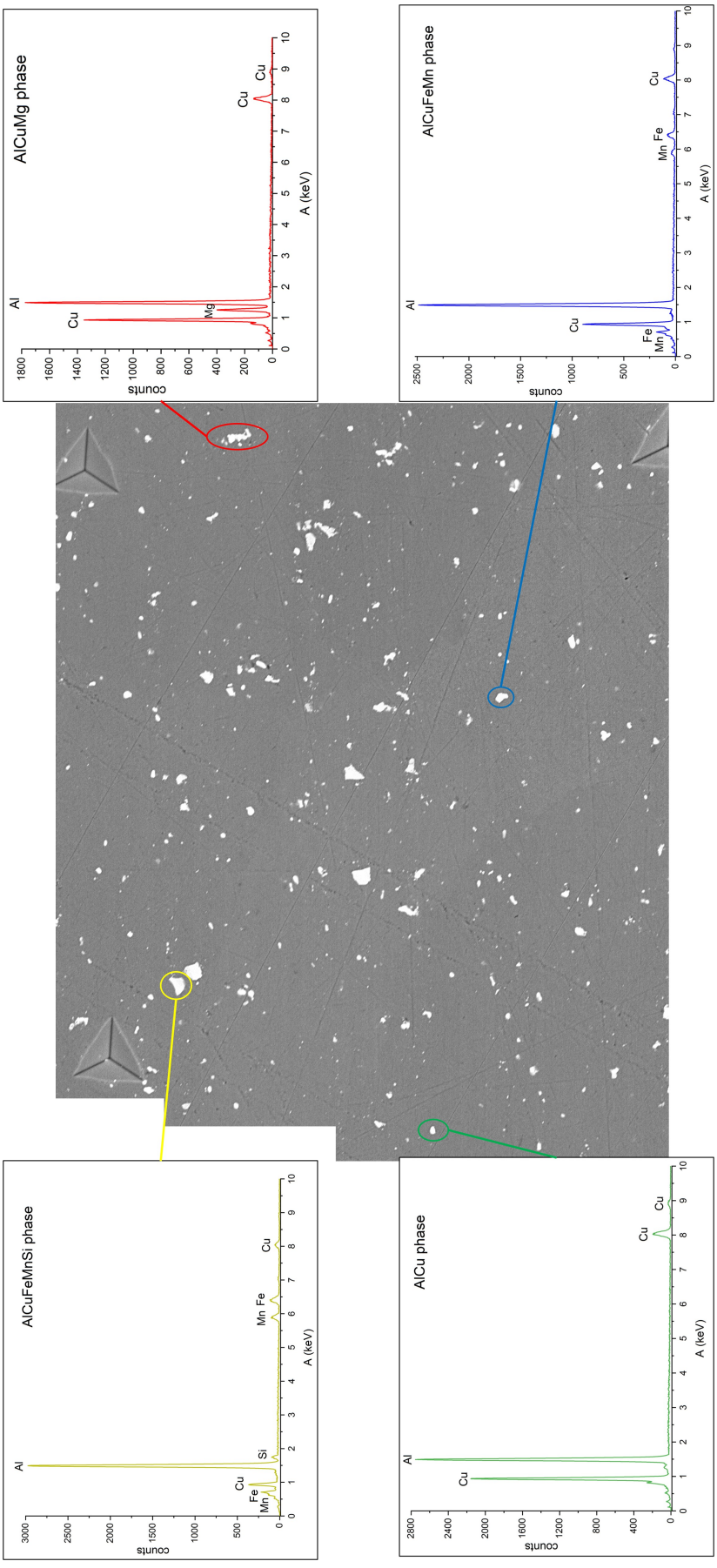

Figure A.1: The various intermetallics and their EDS spectra

A.2. Microstructural analysis of the substrate surface

The spectra of the IMs taken from the AA2024 samples used in the motility study were analyzed and categorized into 4 categories:

1. AlCu (θ-phase)
2. AlCuMg (S-phase)
3. AlCuFeMn
4. AlCuFeMnSi

The results for each can be seen in Figure A.2. All samples were cut from the same plate, please note that the compositions are given as a percentage of the *analyzed* IMs and not of the total number of IMs on the sample. In all samples, the S-phase makes up the biggest part of the measured IMs. However, in the characterization of the IMs it was decided to focus on the largest IMs, which might introduce bias. Within the regions of interest, the IMs make up 1.6-2.5% of the total area. It is important to check the nearest neighbor distance to ensure that it was possible for the diatoms to reach a considerable number of IMs during the measurement time to investigate their influence. Using the *nnd* plugin for ImageJ and visual confirmation, it was found that the distance between the particles varied between 9.4 µm and 9.9 µm, which is small enough compared to the traveled path of the diatoms. The total number of particles registered by during *nnd* plugin were 318 for sample A, 245 for sample B and 276 for sample C.

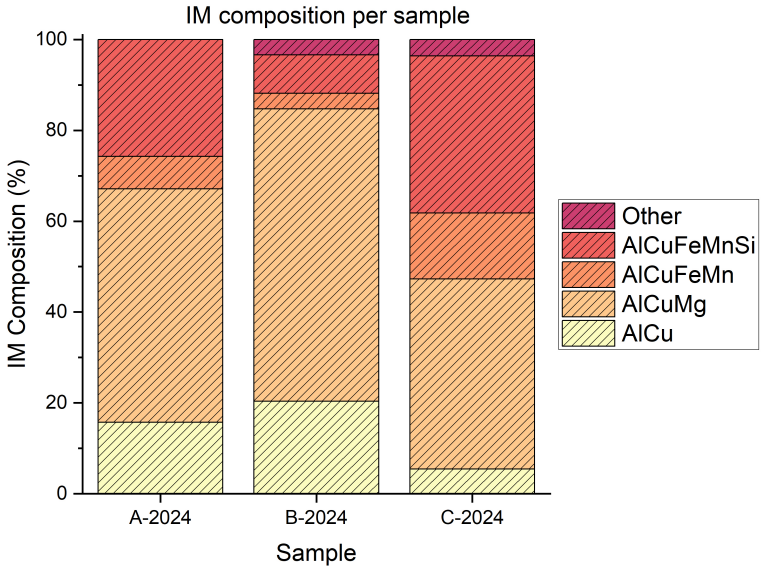

Figure A.2: The composition of the various measured IMs for the samples used in the motility study; the percentage is relative percentage of the IMs analyzed; for sample A 55 IMs were analyzed, for sample B 59 IMs were analyzed, for sample C 70 IMs were analyzed; the category ”other” contains IMs with compositions that could not be sorted into one of the categories

A.3. Motility & intermetallics

This section contains the diatoms' tracks overlaid with the IM map on the AA2024 samples used in section 3.4. The color coding is as follows: green = AlCu, red = AlCuMg, blue = AlCuFeMn, yellow = AlCuFeMnSi, cyan = other. The red oval indicate areas that appear to be avoided by the diatoms.

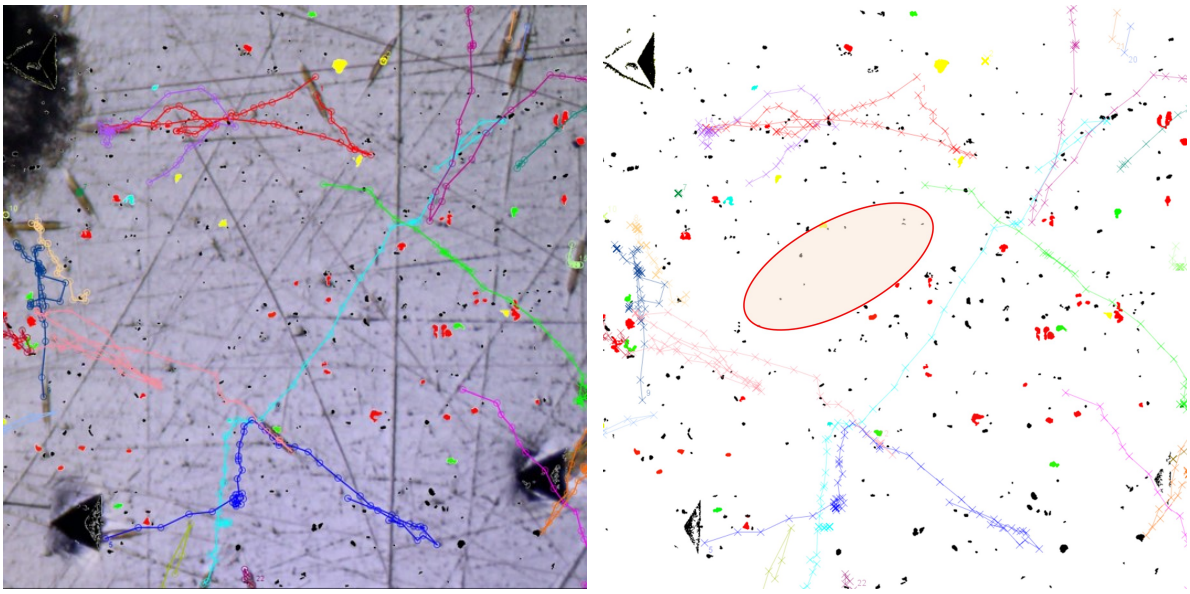

(a) Optical image of the tracks on B-AA2024 after 1h

(b) Tracks on B-AA2024 after 1h on the intermetallics mask

Figure A.3: B-2024 tracks at the 1h measurement

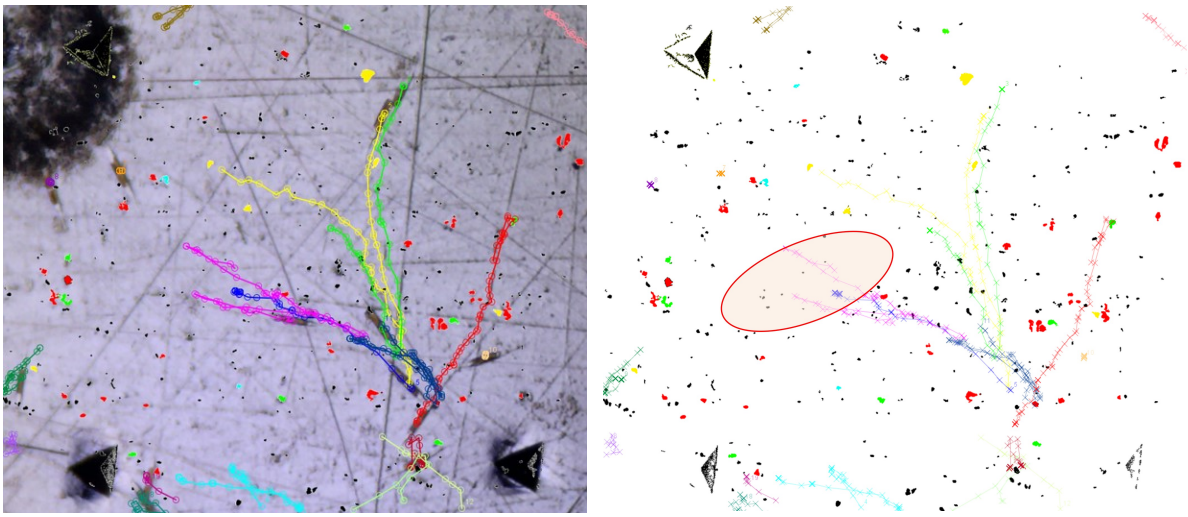

(a) Optical image of the tracks on B-AA2024 after 16h

(b) Tracks on B-AA2024 after 16h on the intermetallics mask

Figure A.4: B-2024 tracks at the 16h measurement

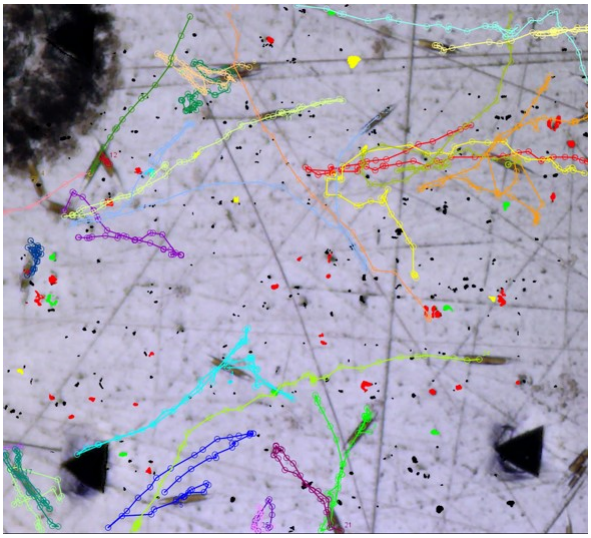

(a) Optical image of the tracks on B-AA2024 after 20h

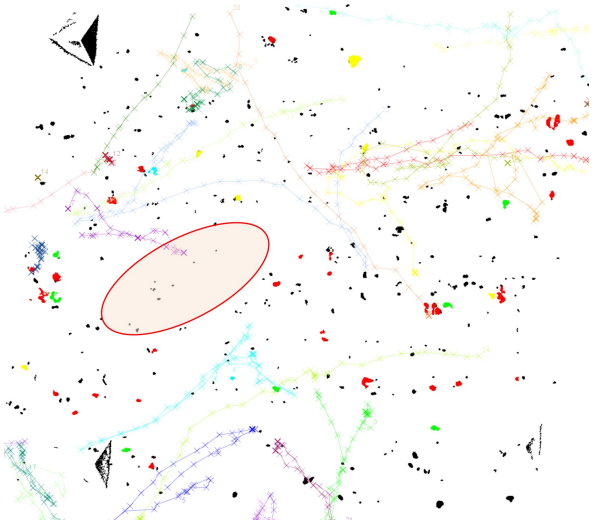

(b) Tracks on B-AA2024 after 20h on the intermetallics mask

Figure A.5: B-2024 tracks at the 20h measurement

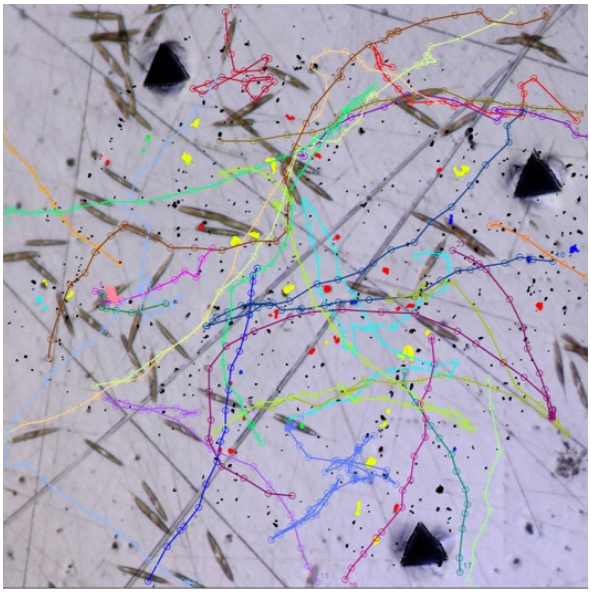

(a) Optical image of the tracks on C-AA2024 after 4h

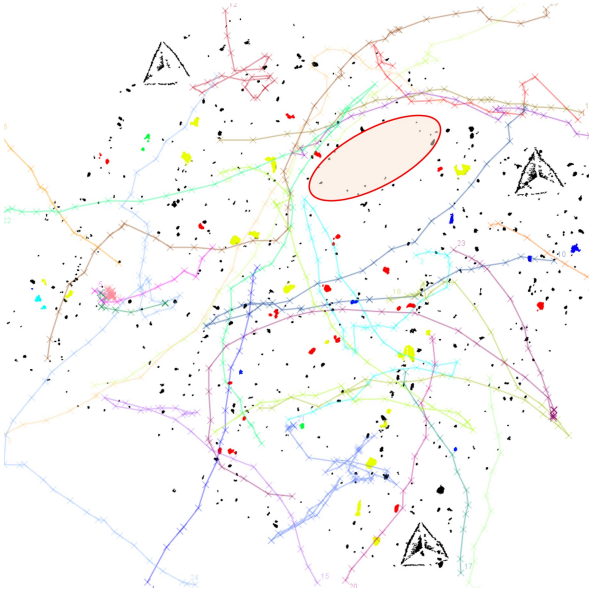

(b) Tracks on C-AA2024 after 4h on the intermetallics mask

Figure A.6: C-2024 tracks at the 4h measurement

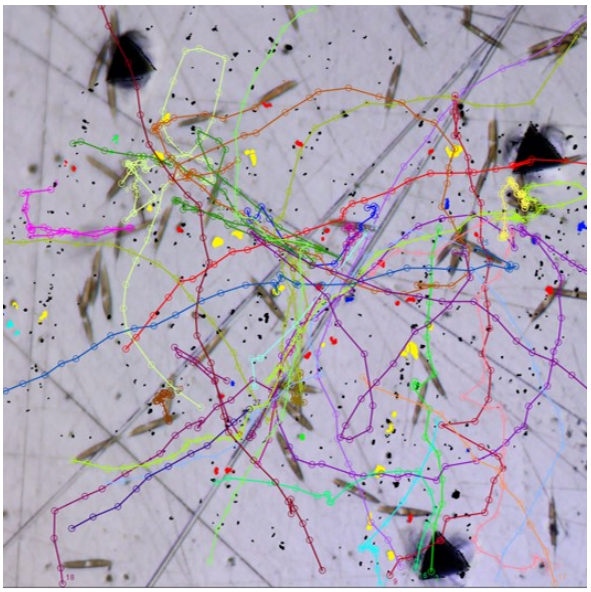

(a) Optical image of the tracks on C-AA2024 after 8h

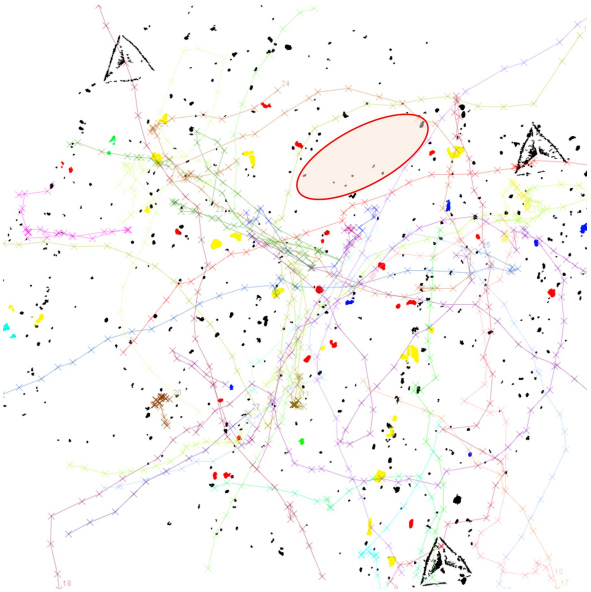

(b) Tracks on C-AA2024 after 8h on the intermetallics mask

Figure A.7: C-2024 tracks at the 8h measurement

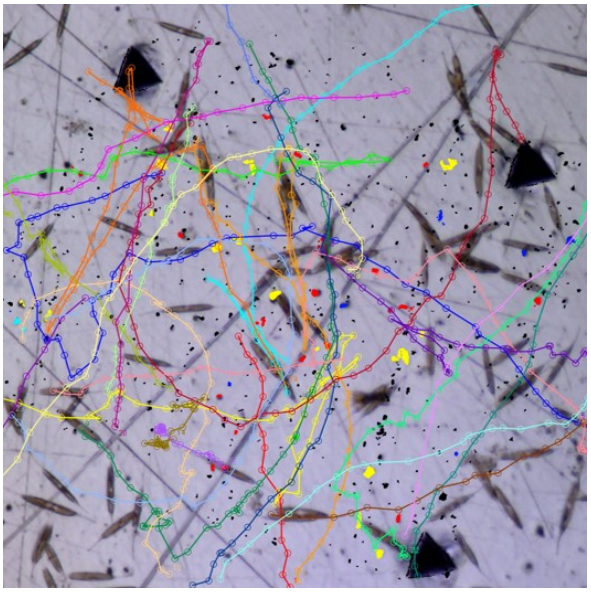

(a) Optical image of the tracks on C-AA2024 after 24h

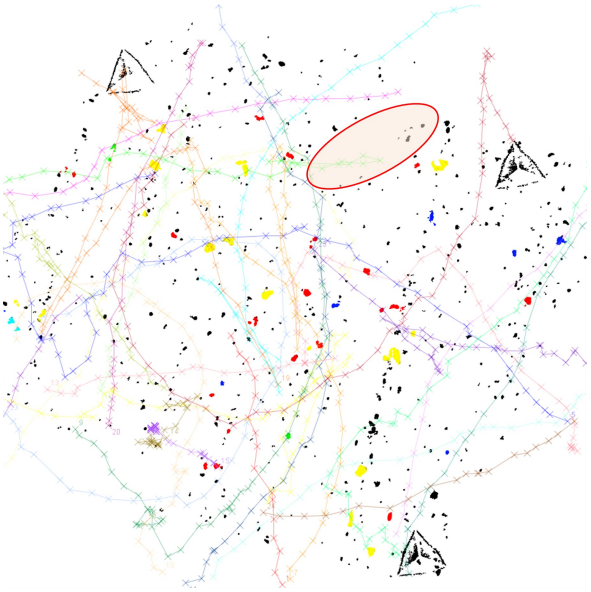

(b) Tracks on C-AA2024 after 24h on the intermetallics mask

Figure A.8: C-2024 tracks at the 24h measurement

A.4. Paths of the diatoms on Al99.5

This section contains the diatoms' tracks on the Al99.5 samples used in section 3.4.

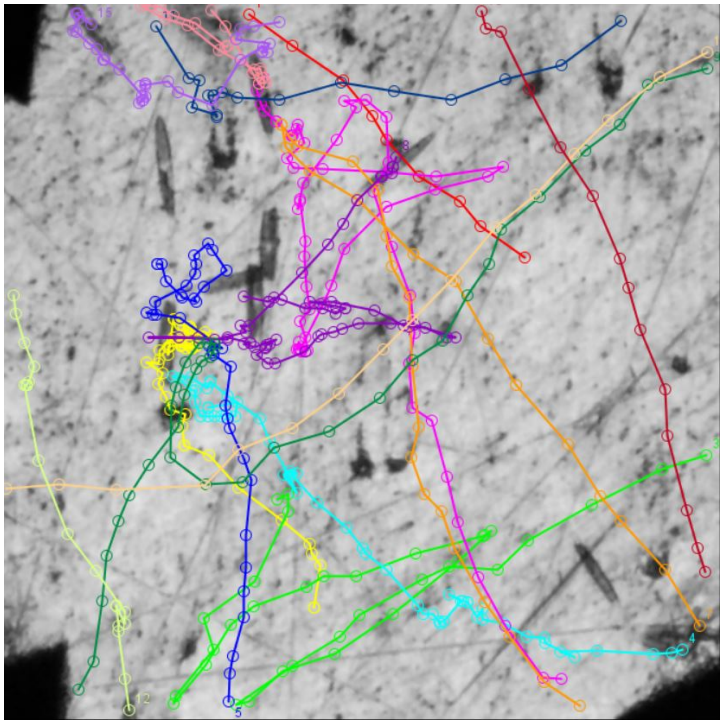

Figure A.9: Tracks on A-99.5 after 2h

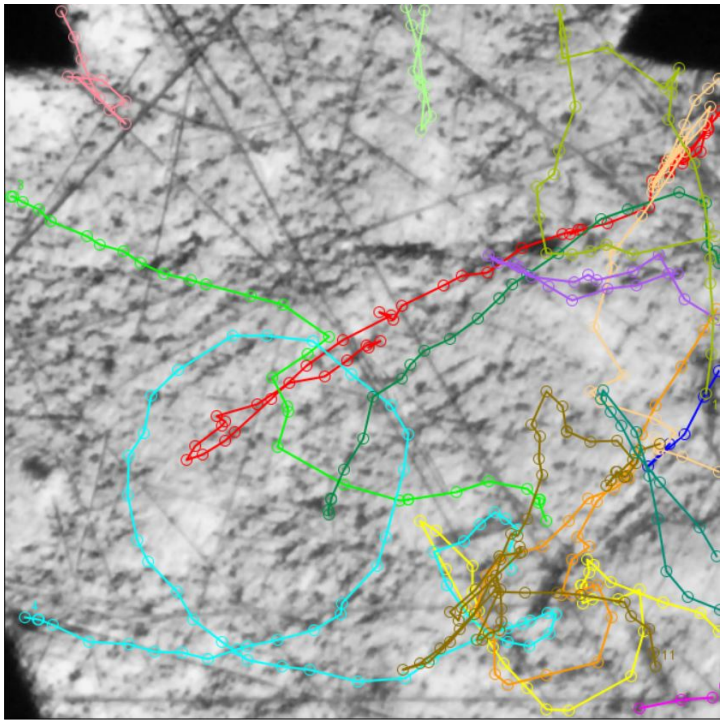

Figure A.10: Tracks on B-99.5 after 1h

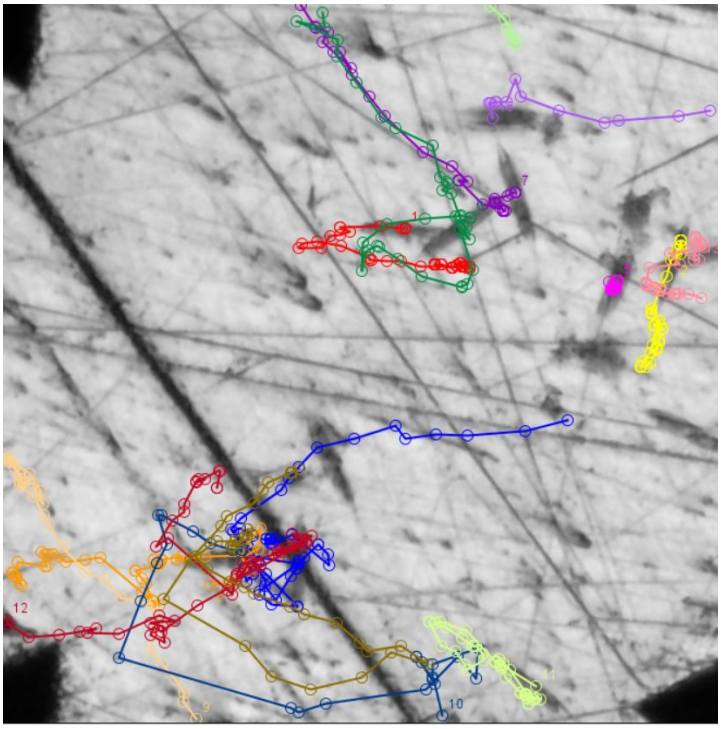

Figure A.11: Tracks on C-99.5 after 4h

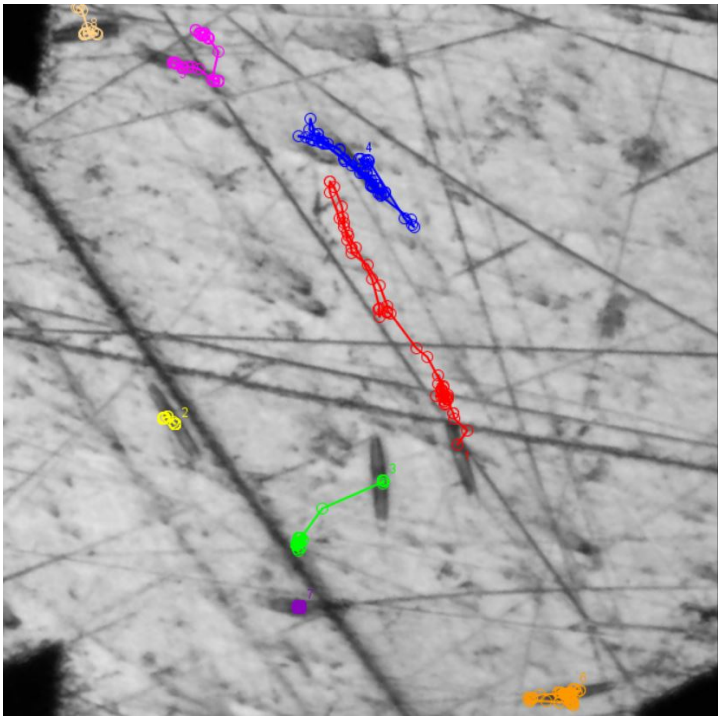

Figure A.12: Tracks on C-99.5 after 8h

B

Appendix

B.1. FTIR results

An FTIR spectrum was taken of the medium to compare to the biofilm spectra, see Figure B.1. The medium spectrum shows three clear peaks. The peak around 3350 cm^{-1} is the O—H stretch, which is consistent with the medium being water based. The peak at 1640 cm^{-1} may be due by compounds in the medium or to scissoring of H—O—H of H_2O. A smaller broad peak is centered around 2100 cm^{-1}, which is not present in the spectra taken from the biofilms.

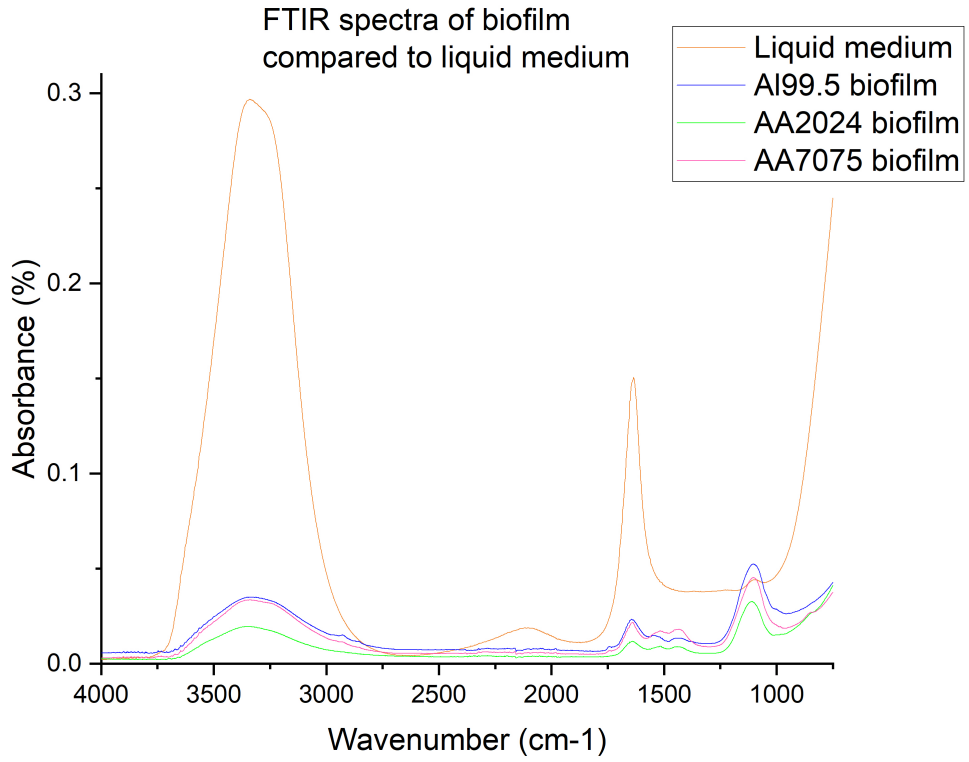

Figure B.1: FTIR spectra of the dried biofilm on various substrates compared with the liquid Mix Si medium

FTIR spectra were also obtained for the bare Al99.5 and AA2024 plates, see Figure B.2. The only peak that stands out it the peak registered on the bare AA2024 around 935 cm^{-1}, which remains unexplained..

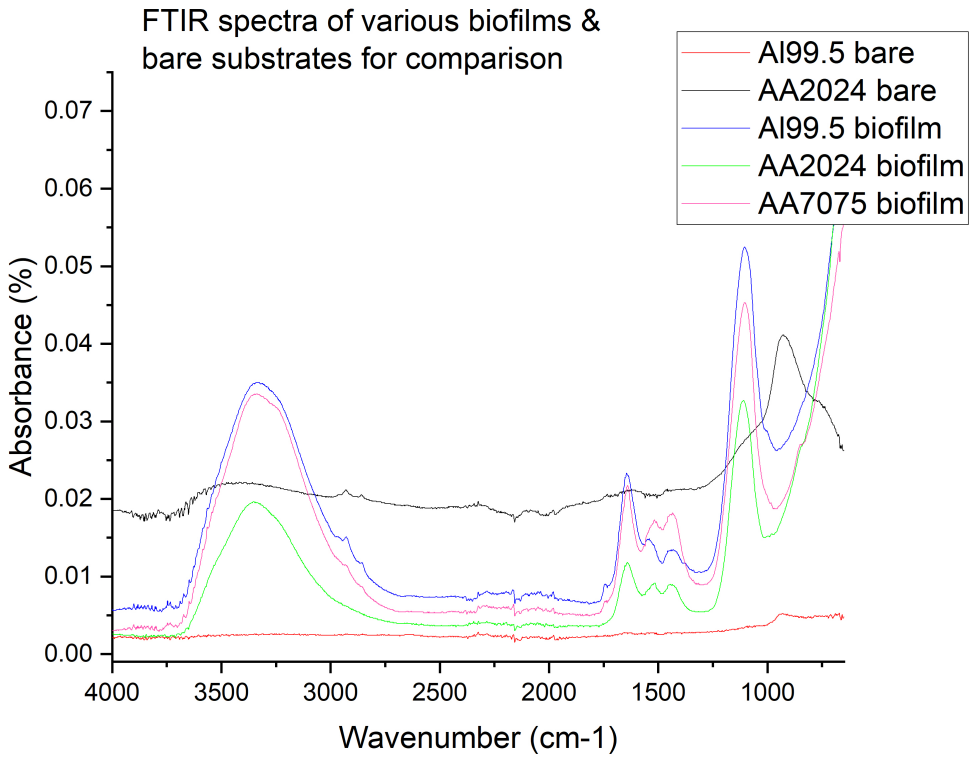

Figure B.2: FTIR spectra of the dried biofilm on various substrates compared with the bare substrates

B.2. SEM images

B.2.1. Surface after biofilm removal

After biofilm removal, the surfaces of the Al99.5, AA2024-T3 and AA7075-T6 substrates were also sputtered and imaged using the SEM. They all show a similar structure on the surface, which may be the remaining EPS layer. The porous structure may be caused by damage done during the removal of the biofilm layer. To confirm, additional chemical analysis should be performed.

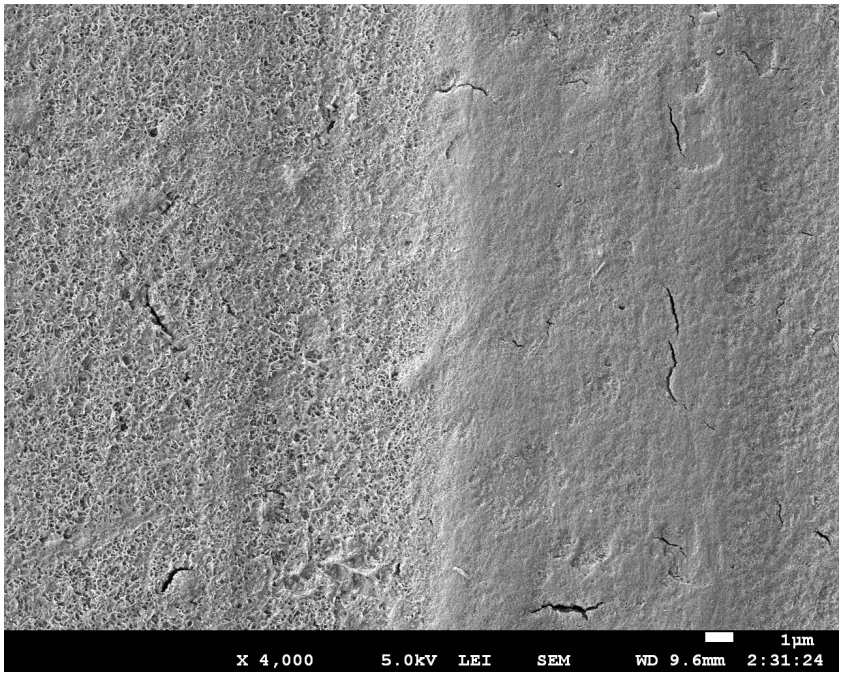

Figure B.3: Surface of Al99.5 after biofilm removal imaged with the SEM (mag:4000x)

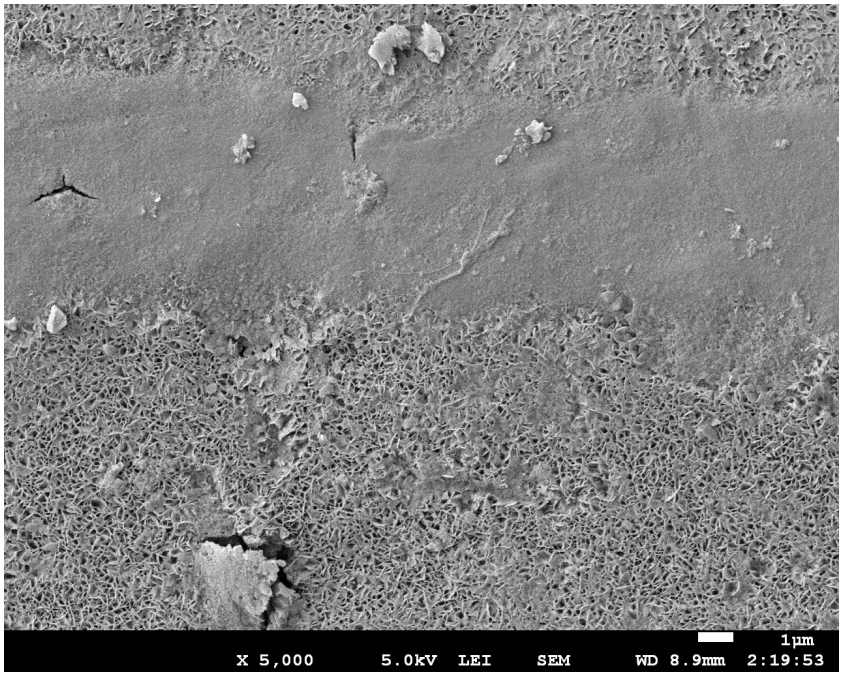

Figure B.4: Surface of AA2024-T3 after biofilm removal imaged with the SEM (mag:5000x)

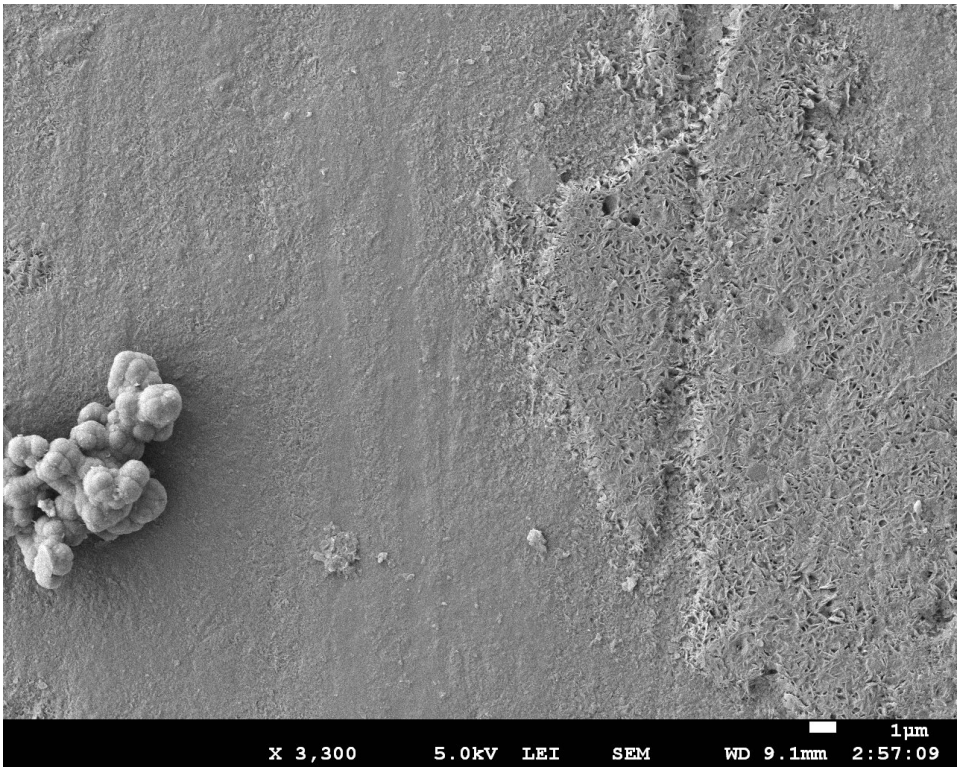

Figure B.5: Surface of AA7075-T6 after biofilm removal imaged with the SEM (mag:3300x)

B.2.2. Surfaces of samples exposed to a low concentration cell suspension for 24h

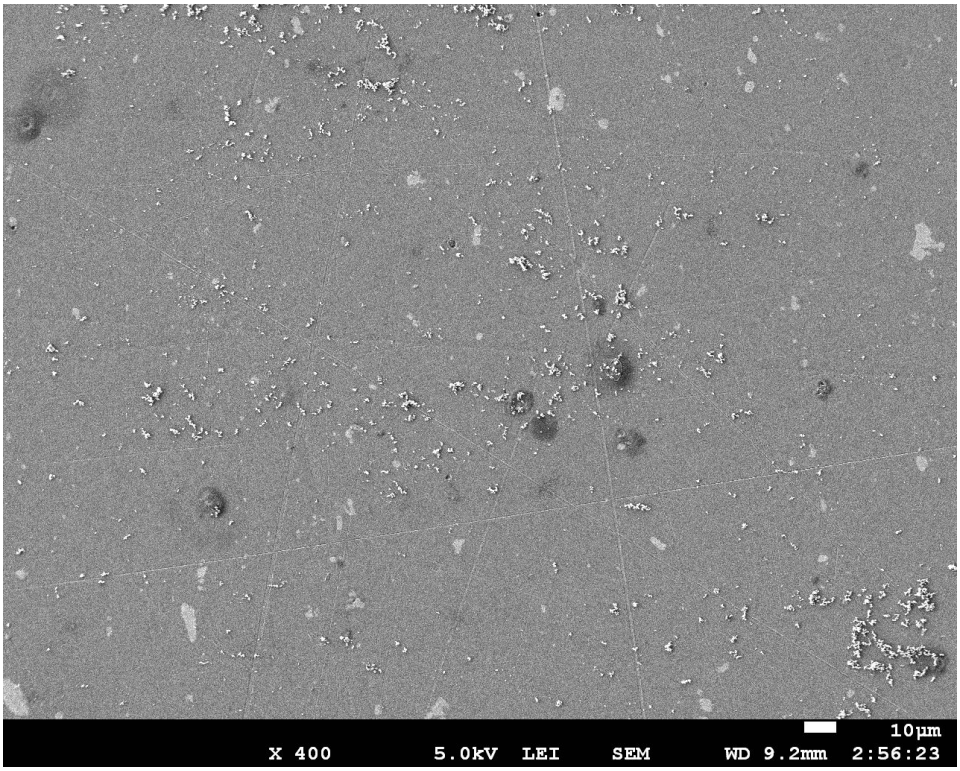

Figure B.6: Surface of C-2024 imaged with the SEM (mag:400x)

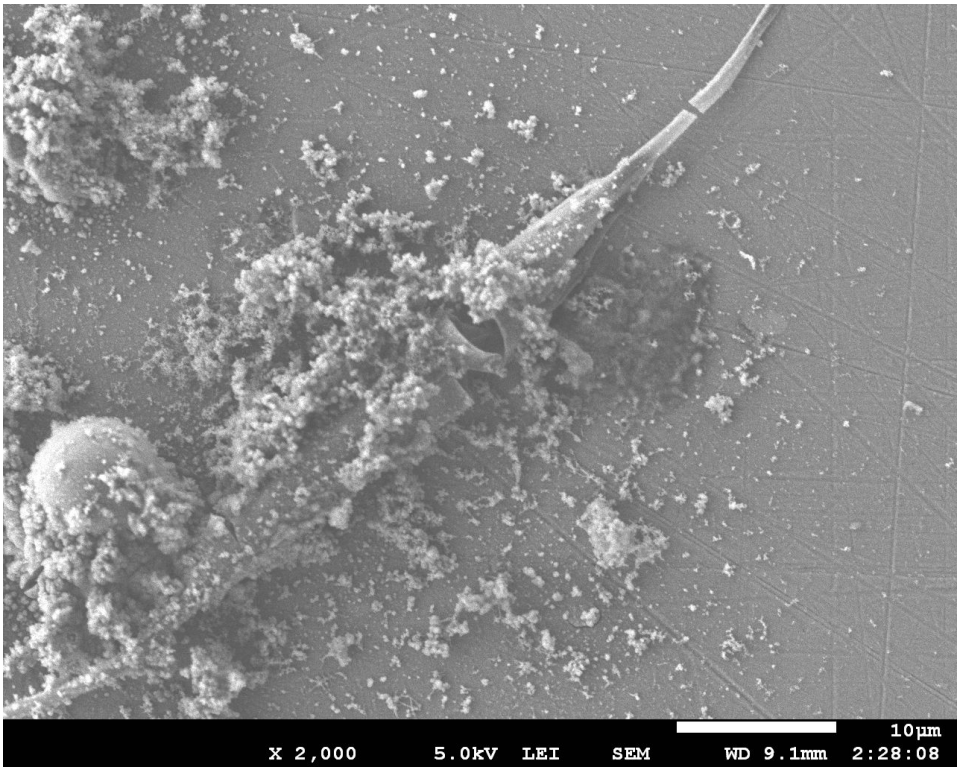

Figure B.7: Surface of C-2024 imaged with the SEM (mag:2000x), a broken frustule can be seen, likely kept in place by EPSs

B.2.3. Surfaces of the samples in the biofilm experiment exposed to medium with diatoms

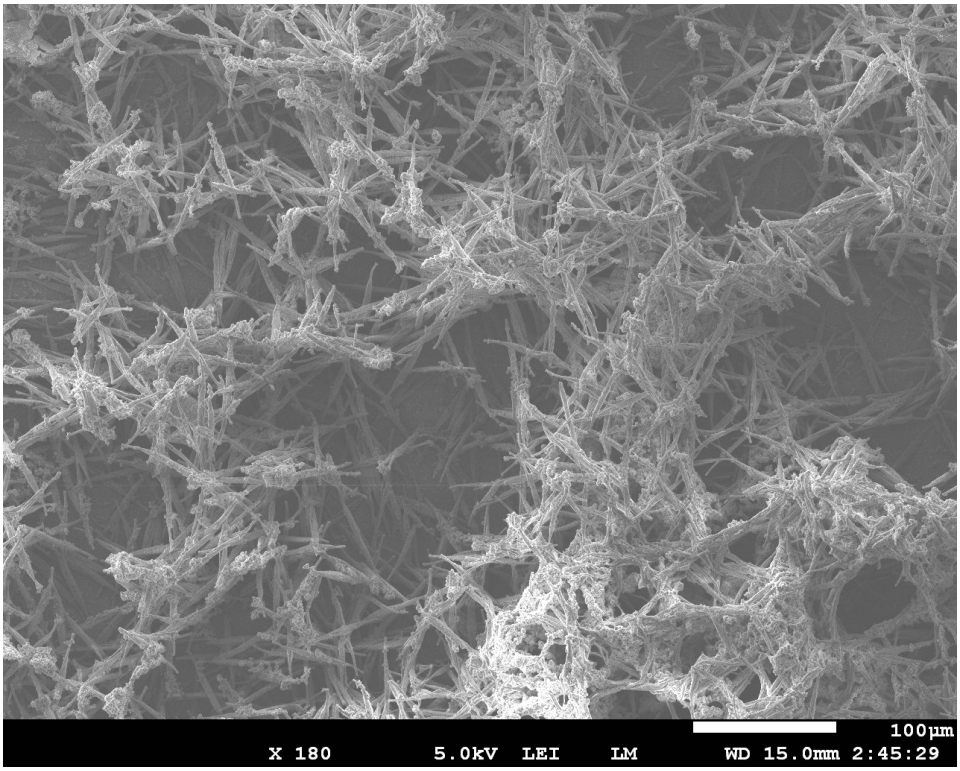

Figure B.8: Biofilm on polished AA2024-T3 exposed to diatoms in medium for 14 days (mag:180x)

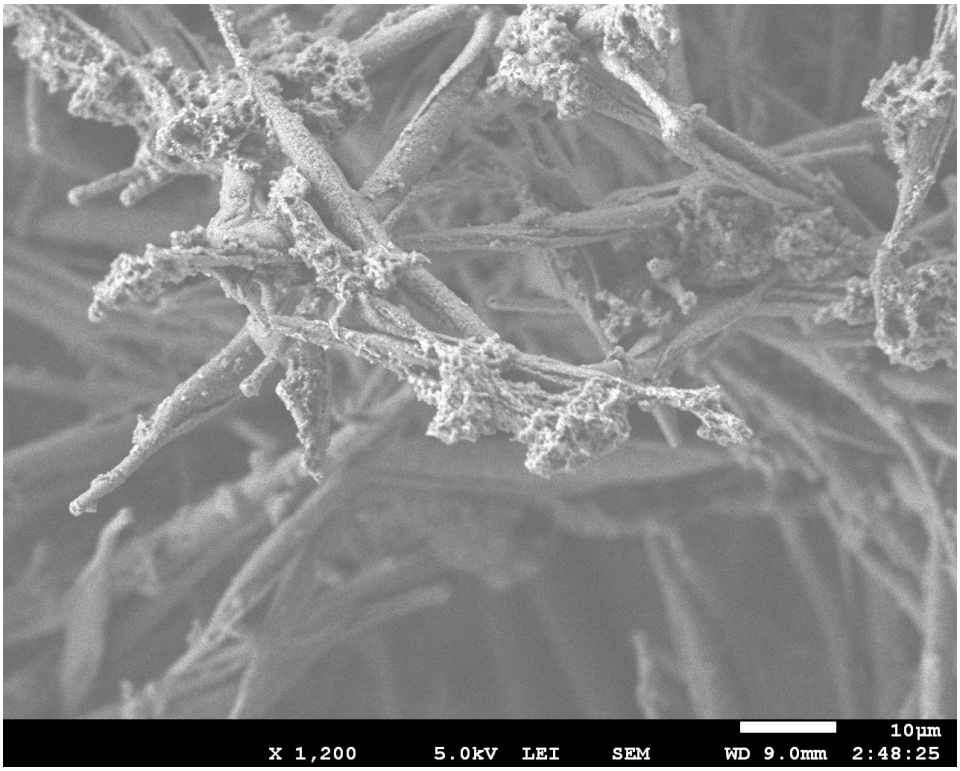

Figure B.9: Biofilm on polished AA2024-T3 exposed to diatoms in medium for 14 days (mag:1200x)

B.2.4. Surfaces of the samples in the biofilm experiment exposed to NSW with diatoms

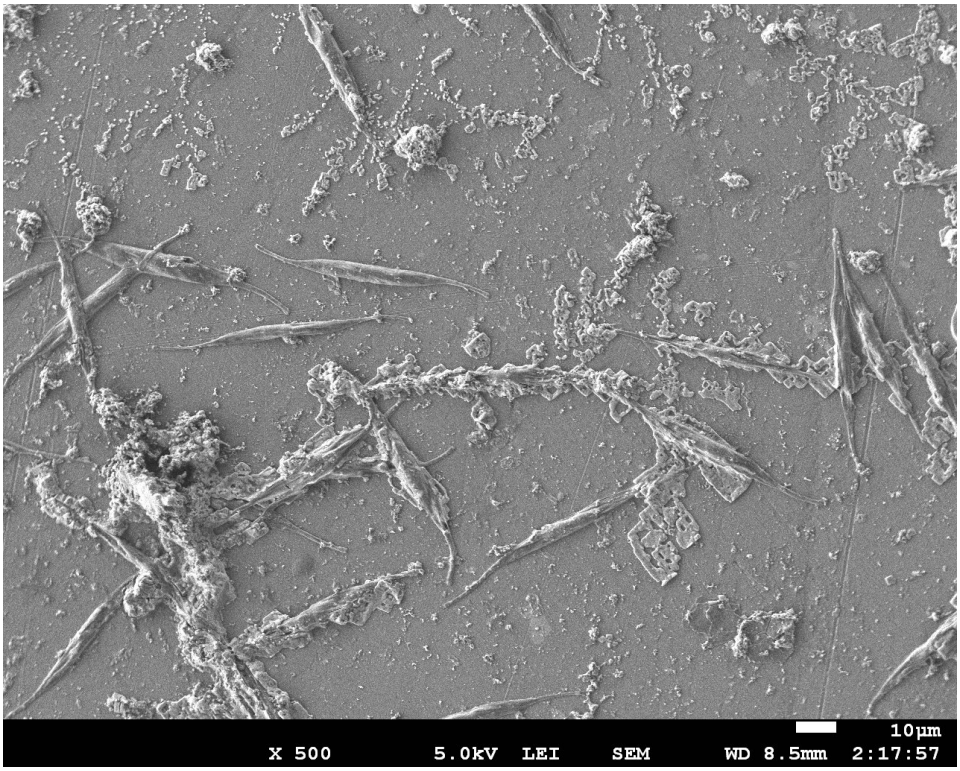

Figure B.10: Biofilm on polished AA2024-T3 exposed to diatoms in NSW for 14 days (mag:500x)

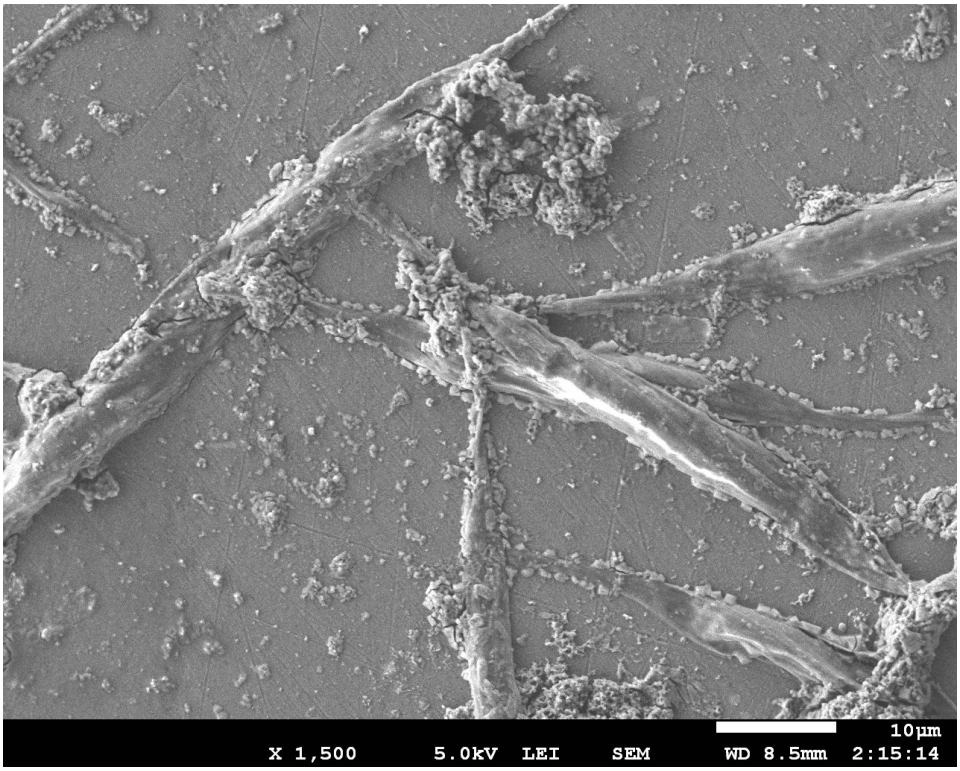

Figure B.11: Several cells from the biofilm on polished AA2024-T3 exposed to diatoms in NSW for 14 days (mag:1500x); the amorphous structures may be EPS

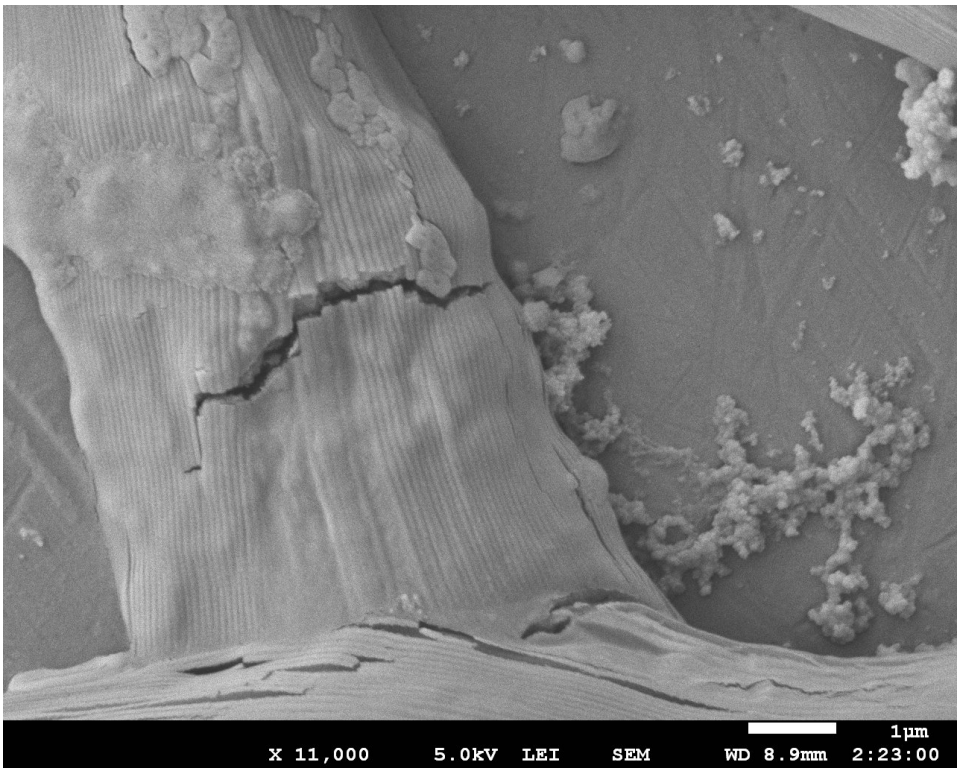

Figure B.12: Broken frustule on the biofilm on polished AA2024-T3 exposed to diatoms in NSW for 14 days (mag:11000x)

B.3. Staining with Stains-All

Based on literature, Stains-All was tried to visualize the tracks left by the diatoms during motility. Various protocols were tried, varying the substrate and staining procedure. A representative surface after 24h diatom exposure and staining with Stains-All can be seen in Figure B.13. In some places a faint blue hue can be seen, but track visualization was not achieved.

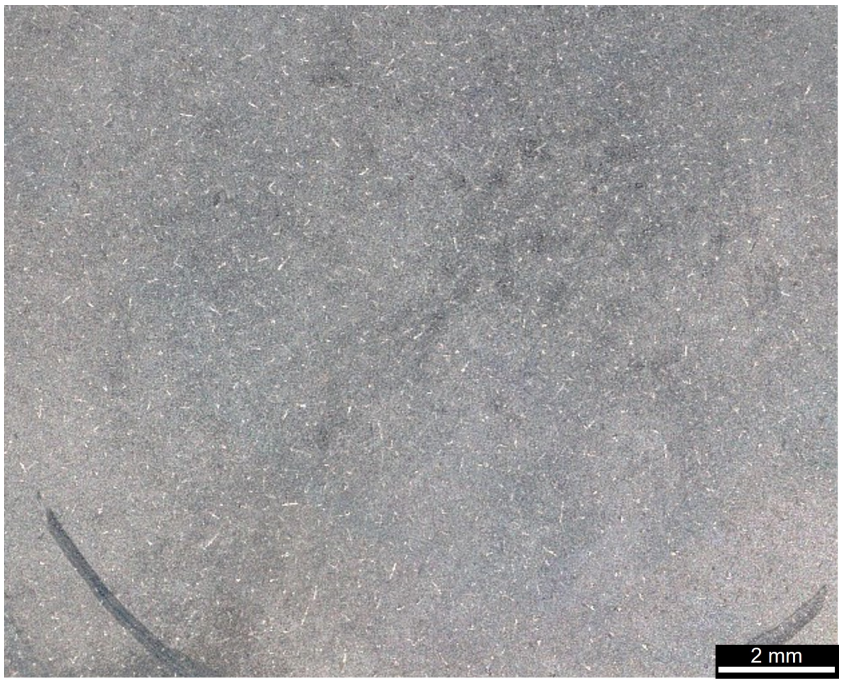

Figure B.13: Aluminum surface after 24h diatom exposure stained with Stains-All

C

Appendix

C.1. Substrates after 24h of medium only exposure

To study the corrosion processes on Al99.5 and AA2024 without the influence of the diatoms, a Al99.5 and AA2024 were prepared the same as the motility samples and exposed to the mix Si medium for 24h, the results can be seen in Figure C.1. Corrosion during immersion was observed to be minimal om both substrates. There were some corrosion spots forming on the AA2024 sample (see Figure C.2), but this seemed to be limited to local spots not progressing to global corrosion of the substrate.

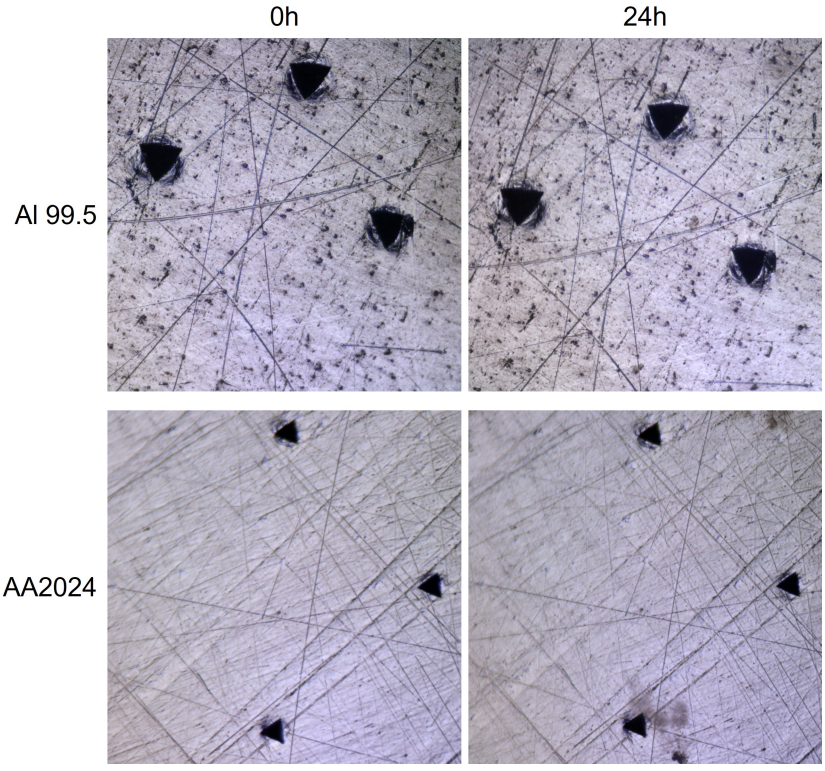

Figure C.1: An Al99.5 and AA2024-T3 which were exposed to 1 mL of mix Si medium for 24h to study corrosion; the spot that can be seen in the bottom right figure is not corrosion, but some contamination of the medium floating around

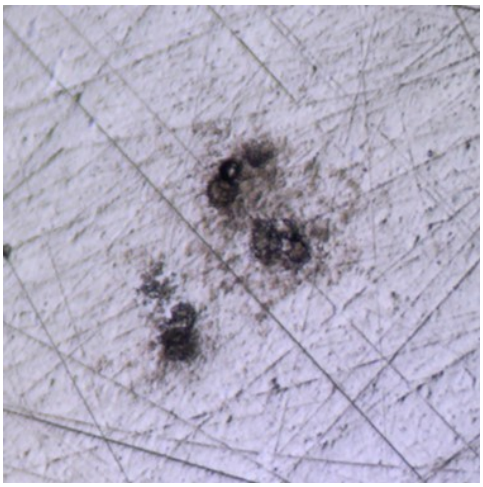

Figure C.2: A corrosion spot observed on AA2024-T3 after 8h immersion into the medium

C.2. Effect UV treatment

The effect of the UV treatment to remove the potential carbon build-up was tested through a corrosion experiment. Two 30x30mm^2 polished AA2024-T3 were indented. A selected area was exposed to the SEM beam for 3h to simulate the exposure of the samples used for the motility experiment. One of these samples was UV treated for 10 minutes, while the other was not. Subsequently, they were exposed to a 0.05M NaCl solution for 6h. In case there is carbon build-up, there would be different corrosion behavior for that region compared to the rest of the substrate. The UV treatment should remove this build-up, meaning the substrate should corrode equally in the exposed area as the rest of the substrate. The results can be seen in Figure C.3, the areas in the red rectangles were exposed to the SEM.

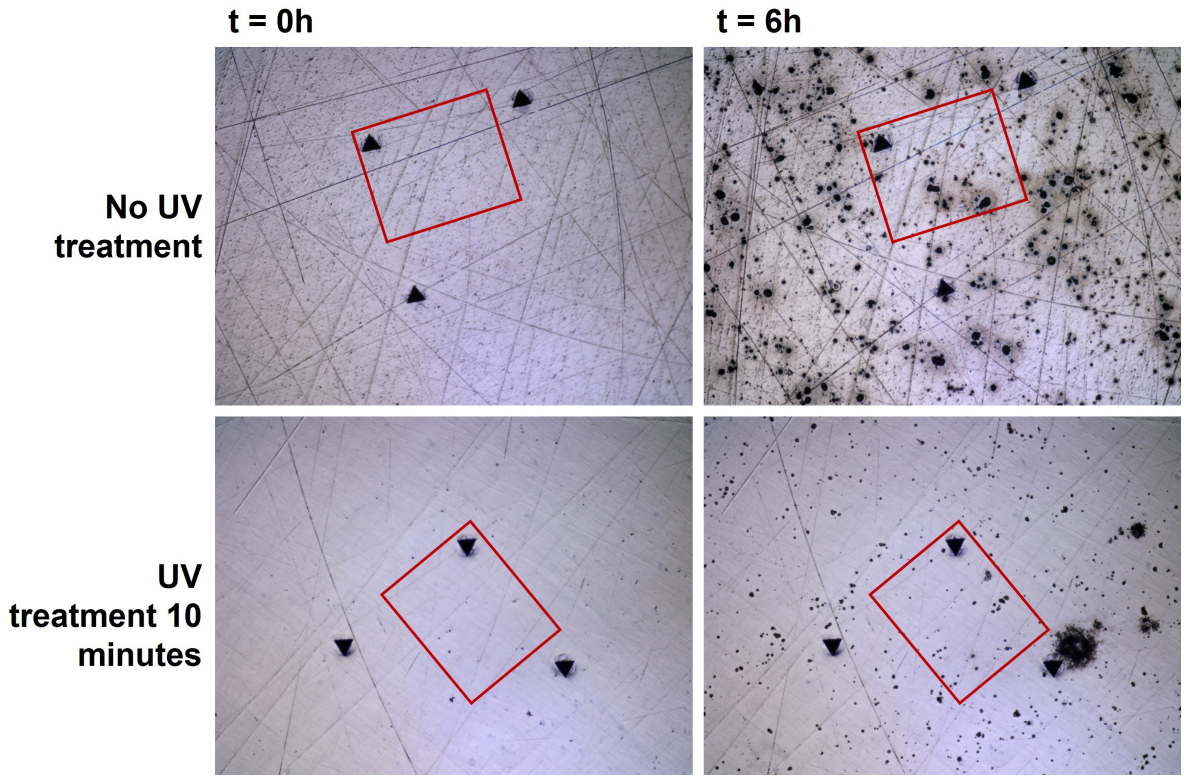

Figure C.3: Effect of 10 min UV treatment on polished AA2024-T3 visualized upon exposure to 0.05M NaCl solution; the areas in the red rectangles were exposed to the SEM beam for 3h prior to immersion

The result for this test is inconclusive. For the top row, a difference would be expected between the area in the red rectangle and the rest of the substrate. However, no clear difference can be discerned. Similarly, the bottom row does not show a considerable difference between the area in the red rectangle and the area outside it. Interestingly, there appears to be a considerably less corrosion on the UV treated sample compared to no UV treatment.

D

Appendix

D.1. Chl-a measurements

Figure D.1 contains the growth curve for one of the cultures as well as the concentration chl-a. As can be seen from the figure, the chl-a concentration follows the expectations as it increases exponentially during the exponential growth phase and decreases in the stationary phase.However, the concentrations as displayed here differ considerably from earlier chl-a measurements taken for similar concentrations of cells [16]. Additionally, it became clear during measurements that the chl-a present in 1 mL aliquots was close to the detection limit to the machine. Therefore it is advised to use higher volume samples for chl-a extraction in future and that this technique is further optimized and validated before using it in future research.

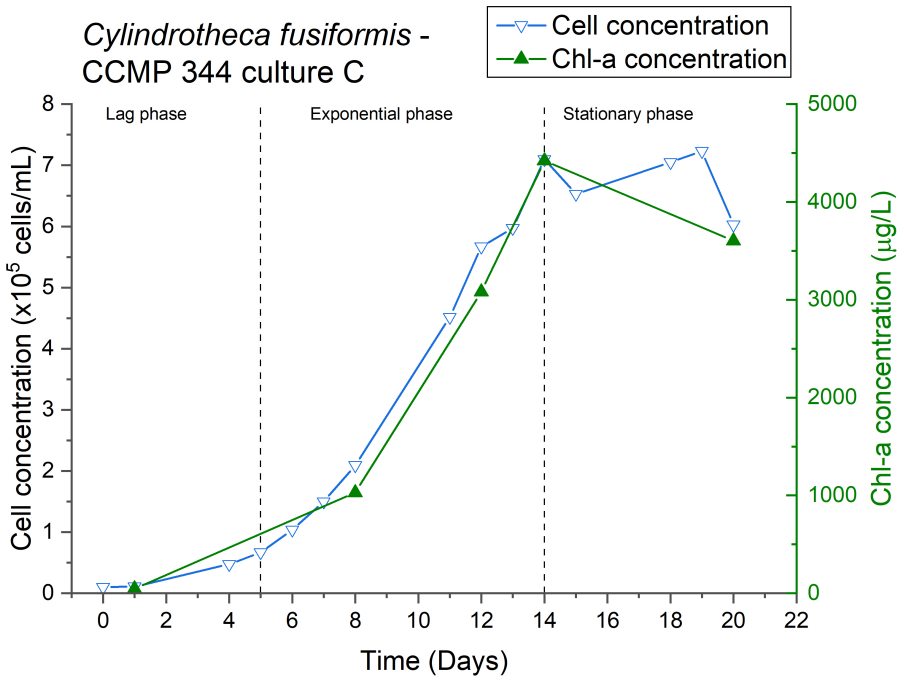

Figure D.1: Growth curve of *Cylindrotheca fusiformis* culture C compared to the chl-a concentration

During the motility study chl-a samples were taken of the mother-lines and cell suspensions. The concentrations of the cells suspensions were below the detection limit of the machine, the results for the mother-lines are displayed in Figure D.2.

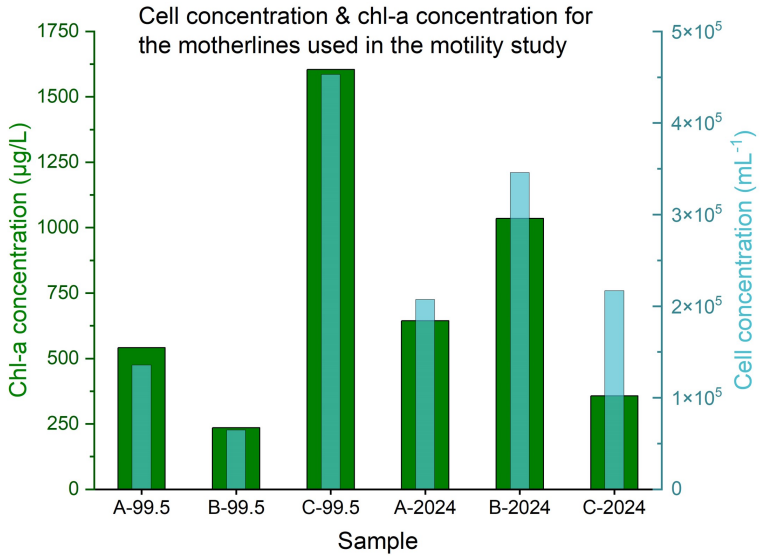

Figure D.2: Cell concentrations and chl-a concentrations for the mother-lines of *Cylindrotheca fusiformis* used in the motility study

A spectrum for a higher chl-a concentration taken using the *Jasco J815 spectrophotometer* can be seen in Figure D.3. It shows the excitation peak at 431 nm as well as the characteristic emission peak at 671nm.

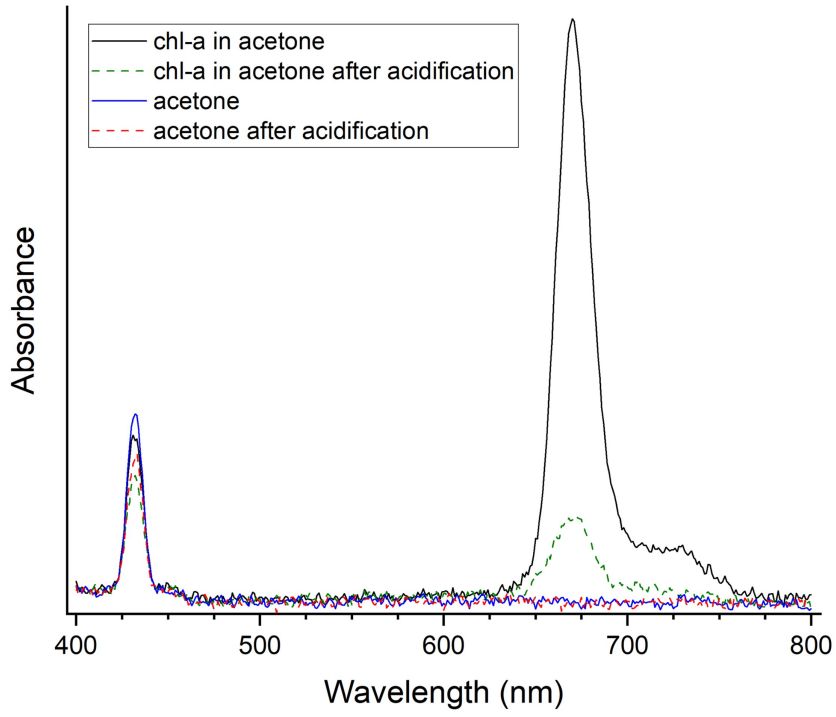

Figure D.3: Spectrum for acetone with and without chl-a before and after acidification with HCl; note the decrease in the peak around 671 nm upon acidification

D.2. TEP measurements

While the TEP setup did not function optimally, a calibration curve was successfully obtained, see Figure D.4. This indicates that with the right optimization, TEP measurements can be made in future.

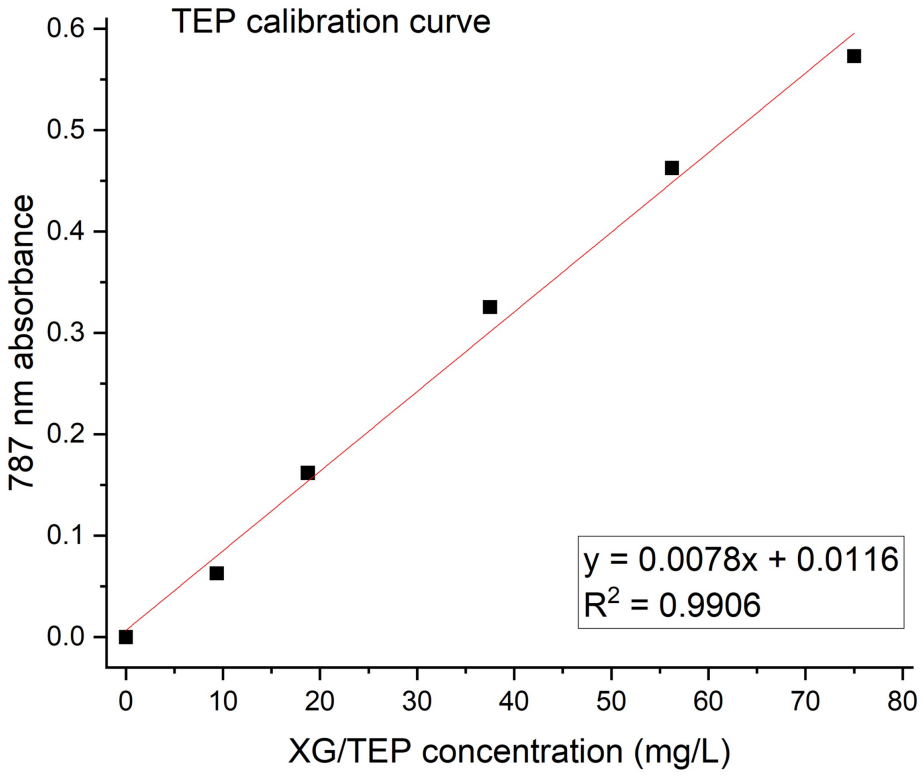

Figure D.4: A successful calibration curve obtained using the *Perkin Elmer Lambda 35* spectrophotometer

E

Appendix

E.1. Growth curve for alternative species *Chaetoceros calcitrans*

During the initial phases of this project, another marine species *Chaetoceros calcitrans* was also kept and a growth curve was generated (see). As *Cylindrotheca fusiformis* showed more potential, it was decided discontinue experiments using *Chaeroceros calcitrans*.

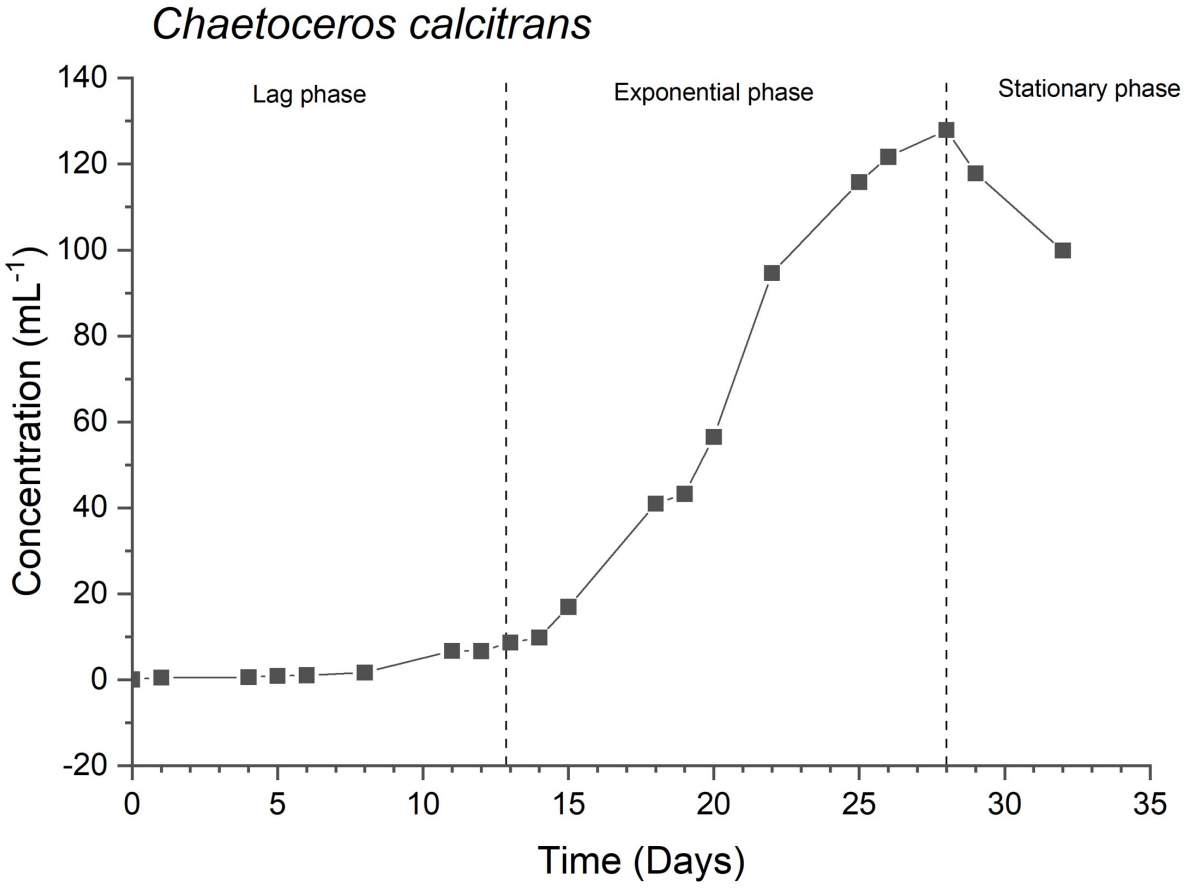

Figure E.1: Growth curve for *Chaetoceros calcitrans*

Bibliography

[1] E. Haeckel, *Kunstformen der Natur*. 1904.

[2] G. Koch, “1 - cost of corrosion,” in *Trends in Oil and Gas Corrosion Research and Technologies*, A. M. El-Sherik, Ed. Boston: Woodhead Publishing, 2017, pp. 3–30, ISBN: 978-0-08-101105-8. DOI: https://doi.org/10.1016/B978-0-08-101105-8.00001-2.

[3] P. Visser, H. Terryn, and J. M. C. Mol, “Aerospace coatings,” in *Active Protective Coatings: New-Generation Coatings for Metals*, A. E. Hughes, J. M. C. Mol, M. L. Zheludkevich, and R. G. Buchheit, Eds. Dordrecht: Springer Netherlands, 2016, pp. 315–372, ISBN: 978-94-017-7540-3. DOI: 10.1007/978-94-017-7540-3_12.

[4] A. D. Roberts, W. Finnigan, E. Wolde-Michael, P. Kelly, J. J. Blaker, S. Hay, R. Breitling, E. Takano, and N. S. Scrutton, “Synthetic biology for fibers, adhesives, and active camouflage materials in protection and aerospace,” *MRS Communications*, vol. 9, no. 2, pp. 486–504, 2019, ISSN: 2159-6859. DOI: 10.1557/mrc.2019.35.

[5] P. J. Denissen and S. J. Garcia, “Cerium-loaded algae exoskeletons for active corrosion protection of coated aa2024-t3,” *Corrosion Science*, vol. 128, pp. 164–175, 2017, ISSN: 0010-938X. DOI: https://doi.org/10.1016/j.corsci.2017.09.019.

[6] A. Demirbas, “Use of algae as biofuel sources,” *Energy Conversion and Management*, vol. 51, no. 12, pp. 2738–2749, 2010, ISSN: 0196-8904. DOI: 10.1016/j.enconman.2010.06.010.

[7] M. P. Schultz, “Effects of coating roughness and biofouling on ship resistance and powering,” *Biofouling*, vol. 23, no. 5, pp. 331–341, 2007, ISSN: 0892-7014. DOI: 10.1080/08927010701461974.

[8] Z. Lewandowski and H. Beyenal, “Mechanisms of microbially influenced corrosion,” in *Marine and Industrial Biofouling*, H.-C. Flemming, P. S. Murthy, R. Venkatesan, and K. Cooksey, Eds. Berlin, Heidelberg: Springer Berlin Heidelberg, 2009, pp. 35–64, ISBN: 978-3-540-69796-1. DOI: 10.1007/978-3-540-69796-1_3.

[9] H. A. Videla and L. K. Herrera, “Understanding microbial inhibition of corrosion. a comprehensive overview,” *International Biodeterioration and Biodegradation*, vol. 63, no. 7, pp. 896–900, 2009, ISSN: 0964-8305. DOI: 10.1016/j.ibiod.2009.02.002.

[10] R. Zuo, “Biofilms: Strategies for metal corrosion inhibition employing microorganisms,” *Applied Microbiology and Biotechnology*, vol. 76, no. 6, pp. 1245–1253, 2007, ISSN: 1432-0614. DOI: 10.1007/s00253-007-1130-6. [Online]. Available: https://doi.org/10.1007/s00253-007-1130-6.

[11] R. Xiao and Y. Zheng, “Overview of microalgal extracellular polymeric substances (eps) and their applications,” *Biotechnology Advances*, vol. 34, no. 7, pp. 1225–1244, 2016. DOI: 10.1016/j.biotechadv.2016.08.004.

[12] P. J. Molino, O. M. Hodson, J. F. Quinn, and R. Wetherbee, “Utilizing qcm-d to characterize the adhesive mucilage secreted by two marine diatom species in-situ and in real-time,” *Biomacromolecules*, vol. 7, no. 11, pp. 3276–3282, 2006, ISSN: 1525-7797. DOI: 10.1021/bm0605661.

[13] P. J. Molino and R. Wetherbee, “The biology of biofouling diatoms and their role in the development of microbial slimes,” *Biofouling*, vol. 24, no. 5, pp. 365–379, 2008, ISSN: 0892-7014. DOI: 10.1080/08927010802254583.

[14] D. G. Mann, “The species concept in diatoms,” *Phycologia*, vol. 38, no. 6, pp. 437–495, 1999, ISSN: 0031-8884. DOI: 10.2216/i0031-8884-38-6-437.1.

[15] B. E. F. Reimann, J. C. Lewin, and B. E. Volcani, “Studies on the biochemistry and fine structure of silica shell formation in diatoms : I. the structure of the cell wall of cylindrotheca fusiformis reimann and lewin,” *Journal of Cell Biology*, vol. 24, no. 1, pp. 39–55, 1965, ISSN: 0021-9525. DOI: 10.1083/jcb.24.1.39.

[16] S. Zalman, “Flying algae - diatoms’ potential as an aerospace coating,” Research facilitated by the Royal Netherlands Institute for Sea Research, Dec. 2020.

[17] L. Karp-Boss, R. Gueta, and I. Rousso, “Judging diatoms by their cover: Variability in local elasticity of lithodesmium undulatum undergoing cell division,” *PLOS ONE*, vol. 9, no. 10, e109089, 2014. DOI: 10.1371/journal.pone.0109089.

[18] A. Garrison and R. Huigens, “Eradicating bacterial biofilms with natural products and their inspired analogues that operate through unique mechanisms,” *Current topics in medicinal chemistry*, vol. 17, Dec. 2016. DOI: 10.2174/1568026617666161214150959.

[19] M. J. Higgins, S. A. Crawford, P. Mulvaney, and R. Wetherbee, “Characterization of the adhesive mucilages secreted by live diatom cells using atomic force microscopy,” *Protist*, vol. 153, no. 1, pp. 25–38, 2002, ISSN: 1434-4610. DOI: https://doi.org/10.1078/1434-4610-00080.

[20] C. Y. Tong and C. J. C. Derek, “Biofilm formation of benthic diatoms on commercial polyvinylidene fluoride membrane,” *Algal Research*, vol. 55, p. 102 260, 2021, ISSN: 2211-9264. DOI: https://doi.org/10.1016/j.algal.2021.102260.

[21] U. Passow, “Transparent exopolymer particles (tep) in aquatic environments,” *Progress in Oceanography*, vol. 55, no. 3, pp. 287–333, 2002, ISSN: 0079-6611. DOI: https://doi.org/10.1016/S0079-6611(02)00138-6.

[22] T. Berman and C. G. Mizrahi R.and Dosoretz, “Transparent exopolymer particles (tep): A critical factor in aquatic biofilm initiation and fouling on filtration membranes,” *Desalination*, vol. 276, no. 1, pp. 184–190, 2011, ISSN: 0011-9164. DOI: 10.1016/j.desal.2011.03.046.

[23] C. Y. Tong and C. J. C. Derek, “The role of substrates towards marine diatom cylindrotheca fusiformis adhesion and biofilm development,” *Journal of Applied Phycology*, vol. 33, no. 5, pp. 2845–2862, 2021, ISSN: 1573-5176. DOI: 10.1007/s10811-021-02504-1.

[24] K. A. Whitehead and J. Verran, “The effect of substratum properties on the survival of attached microorganisms on inert surfaces,” in *Marine and Industrial Biofouling*, H.-C. Flemming, P. S. Murthy, R. Venkatesan, and K. Cooksey, Eds. Berlin, Heidelberg: Springer Berlin Heidelberg, 2009, pp. 13–33, ISBN: 978-3-540-69796-1. DOI: 10.1007/978-3-540-69796-1_2.

[25] J. Landoulsi, K. E. Cooksey, and V. Dupres, “Review – interactions between diatoms and stainless steel: Focus on biofouling and biocorrosion,” *Biofouling*, vol. 27, no. 10, pp. 1105–1124, 2011, ISSN: 0892-7014. DOI: 10.1080/08927014.2011.629043.

[26] F. T. Arce, R. Avci, I. B. Beech, K. E. Cooksey, and B. Wigglesworth-Cooksey, “A live bioprobe for studying diatom-surface interactions,” *Biophysical Journal*, vol. 87, no. 6, pp. 4284–4297, 2004, ISSN: 0006-3495. DOI: 10.1529/biophysj.104.043307.

[27] B. Wigglesworth-Cooksey, H. van der Mei, H. J. Busscher, and K. E. Cooksey, “The influence of surface chemistry on the control of cellular behavior: Studies with a marine diatom and a wettability gradient,” *Colloids and Surfaces B: Biointerfaces*, vol. 15, no. 1, pp. 71–80, 1999, ISSN: 0927-7765. DOI: https://doi.org/10.1016/S0927-7765(98)00102-7.

[28] S. Dobretsov, R. M. M. Abed, and C. R. Voolstra, “The effect of surface colour on the formation of marine micro and macrofouling communities,” *Biofouling*, vol. 29, no. 6, pp. 617–627, 2013. DOI: 10.1080/08927014.2013.784279.

[29] L. A. Edgar, J. D. Pickett-Heaps, and G. E. Fogg, “The mechanism of diatom locomotion. i. an ultrastructural study of the motility apparatus,” *Proceedings of the Royal Society of London. Series B. Biological Sciences*, vol. 218, no. 1212, pp. 331–343, 1983. DOI: doi:10.1098/rspb.1983.0042.

[30] N. Poulsen, N. Kröger, M. J. Harrington, E. Brunner, S. Paasch, and M. T. Buhmann, “Isolation and biochemical characterization of underwater adhesives from diatoms,” *Biofouling*, vol. 30, no. 4, pp. 513–523, 2014, ISSN: 0892-7014. DOI: 10.1080/08927014.2014.895895.

[31] “8 - aluminium alloys for aircraft structures,” in *Introduction to Aerospace Materials*, A. P. Mouritz, Ed. Woodhead Publishing, 2012, pp. 173–201, ISBN: 978-1-85573-946-8. DOI: https://doi.org/10.1533/9780857095152.173.

[32] A. A. S. M. Inc. (). “Aluminum 2024-t3,” [Online]. Available: http://asm.matweb.com/search/SpecificMaterial.asp?bassnum=ma2024t3.

[33] ——, (). “Aluminum 7075-t6,” [Online]. Available: http://asm.matweb.com/search/SpecificMaterial.asp?bassnum=ma7075t6.

[34] A. E. Hughes, N. Birbilis, J. M. Mol, S. J. Garcia, X. Zhou, and G. E. Thompson, “High strength al-alloys: Microstructure, corrosion and principles of protection,” *Recent Trends in Processing and Degradation of Aluminium Alloys*, vol. 1, pp. 223–262, 2011.

[35] A. Boag, A. E. Hughes, A. M. Glenn, T. H. Muster, and D. McCulloch, “Corrosion of aa2024-t3 part i: Localised corrosion of isolated im particles,” *Corrosion Science*, vol. 53, no. 1, pp. 17–26, 2011, ISSN: 0010-938X. DOI: https://doi.org/10.1016/j.corsci.2010.09.009.

[36] M. Olgiati, P. J. Denissen, and S. J. Garcia, “When all intermetallics dealloy in aa2024-t3: Quantifying early stage intermetallic corrosion kinetics under immersion,” *Corrosion Science*, vol. 192, p. 109 836, 2021, ISSN: 0010-938X. DOI: https://doi.org/10.1016/j.corsci.2021.109836.

[37] J. Evertsson, F. Bertram, F. Zhang, L. Rullik, L. R. Merte, M. Shipilin, M. Soldemo, S. Ahmadi, N. Vinogradov, F. Carlà, J. Weissenrieder, M. Göthelid, J. Pan, A. Mikkelsen, J. O. Nilsson, and E. Lundgren, “The thickness of native oxides on aluminum alloys and single crystals,” *Applied Surface Science*, vol. 349, pp. 826–832, 2015, ISSN: 0169-4332. DOI: https://doi.org/10.1016/j.apsusc.2015.05.043.

[38] P. Cornette, S. Zanna, A. Seyeux, D. Costa, and P. Marcus, “The native oxide film on a model aluminium-copper alloy studied by xps and tof-sims,” *Corrosion Science*, vol. 174, p. 108 837, 2020, ISSN: 0010-938X. DOI: https://doi.org/10.1016/j.corsci.2020.108837.

[39] K. Xhanari and M. Finšgar, “Organic corrosion inhibitors for aluminum and its alloys in chloride and alkaline solutions: A review,” *Arabian Journal of Chemistry*, vol. 12, no. 8, pp. 4646–4663, 2019, ISSN: 1878-5352. DOI: https://doi.org/10.1016/j.arabjc.2016.08.009.

[40] NIOZ, “Adapted enriched artificial seawater medium,” Standard Operating Procedure for the Royal Netherlands Institute for Sea Research, Dec. 2018.

[41] A. Noordeloos and K. Kooijman, “F/2 medium,” Standard Operating Procedure for the Royal Netherlands Institute for Sea Research, Jan. 2017.

[42] K. Kooijman, “Mix-tx medium,” Standard Operating Procedure for the Royal Netherlands Institute for Sea Research, Jan. 2017.

[43] R. R. Guillard and J. H. Ryther, “Studies of marine planktonic diatoms. i. cyclotella nana hustedt, and detonula confervacea (cleve) gran,” *Can J Microbiol*, vol. 8, pp. 229–39, 1962, ISSN: 0008-4166 (Print) 0008-4166. DOI: 10.1139/m62-029.

[44] R. R. L. Guillard, “Culture of phytoplankton for feeding marine invertebrates,” in *Culture of Marine Invertebrate Animals: Proceedings — 1st Conference on Culture of Marine Invertebrate Animals Greenport*, W. L. Smith and M. H. Chanley, Eds. Boston, MA: Springer US, 1975, pp. 29–60, ISBN: 978-1-4615-8714-9. DOI: 10.1007/978-1-4615-8714-9_3.

[45] E. J. Arar, *Method 445.0 [electronic resource] : in vitro determination of chlorophyll a and pheophytin a in marine and freshwater algae by fluorescence / Elizabeth J. Arar and Gary B. Collins*. [Cincinnati, OH]: United States Environmental Protection Agency, Office of Research and Development, National Exposure Research Laboratory, 1997.

[46] T. B. Bittar, U. Passow, L. Hamaraty, K. D. Bidle, and E. L. Harvey, “An updated method for the calibration of transparent exopolymer particle measurements,” *Limnology and Oceanography: Methods*, vol. 16, no. 10, pp. 621–628, 2018, ISSN: 1541-5856. DOI: https://doi.org/10.1002/lom3.10268.

[47] U. Passow and A. L. Alldredge, “A dye-binding assay for the spectrophotometric measurement of transparent exopolymer particles (tep),” *Limnology and Oceanography*, vol. 40, no. 7, pp. 1326–1335, 1995, ISSN: 0024-3590. DOI: https://doi.org/10.4319/lo.1995.40.7.1326.

[48] S. Marienfeld, *Counting chambers sedgewick rafter*, Accessed on 24 September 2020. [Online]. Available: https://www.marienfeld-superior.com/counting-chambers-sedgewick-rafter.html.

[49] P. J. Denissen, A. M. Homborg, and S. J. Garcia, "Interpreting electrochemical noise and monitoring local corrosion by means of highly resolved spatiotemporal real-time optics," *Journal of The Electrochemical Society*, vol. 166, no. 11, p. C3275, 2019, ISSN: 1945-7111.

[50] L. A. Ardila-Rodríguez, B. Boshuizen, C. Rans, and J. A. Poulis, "The influence of grit blasting and uv/ozone treatments on ti-ti adhesive bonds and their durability after sol-gel and primer application," *International Journal of Adhesion and Adhesives*, vol. 104, p. 102 750, 2021, ISSN: 0143-7496. DOI: https://doi.org/10.1016/j.ijadhadh.2020.102750.

[51] *Ir spectrum table & chart*. [Online]. Available: https://www.sigmaaldrich.com/NL/en/technical-documents/technical-article/analytical-chemistry/photometry-and-reflectometry/ir-spectrum-table.

[52] A. B. D. Nandiyanto, R. Oktiani, and R. Ragadhita, "How to read and interpret ftir spectroscope of organic material," *2019*, vol. 4, no. 1, p. 22, 2019, ISSN: 2527-8045. DOI: 10.17509/ijost.v4i1.15806.

[53] A. Chiovitti, P. Heraud, T. M. Dugdale, O. M. Hodson, R. C. Curtain, R. R. Dagastine, B. R. Wood, and R. Wetherbee, "Divalent cations stabilize the aggregation of sulfated glycoproteins in the adhesive nanofibers of the biofouling diatom toxarium undulatum," *Soft Matter*, vol. 4, no. 4, pp. 811–820, 2008.

[54] F. Mallamace, C. Corsaro, D. Mallamace, S. Vasi, C. Vasi, and G. Dugo, "The role of water in protein's behavior: The two dynamical crossovers studied by nmr and ftir techniques," *Computational and Structural Biotechnology Journal*, vol. 13, 2014. DOI: 10.1016/j.csbj.2014.11.007.

[55] M. Foggia, P. Taddei, A. Torreggiani, M. Dettin, and A. Tinti, "Self-assembling peptides for biomedical applications: Ir and raman spectroscopies for the study of secondary structure," *Proteomics Research Journal*, vol. 2, pp. 231–272, 2012.

[56] K. Zakowski, M. Narozny, M. Szocinski, and K. Darowicki, "Influence of water salinity on corrosion risk-the case of the southern baltic sea coast," *Environmental monitoring and assessment*, vol. 186, no. 8, pp. 4871–4879, 2014, ISSN: 1573-2959 0167-6369. DOI: 10.1007/s10661-014-3744-3.

[57] I. Moreno-Garrido, L. M. Lubián, and A. M. V. M. Soares, "Influence of cellular density on determination of ec50 in microalgal growth inhibition tests," *Ecotoxicology and Environmental Safety*, vol. 47, no. 2, pp. 112–116, 2000, ISSN: 0147-6513. DOI: https://doi.org/10.1006/eesa.2000.1953.

[58] K. G. V. Bondoc, J. Heuschele, J. Gillard, W. Vyverman, and G. Pohnert, "Selective silicate-directed motility in diatoms," *Nature Communications*, vol. 7, no. 1, p. 10 540, 2016, ISSN: 2041-1723. DOI: 10.1038/ncomms10540.

[59] B. Cooksey and K. E. Cooksey, "Chemical signal-response in diatoms of the genus amphora," *Journal of Cell Science*, vol. 91, no. 4, pp. 523–529, 1988, ISSN: 0021-9533. DOI: 10.1242/jcs.91.4.523.

[60] L. Chen, D. Weng, C. Du, J. Wang, and S. Cao, "Contribution of frustules and mucilage trails to the mobility of diatom navicula sp," *Scientific Reports*, vol. 9, no. 1, p. 7342, 2019, ISSN: 2045-2322. DOI: 10.1038/s41598-019-43663-z.

[61] S. A. Cohn and N. C. Disparti, "Environmental factors influencing diatom cell motility1," *Journal of Phycology*, vol. 30, no. 5, pp. 818–828, 1994, ISSN: 0022-3646. DOI: https://doi.org/10.1111/j.0022-3646.1994.00818.x.

[62] B. Cooksey and K. E. Cooksey, "Chemical signal-response in diatoms of the genus amphora," *Journal of Cell Science*, vol. 91, no. 4, pp. 523–529, 1988, ISSN: 0021-9533. DOI: 10.1242/jcs.91.4.523.

[63] R. Holland, T. M. Dugdale, R. Wetherbee, A. B. Brennan, J. A. Finlay, J. A. Callow, and M. E. Callow, "Adhesion and motility of fouling diatoms on a silicone elastomer," *Biofouling*, vol. 20, no. 6, pp. 323–329, 2004, ISSN: 0892-7014. DOI: 10.1080/08927010400029031.

[64] M. L. Gillmore, L. A. Golding, B. M. Angel, M. S. Adams, and D. F. Jolley, “Toxicity of dissolved and precipitated aluminium to marine diatoms,” *Aquat Toxicol*, vol. 174, pp. 82–91, 2016, ISSN: 1879-1514 (Electronic) 0166-445X (Linking). DOI: 10.1016/j.aquatox.2016.02.004.

[65] S. Garcia, “Designing against aircraft corrosion,” From lecture series: Designing materials with aerospace specific properties, Sep. 2020.

[66] K. M. Elkins and D. J. Nelson, “Spectroscopic approaches to the study of the interaction of aluminum with humic substances,” *Coordination Chemistry Reviews*, vol. 228, no. 2, pp. 205–225, 2002, ISSN: 0010-8545. DOI: https://doi.org/10.1016/S0010-8545(02)00040-1.

[67] R. Stadler, W. Fuerbeth, K. Harneit, M. Grooters, M. Woellbrink, and W. Sand, “First evaluation of the applicability of microbial extracellular polymeric substances for corrosion protection of metal substrates,” *Electrochimica Acta*, vol. 54, no. 1, pp. 91–99, 2008. DOI: 10.1016/j.electacta.2008.04.082.